Master Thesis

INVESTIGATION OF THE AIR–LUBRICATION EFFECT ON FRICTION RESISTANCE

Naval Architecture & Marine Engineering

Thesis directors

Assoc. Prof. Dr. Stefan Kyulevcheliev
Technical University of Varna (Bulgaria)

Dr. José Enrique Gutiérrez Romero
Polytechnic University of Cartagena (Spain)

Author

Antonio Gallardo Martínez
Polytechnic University of Cartagena (Spain)

December 2016

ACKNOWLEDGEMENTS

Upon completion of this master thesis for the title of Naval Architect and Marine engineer, I want to extend the special thanks:

First, to Stefan Kyulevcheliev, for supervise and helping me with this thesis. I have had the pleasure of meeting and working with Stefan during my stay in the Technical University of Varna (Bulgaria) for two semesters in 2014 - 2015 under the Erasmus students' mobility program. He was the one who told me about the air-lubrication and its potential benefits on fuel consumption savings. So we started to work with the aim of make our contribution there too.

Second, to José Enrique Gutiérrez Romero, from the Polytechnic University of Cartagena (Spain). Thanks to him, I could carry out the second part of this project which envelops the use of CFD Software. He gave me his knowledge about Computational Fluid Dynamics which was very useful for me at the time of running the simulations on pc.

I am especially grateful to both teachers for their role as directors of this thesis, for his countless contributions and because his excitement to research that always transmitted an extra motivation.

Moreover, I would like to thank the Technical University of Varna. Thanks to its infrastructure I could grab such an important knowledge for a naval architect as is the hydrodynamic experimentation. I want also thank the Polytechnic University of Cartagena for receiving comprehensive and sufficient training, ethics and human formation to graduate as useful professional for society. I do not forget either the company located in Barcelona who gave us the chance to use its multiphase module of the software they develop 'Tdyn', so thanks to Compass company.

Finally, thanks to my family and friends, who are always there, are patient with me and support me whenever I need it.

Thank you very much to all of you.

ABSTRACT

The new IMO (International Maritime Organization) regulations introduced new requirements (some of them compulsory) for reducing the GHG (Green House Gas) emissions from shipping. These requirements stimulated the implementation of new energy saving devices and methods, and revived the interest to some methodologies already known but not sufficiently studied. One of the latter is the idea of air lubrication of the hull.

The drag resistance of a ship is mainly composed by a part due to the friction and another due to the wave formation and first one is about a 60% of the total. The air lubrication affects mostly to the frictional resistance and seeks its reduction because it would have the most direct and considerable effect on ship's powering performance.

The air lubrication system involves injecting air beneath the hull, so that it moves on the layer of air created between the hull and the surrounding water which it is less viscous.

The thesis is composed by two parts. First one analyzes the behavior of a simplified model of a flat plate in hydrodynamic tests. The second one focuses on the use of CFD software (ANSYS Fluent & Tdyn CFD) for numerical simulations. Different configurations of air-injection openings/slots are investigated with varying combinations of air flow rate and water flow velocities. The numerical computations verify the air-layer pattern and thickness and the effect on frictional resistance.

Experiments are carried out with a flat-bottom barge to validate the numerical results; the towing tank of TU-Varna is the place where tests are performed.

An estimation of the power demand for air injection is also considered to evaluate the trade-off between resistance reduction and air-blow expenses. Finally, a 10% drag reduction is demonstrated to be feasible with this system.

RESUMEN

Los nuevos reglamentos de la IMO (Organización Marítima Internacional) han introducido nuevos requisitos (algunos de ellos de obligado cumplimiento) para reducir las emisiones de Gases de Efecto Invernadero (GEI o GHG de sus siglas en inglés) emitidos por los buques. Estos requisitos han incentivado la implementación de nuevos métodos y dispositivos para el ahorro de energía, y han revivido el interés de algunos ya conocidos, pero no lo suficientemente estudiados. Uno de estos últimos es la idea de lubricar el casco con aire.

La resistencia al avance de un barco se compone principalmente por una parte debida a la fricción y otra a la formación de olas y la primera es de aproximadamente un 60% del total. La lubricación por aire afecta sobre todo a la resistencia de fricción y busca su reducción, ya que tendría el efecto más directo y considerable en el rendimiento propulsivo de la nave.

El sistema de lubricación con aire consiste en la inyección de aire por debajo del casco, de tal forma que este se desplace sobre la capa de aire creada entre el casco y el agua colindante, la cual es menos viscosa.

El estudio está compuesto por dos partes. La primera analiza el comportamiento de un modelo simple de fondo plano en test hidrodinámicos. La segunda se centra en el uso de software CFD (ANSYS Fluent & Tdyn CFD) para simulación numérica. Se investigan diferentes configuraciones de inyección de aire variando combinaciones de flujo de aire y velocidades de arrastre. Las simulaciones por ordenador mostrarán el patrón de la capa de aire y el espesor de la misma, así como su efecto en la resistencia de fricción.

Los experimentos se llevan a cabo con una barcaza de fondo plano para validar los resultados numéricos; el lugar de ensayo es el canal de remolque de la TU-Varna.

Se hace también una estimación de la energía demandada por la inyección de aire con el fin de hacer balance entre la reducción de resistencia y el gasto de aire soplado. Finalmente resulta que una reducción de la resistencia al avance de en torno al 10% es factible.

Table of Contents

Section I

State of The Art

1.1 Objectives

The aim of the work is to investigate the flow around a body in water with injecting air through the surface, as well as its effect on frictional resistance. This is an old idea becoming topical again with the new IMO requirements.

The project is intended to include model tests on a barge-shaped hull model, CFD simulations for comparison and cost-benefit analysis of the method. The experiments are planned to be carried out in the towing tank of the naval architecture department of TU-Varna. The barge model was partially prepared and supported by another earlier project.

The aim of the work is to obtain a drag reduction of around 10% according to results founded out by others previous experiments.

The air lubrication personally captured my attention because there is still a waste knowledge to explore and discover. The best universities and companies are working together to develop such an ambitious progress like the one studied in this thesis.

1.2 Scope

As well as it has mentioned in the abstract, new IMO requirements go after an improvement in the ship efficiency. Currently an optimization of the hull forms, engine and propeller are already studied. The wave and shape resistance can be reduced by optimizing the hull form, but the drag remains proportional to the wetted surface. So, energy saving system like air lubrication and other hi-tech machinery are welcome to attain the goal.

The world economy is moved by ships, that is a fact, so a reduction in the cost of shipping is continuously pursued, the consumption of fuel is only a small advantage in this area, because the main goal is to allow for a more sustainable and clean environment.

It can be remarked that the air lubrication system requires a flat bottom to keep the air below the hull and inside the beam. Containerships, bulk-carriers and oil tankers are a good example of this.

1.3 Phases of the project

The guideline below is the ‘modus operandi’ to get the advance of this project:

a. IMO emissions requirements.
b. Introduction to air lubrication system.
c. Study of literature on air lubrication effects.
d. Cost-benefit analysis.
e. Formulation and settings test of the flat-plate model.
f. Experimental tests with flat-plate models.
g. Introduction to CFD and multi-phase flow method VOF.
h. Introduction to ANSYS Fluent.
i. Introduction to Tdyn CFD.
j. Parametric numerical simulations of air lubrication.
k. Validation between numerical and experimental results.
l. Conclusions.

Basically an introduction to IMO requirements is given, which are precursors of the energy saving pursued and the continuous evolution of different air lubrication systems and researches carried out until now.

The current thesis is part of a long-term study considering that it requires an extensive research involving many tests with the flat-plate model till get coherent results in the towing tank. It is necessary to explain all the details concerning to the experimental set-up and changes in the model test.

Another part of the task focuses in numerical simulations with the flat-plate barge. ANSYS Fluent and Tdyn codes are necessary to reach results in this field. Also it will be studied several turbulence models to use as well as the boundary conditions of the experiment in order to reproduce the experimental results.

Finally, the conclusions will be established according to a comparison between numerical and experimental results. Cost-benefit estimation will take in account as well.

1.4 Introduction

Shipping is vital for global commerce, as it is generally one of the most economical and environmental friendly transportation methods. In addition to the commercial shippers, the world's navies and innumerous cruise lovers need and want, respectively, shipping to be as economical as possible with minimal environmental harm.

Since approximately 60% of a typical ship's propulsive power is required to overcome frictional drag when *Fr* < 0.2 (Fr = U/$\sqrt{gL}$), i.e. for speed ranges usual for merchant ships, any technique that could significantly reduce a ship's frictional resistance might have a substantial impact both economically and environmentally.

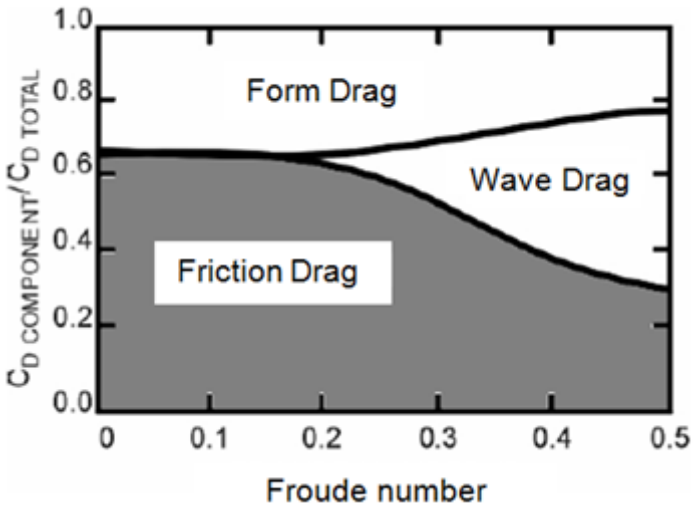

Figure 1.1: Relative share of ship resistance components as a function of Froude number.

Frictional drag stems from the velocity of a fluid on a solid surface being the same as the velocity of the surface due to the no-slip condition. Momentum is transferred from free stream to near-wall-region by structures in the boundary layer and shear. Methods proposed for frictional drag reduction (FDR) are based on reducing the density or viscosity of fluid near the wall (air lubrication) or alter the momentum transport in the boundary layer (air or polymers). Throughout the last two centuries, various methods to reduce the frictional component of drag have been proposed. These include injection of polymers, compliant walls, electromagnetic methods, and various air lubrication techniques.

It will consider only air lubrication in this investigation. A simple test to illustrate how air lubrication works is running a thin but sturdy plate, first through air and then through water, while keeping the widest area on the sides. The resistance is mostly due to frictional drag, and it can immediately observe that the resistance in air is much less than in water. This is because the dynamic viscosity (the natural resistance to flow) and density of air are much less than those of water. In fact, at the same speed the frictional drag for a flat plate is more than 500 times greater in water than air.

So, the air lubrication is achieved pumping air beneath the hull and thus reducing the area of hull in direct contact with the liquid flow, or in the case of discrete bubbles by modification of momentum transport and average density in the boundary layer. Successful application of air lubrication to both existing and new craft would save fuel and reduce exhaust emissions. The challenge is to efficiently deliver the air to the hull and manage its flow for the maximum reduction of friction drag. If properly implemented, the air lubrication has been estimated to lead to fuel saving between 5 and 20%.

These savings of fuel and GHG emissions (NO_x, SO_x, and CO_2 emissions) are promoted by IMO through the Energy Efficiency Design Index (EEDI) which is mandatory for new ships and the Ship Energy Efficiency Management Plan (SEEMP) mandatory for all ships.

The IMO regulations (Chapter 4 of MARPOL Annex VI) are applied to ships of at least 400GT and was implemented on 1 January 2013, however a waiver may be granted to delay implementation of the regulations up to four years for new ships registered in developing countries. The EEDI sets a minimum efficiency standard that new ships must accomplish, but it permits owners to choose which technologies they use to achieve the EEDI standard. The EEDI is based on the ship type and cargo carrying capacity of the ship and the IMO will gradually reduce the permitted maximum EEDI over time. To the interested reader is strongly recommended to review the resolution of “EEDI amendments MEPC.203 (62)”.

The SEEMP aims to improve the energy efficiency of a ship’s operation via various energy management methods, such as increased fuel efficiency and

improved voyage planning. It requires ships to keep a ship-specific energy use and management plan on board. The presence of a SEEMP is verified at intermediate and renewal surveys.

The idea of reducing drag friction by placing a thin layer of air between a ship and its water boundary was patented already in the nineteenth century. In 1883 the inventor Gustav de Laval experimented with releasing compressed air along the girths of numerous sections on the hull of a test boat. He had hoped that a thin layer of air would adhere to the hull. However, air bubbles formed instead and there was no detectable reduction in resistance.

Nowadays this technique is gaining importance in order to protect the environment and overcome IMO requirements among others purposes.

1.5 Physics and methods of Air Lubrication

The friction resistance is mainly affected, because the dynamic viscosity and density of air are much less than those of water. There are three basic methods of air-lubrication and Figure 1.2 shows the conceptual differences between the different techniques that will be discussed after.

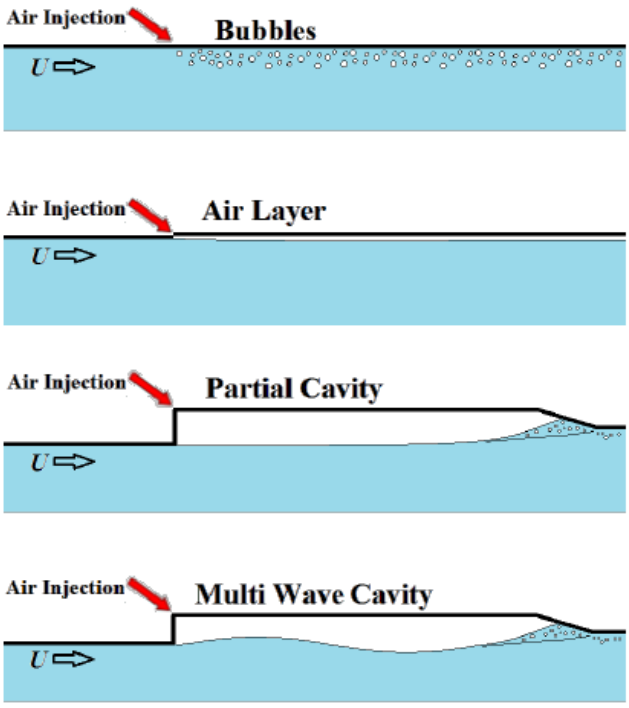

Figure 1.2: Types of air lubrication. It is shown the air pattern layer created according to the Physical mechanisms used.

1.5.1 Bubbles Drag Reduction (BDR)

In Bubble Drag Reduction (BDR) small bubbles are injected into the boundary layer. The dispersed bubbles act to reduce the bulk density and to modify turbulent momentum transport. The technique is sometimes referred to as micro bubble drag reduction, when the bubbles are very small compared to the boundary layer. This technique is subject of many studies and some discuss whether the drag reduction mainly comes from modification of effective viscosity, density change, turbulence modification, or change in momentum transport. However, many of the early and most promising studies were conducted at the laboratory scale and questions remain regarding the technique's suitability to ship scale; how much gas injection is needed, how far downstream from injection site will the bubbles persist, how important is the bubble size, performance in salt water, what is the best injection method, etc.

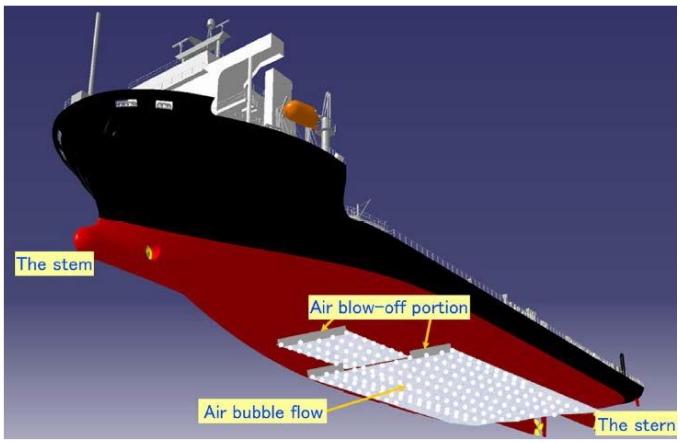

Figure 1.3: Example of bubbles injection system.

1.5.2 Air Layer Drag Reduction (ALDR)

In Air Layer Drag Reduction (ALDR) the gas creates a continuous lubricating layer between hull and water. Surface devices (small backward step for instance) may be used to enforce boundary layer separation upstream of the injection point to aid in the initial formation of the layer. In ALDR, as in BDR, no effort is made to re-circulate the injected gas. Air is injected beneath the hull of a ship, forms a film on the flat (horizontal) part of the hull and reduces the frictional drag on the area covered by over 80%.

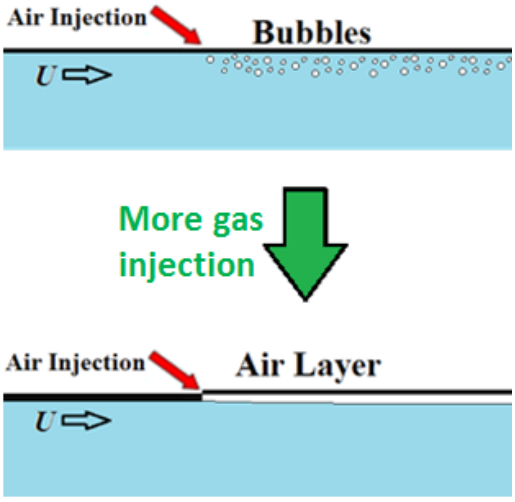

With sufficient gas flux, the injected gas bubbles coalesce into a film. The system employed for BDR could be used for ALDR as well, just increasing air flow supply.

Figure 1.4: Conceptual sketches illustrating ALDR.

1.5.3 Partial Cavity Drag Reduction (PCDR)

In Partial Cavity Drag Reduction (PCDR) the gas creates a lubricating layer between the hull and liquid by filling a recess, much thicker than the ship-hull boundary layer thickness, with gas. To apply PCDR on a ship's hull, the bottom of the hull needs to have indentations, which are to be filled with gas, usually air. A backward-facing step on the upstream end of the recess and a gently downwards sloping closure on the downstream side normally form the recess which traps the gas, thus forming a ventilated partial cavity. Gas is injected continuously into the cavity to make up for that which is lost to entrainment, but with proper cavity design the gas loss is minimized.

The following pictures illustrate an example of air cavity application in vessels:

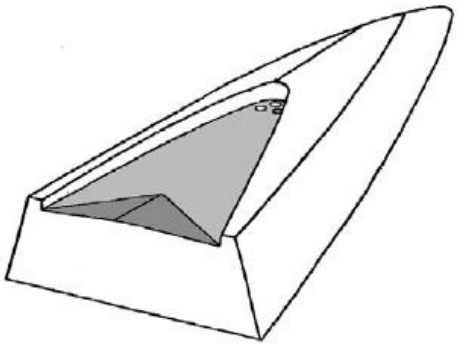

Figure 1.5: Artificial air cavity ship concept.

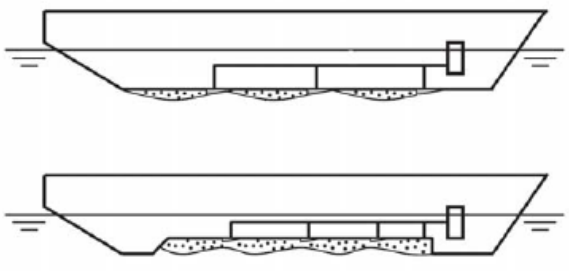

Figure 1.6: Artificial air cavity ship concept for low speed hull forms.

1.6 Current framework of Air Lubrication

Theoretical & experimental investigations and full-scale implementations

Though the idea of air lubrication is an old one (patented in the 19th century), the interest to it related to ships was revived and reinforced in the last decade. There are numerous model test studies, both on flat plates and ship models, including seakeeping aspect, as well as CFD simulations.

More importantly, there are already full-scale implementations of air lubrication systems. So, some of these studies with their observations and conclusions are briefly summarized then in describing the three basic types of air lubrication.

On example of these full-scale implementations is The Mitsubishi Air Lubrication System (MALS) was the first air lubrication system in the world to be applied to a newly built ship, and resulted in a substantial reduction in the ship's resistance. Sea trials confirmed from 8 to 12 % net energy savings depending on the bubble diameter/air layer thickness.

Another system, Stena AirMax PCDR Project is being carried out by the Swedish shipping company Stena Bulk. This model expects energy savings according to results found in tests on a 1:12 prototype. Depending on the type of ship and speed, it is expected energy savings of 20 - 30 %.

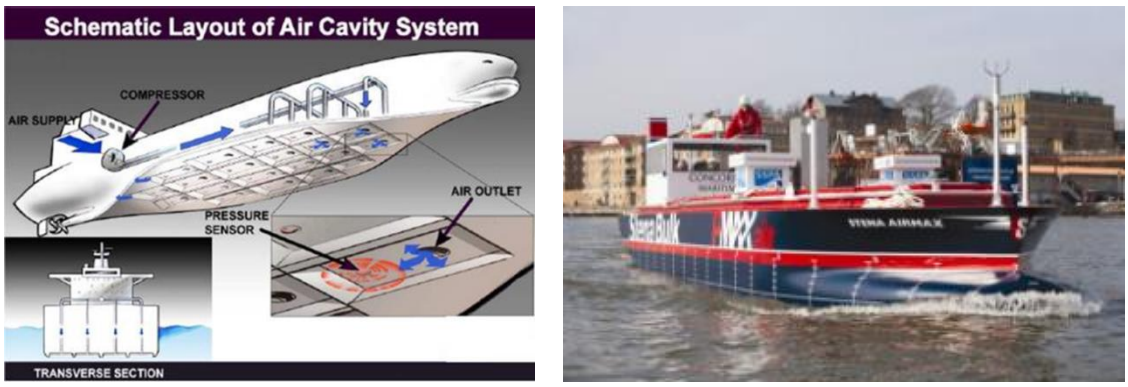

Figure 1.7: Stena AirMax uses the partial cavity drag reduction system. The figure on the right leaves visible the large-scale prototype model (15 m and 25 tons) of the Stena Airmax afloat for the first time.

1.6.1 SMOOTH

Sustainable Methods for Optimal design and Operation of ships with air lubricaTed Hulls

This project [1] was coordinated between 2006 to 2011 by MARIN (Maritime Research Institute Netherlands) organization and Dr. ir. H. Prins.

It speaks of the law of Archimedes. Generally, water or any other fluids are capable to carry bodies such as ships when the integrated pressure forces along the contact surface between body and fluid is equal the weight of the body. It would be possible to be suspected that the boat could sink in the mixture air-water because this mixture is less dense than water, but as long as the air stays under the same pressure than the water, the boat will float with the same draft.

When the boat moves within the water, it is exposed to drag or friction resistance. It is well known that this resistance inside an air ambience is around 2% of the resistance that it would be obtained in water. This involves a large advantage concerning to drag resistance reduction.

The challenge about this project was to supply in an efficient and stable way the air required underneath the ship. The application of this system is difficult, but the physical potential of benefit is high and feasible.

Within 6th frame of the program took place another push to develop and implement this technique in the daily practice of European ships. After three years of research they verify that the potential of an air layer or an air cavity is still free of doubt.

The SMOOTH project investigated the air-lubrication technique of dispersed micro bubbles inside the ship's boundary layer but turned out to be less attractive because just marginal improvements at full scale were found.

The consortium of SMOOTH (Table 1.1) consisted of leading European research institutes and industrial partners from seven different European countries, each of them with unique skills, either as knowledge providers, top hydrodynamic labs and universities, end-users or air-system and maritime paint suppliers, to contribute to the successful implementation of air-lubricated ships.

P001	MARIN – NL	P006	Atlas Copco – NL
P002	Akzo Nobel International Paint – GB	P007	New Logistics – DE
P003	Bureau Veritas – FR	P008	SSPA – SE
P004	Damen Shipyards – NL	P009	DST – DE
P005	Istanbul Technical University – TR	P010	TK Veerhaven – NL (management by DLD – NL)
P011	Imtech – NL		Steering Committee – EU

Table 1.1: A list of partners included in the SMOOTH project.

Furthermore, another project parallel to SMOOTH was PELS; a Dutch national project that esteems a feasible 20% of improvement in the efficiency. The main goal of SMOOTH was to cover all aspects of air-lubricated ships, such as in particular scale effects and to assess the technique in a way that a technology transfer of air-lubrication into daily European shipbuilding and operation practice of both inland and coastal navigating ships is enabled.

Program SMOOTH persecutes a reduction of 15% in the power consumption by means of reduction of the friction resistance thanks to the technique of air lubrication. This would release around 1.2 million tons of CO_2 to the atmosphere. Moreover, ship safety can be improved significantly compared to traditional vessels without air lubrication. Better maneuverability and performance due to frictional resistance in ships can be obtained by locally switching on and off the air-lubrication.

1.6.2 PELS

Project Energy-saving air-Lubricated Ships

This project indicated that an improvement of until 20% in the efficiency of the ship can be feasible; there is not another technique nowadays that augurs such saving. It entails a reduction of the propulsion power to install, the fuel consumption and CO_2 emissions.

This project involved scientific researches worth 1,2 million € intended largely to model building and testing at the research institute MARIN. The three proved techniques were:

1. Air cavity ships.
2. Micro Bubble Drag Reduction.
3. Air-film, generated by air injection onto a super water-repellent coated ship.

The ship efficiency is not limited by the own energetic efficiency but also other aspects should be studied. The stability of the air lubrication during navigation with waves and maneuvering was included here. The seakeeping and safety are influenced by the shapes of ships and air lubrication demands a certain form in order to be effective. The following tests were performed to study all operating conditions and determine the drag reduction:

1. Seakeeping tests, in head, bow- and stern quartering, beam and stern seas.
2. Maneuverability test.
3. Resistance and propulsion tests in the depressurized towing tank, with a correctly scaled down compressibility of the air.

To determine the important issue of possible scale effects, two scale models were made for the tests with different scale ratios. One of these models was divided in ten separate segments to allow for the determination of the distribution of the hydrodynamic forces along the length of the ship. The bottom of each segment was adapted to incorporate the micro-bubble lubrication and the air cavities either way.

In order to experimentally assess the performance of the air lubrication and to investigate the scale effects on air lubrication, two different wooden models were manufactured: a model with a length between perpendiculars L_{pp} of 6 m (scale 1:20) and a second model, larger and geometrically similar (GeoSim) with an L_{pp} of 11.51 m (scale 1:10.4). The main characteristics of the hull form are detailed below:

- A large parallel midship section to maximize the possibilities for air lubrication by either micro-bubbles or air-cavities.
- Small bilge radius to maximize the width of the air cavities.
- Propulsion by twin thrusters in order to be able to position the propellers outside the flow of the air/water mixture.
- A pram-type aft ship to also allow some lubrication at the stern and to facilitate the thrusters.
- A simple stream-lined bow.
- For practical purposes, the model should be easily modified from air-cavities to micro bubble lubrication and vice-versa.

These requirements led to the following hull form. In order to keep air inside cavities, the bottom was built with panels which flush closed the cambers.

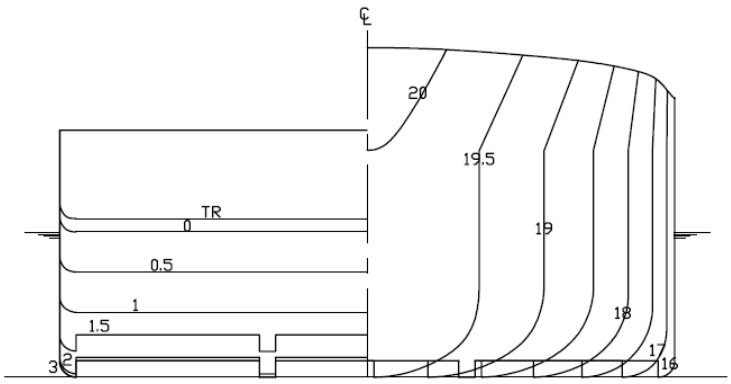

Figure 1.8: Body plan of ship model with air cavities.

Thereafter air lubrication system was described, in every case was used nitrogen stored in bottles. The reason for this was to avoid any fouling during the tests of the porous metal by oxidation. The nitrogen gas was stored under high pressure in cylinders with reduction valves, reducing the pressure in the gas tubes to about 5 bars. The gas was led through mass flow controllers which

were able to control the volume flow of the gas. Several different flow controllers were used to control the air flow to the porous strips.

Air cavities, Micro-Bubbles and Air Film systems are described below. For *air cavities* the length chambers is roughly estimated based on the speed by Matveev's equation (Eq. 1.1).

$$L_{Cavity} = 0.34 \cdot \frac{S^2}{m} \cdot V_s^2 \qquad \text{Eq. (1.1)}$$

The cavities can only cover horizontal or more or less horizontal because in vertical surfaces disappears rapidly due to gravity effects, also inside the cavities an additional wave resistance is generated so the theoretical maximum drag reduction is lower.

In relation with *air film*, the systems involved air injection with a super water repellent (SWR) coating. So, basically the system is the same that *air cavities* or *micro-bubbles* with the difference about the bottom coating.

In the Figure 1.9 and 1.10 are showed two different air lubrication systems, micro bubbles and air cavities respectively:

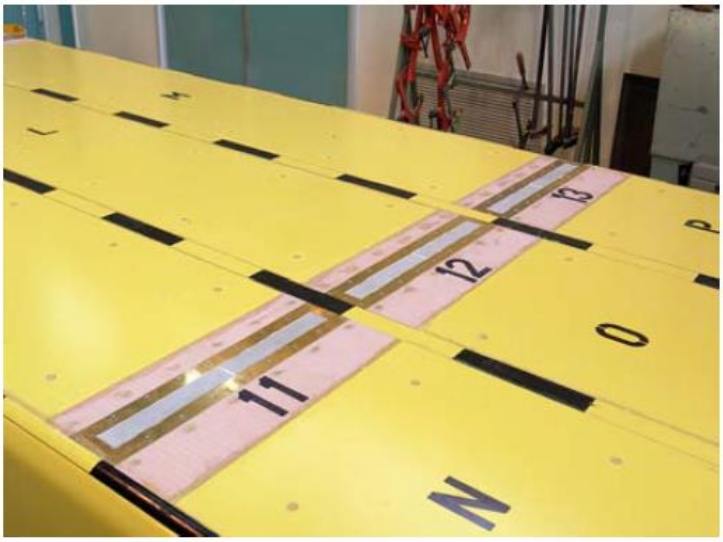

Figure 1.9: Bottom configuration for micro bubbles where porous strips were placed to allow air bubble flow.

To prevent the water flowing in between the segments, small flexible latex strips were mounted between the segments. Figure 1.10 shows the segmented model during preparations. Figure 1.11 presents the ship model fully prepared for the tests.

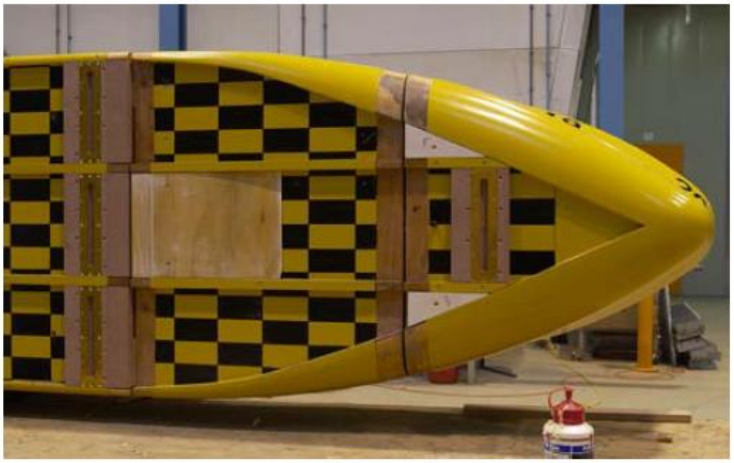

Figure 1.10: Detail of bottom configuration of segmented ship model during preparations.

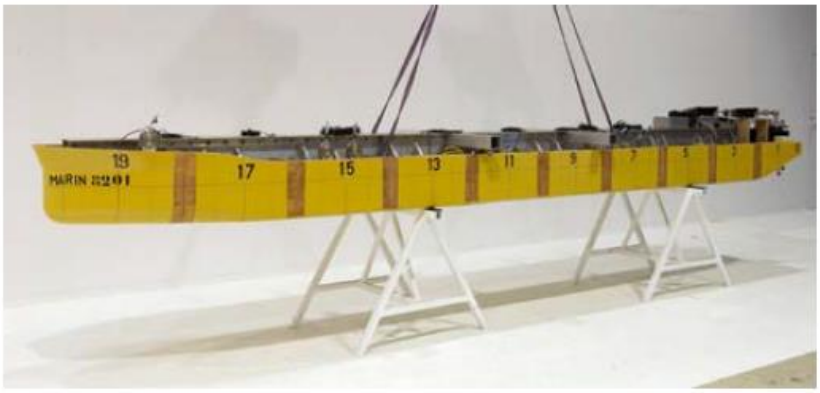

Figure 1.11: Segmented ship model ready for testing.

Tests were performed with the segmented model for the condition without air lubrication, with air chambers and with air bubbles, in regular and irregular waves, at two speeds in wave directions ranging from bow to stern quartering.

The purpose of the tests was to establish whether the air lubrication remained effective in waves, if lost air quantities would appear in the propeller disk area to disturb the propeller efficiency and loading and to which extend the ship motions would be affected by air lubrication. Figure 1.12 shows the model during a run in waves.

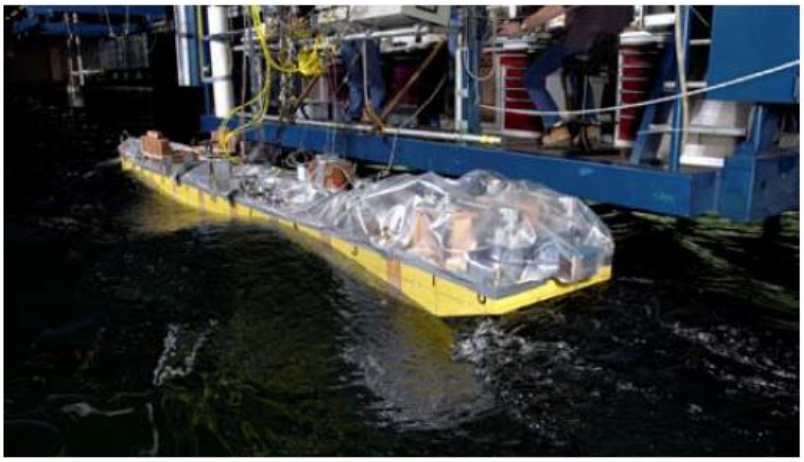

Figure 1.12: Model testing in waves.

In general terms the results of the tests were as follows:

- Ship motions appeared not to be significantly affected by air lubrication. An exception was found in beam seas for which the model with air chambers showed significantly roll due to the change in transversal stability.
- Although power savings reduce when operating in waves, for most conditions with air bubbles power reductions remain possible, while for some low speed conditions with air chambers more power is required with air lubrication than without air lubrication.
- The model with air chambers showed substantial loss of air volume due to ship motions and waves at the lower speeds and substantial quantities of air occasionally arrived in the propeller operating area causing thrust and torque variations.

After experimental test, results had to be validated with computational models. A computational method was required that combines traditional ship hydrodynamics with a description of air chamber flows. The PANSHIP time domain panel code was used to carry out the numerical experimentation.

More information about PANSHIP code can be obtained in ref [2]. The cushion pressure was described through mass conservation equation, also the air supply system with a single fan, as well as the air leakage underneath the air chamber sides when there is a gap.

To validate the motion in waves during experimental phase, the results were compared with the numerical computed by PANSHIP.

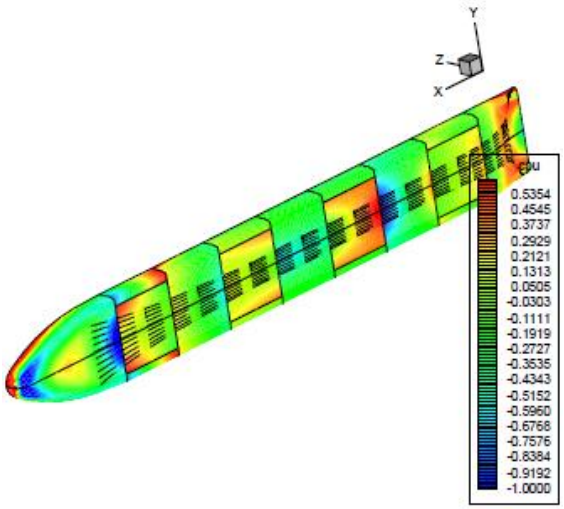

Figure 1.13: Pressure and streamlines on vessel with 6 air chambers.

Figure above shows a pressure and streamline plot for a certain point in time during a simulation in head waves. Discontinuities in dynamic pressure are observed around the air chambers where the air flow either starts or stops.

So finally, investigations agreed that seakeeping characteristics of the ship studied were not significantly affected by the use of either bubbles or air chambers for air lubrication. Power savings were intact with lubrication by means of air bubbles but may become negative when using air chambers at a relatively low speed. Also the leakage of air form chambers may affect the propeller. Predictions for the motions in waves agree well with experimental data.

The last aspect to keep in mind about air lubrication systems is maneuvering characteristics, so for that tests were also carried out including free sailing tests consisted of standard zig-zag and combined turning circle experiments (see Figure 1.14).

The turning ability for all three configurations was found to be good, but the directional stability was poor, due to insufficient damping. In this respect, the best results were found with air cavities.

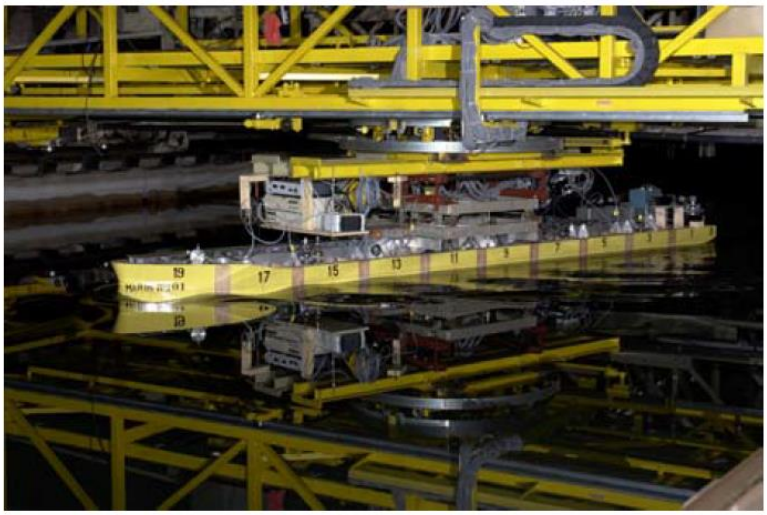

Figure 1.14: Maneuvering test.

Anyway, the effectiveness of air lubrication while maneuvering depends highly on the encountered drift angles. For large drift angles, the air will disappear from the chamber.

After the three techniques were tested the important overall conclusions from the investigations of PELS are:

- A net effective power reduction of 3-10% in calm water.
- In increasing wave heights an increasing part of this advantage is lost, anyway the system does not cause an increase in added resistance or otherwise deterioration of seakeeping at normal operating speeds.
- The application of drag reduction imposes some changes in the design of the ship, specially the bottom of the hull.
- No severe scale effects were found, which is really good.

It should be taken in mind that the model used in the PELS project resembles just a fictitious ship-like body, it is expected that the advantage mentioned above can be overcome with dedicated design strategies. At this point CFD tools will have an important role in optimizing the shape of an air cavity by computing the wavy free surface inside of it.

1.6.3 MALS

Experimental Study of ALM and Verification of Effects on Actual Hull by Means of Sea Trial

Mitsubishi Air Lubrication System [3] was the world's first trial carried out on a newly-built carrier. Prior to the experiment in an actual hull trial, in order to confirm the performance of the air delivery system, a full-size mock-up unit was fabricated and the air delivery conditions were observed in a water tank.

In an actual hull trial, a real energy-saving effect was confirmed as estimated and the effectiveness of this method was validated. Mitsubishi Heavy Industries, Ltd. (MHI) hereafter developed this technology toward general carriers such as VLCCs and bulk carriers.

This system consisted of sending air on the bottom of low speed vessels, so a layer of air bubbles is created between the hull and sea water. This applied technology to general carriers such as VLCCs and bulk carriers, brings successful advances for it.

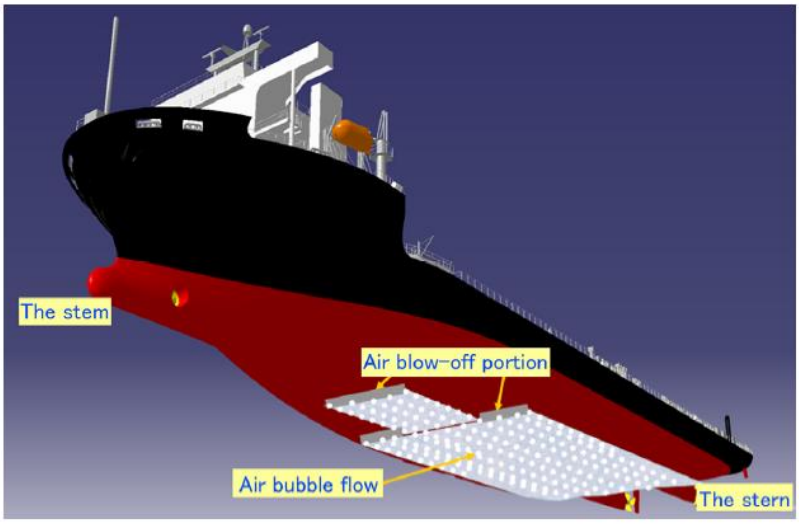

Figure 1.15: Air lubrication method.

Figure 1.15 shows the performance of the system. Air discharged from the air blow-off portion mounted on the bottom turns into air bubbles because of the tearing-off forces of the surrounding flows and the air bubble flow covers the bottom of the hull.

A full size mock was built was built before trials in a real ship. It was measured total and local skin-friction resistance working on that flat plate hull which had a total length of fifty meters, and confirmed a resistance decrease.

After experiments with the model, the system was observed on a real ship, concretely a cement carrier with characteristics showed in table 1.2 and its hull form showed in Figure 1.16. The main feature of the carrier is a wide and shallow draft with a large B/d, so that it has a large flat area in the bottom.

Carrier length	Loa	162 m
Carrier width	B	38 m
Depth	D	9.0 m
Draft	d	4.5 m / 6.37 m
Displacement	△	10,201 t / 19,818 t
Main engine	-	DAIHATSU 6DKM-36×2 Max.3,218 kW×2
Propeller	-	CPP
Designed speed	U	13.25 kt

Table 1.2: Specifications of the carrier tested.

The main engine is a medium-speed diesel engine and the propulsion plant has two engines and two shafts with a Controllable Pitch Propeller (CPP).

In order to cover the bottom of the carrier with air bubbles, three air blow-off portions are installed on the bottom and the air is supplied by two sets of air blowers that are placed in the auxiliary engine room.

Figure 1.16: Mitsubishi air lubrication system.

Prior to sea trials, the ship was moored on a wharf wall and the system was launched by running blowers and then the air blow-off conditions from the apertures in the bottom were photographed by a diver to observe them. Air flow from fifteen branch pipes was also examined; a sketch of the supply system is shown at Figure 1.17.

The curiosity of this experiment was the way how air flow rate was measure. The hull was not equipped with flow meters on the branch pipe

between the butterfly valve and the camber, so flow rate was estimated from the measured pressure instead.

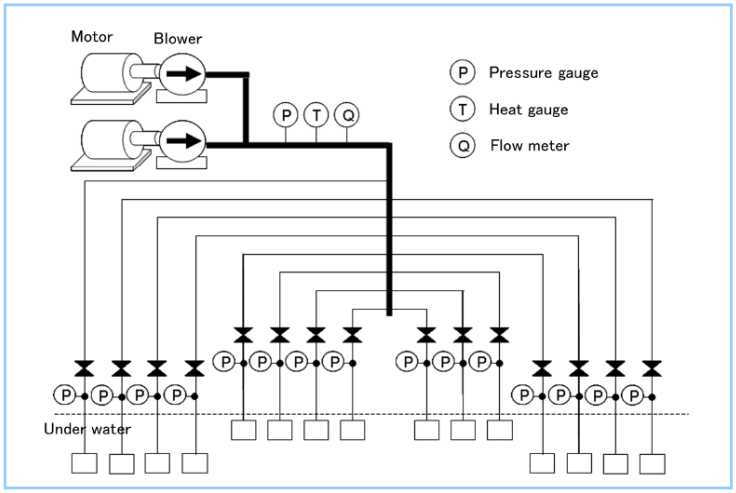

Figure 1.17: Air blow-off conditions of actual hull experiment.

Coming back to the actual hull experiment at sea, air blow-off conditions under sail were photographed by a bottom camera to observe them. Figure 1.18 shows that air from the apertures turns into air bubbles, running backward.

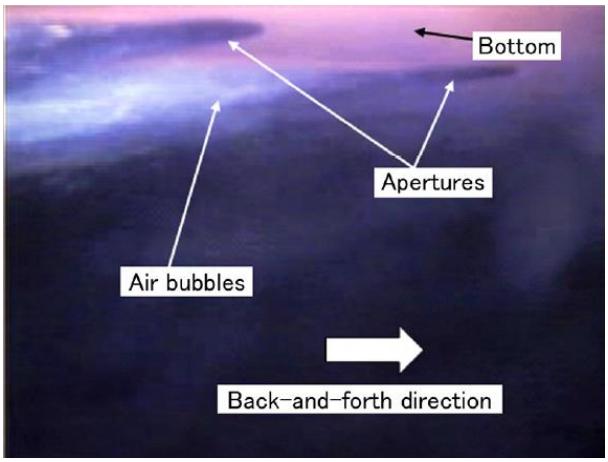

Figure 1.18: Air blow-off conditions of actual hull experiment.

After a normal speed trial test without discharging air, the same speed trial test with air discharged was carried out to measure the energy-saving effect. The speed was compensated by wind and tidal correction and the horsepower of the main engine is calculated from the readings of a load indicator. In a test run, a torsion meter was temporarily installed to simultaneously measure shaft horsepower. Valve openings during the test were restricted based on the results of the wharf wall test.

The speed trial test was carried out varying air blow-off rate in three cases. The air supply rate was calculated, with the equivalent air thickness that is defined in equation (1) taken as 3, 5 and 7 mm, where t_b is the equivalent air thickness at the bottom of the carrier, Q_a is the air supply rate, B_a is the width covered by air bubbles and U is the ship speed.

$$t_b = \frac{\mathrm{Qa}}{\mathrm{Ba} \cdot U} \qquad \text{Eq. (1.2)}$$

The results are summarized in Table 1.3. According to the relationship between speed and horsepower in the speed trial test run, the horsepower appeared to decrease at the time of air blow-off navigation and the speed appeared to increase. So with the increase of air thickness the net energy-saving effect was confirmed.

	Horsepower reduction	Blower electric power consumption	Net energy-saving effect
7 mm	680 kW	211 kW	469 kW (12%)
5 mm	530 kW	143 kW	387 kW (10%)
3 mm	380 kW	72 kW	308 kW (8%)

Table 1.3: A comparison of the energy-saving effects from several tests as a function of different air-layers thickness.

Finally, they were able to confirm a net energy-saving effect of a maximum of 12 percent in a sea trial through the use of an actual carrier. The skin friction resistance of the carrier decreased through the use of an air lubrication method, which is thought to act to decrease the load of the propeller. The carrier was equipped with CPP, so that further improvements in efficiency can be anticipated byre-adjusting the pitch angle of the propellers. After this result they developed a full scale system on a second vessel.

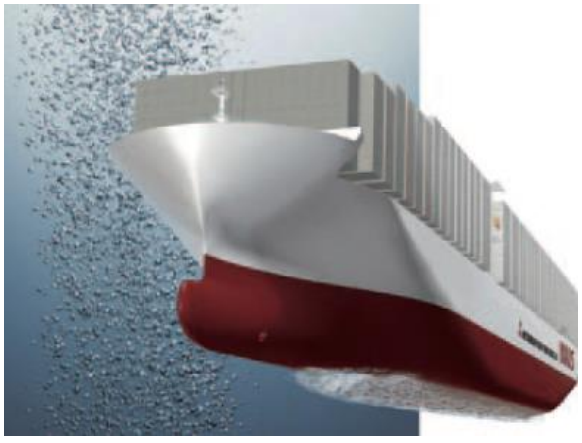

Figure 1.19: MALS adopted for new panama class containership.

1.6.4 CFD predictions of MALS

CFD predictions of Bubbly Flow around an Energy-saving Ship with MALS

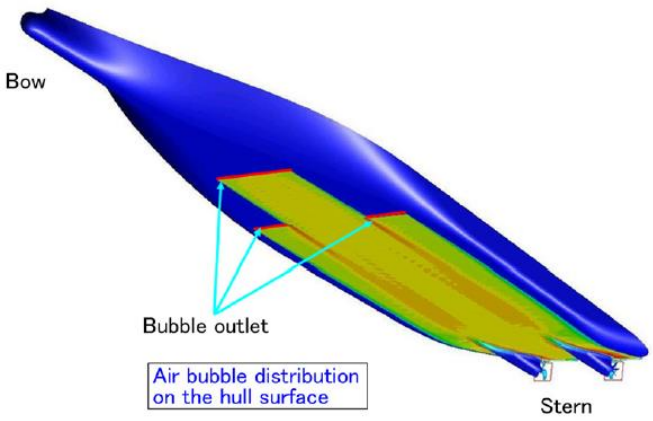

Figure 1.20: Sketch of MALS.

As have been shown in previous section, the Mitsubishi Air Lubrication System (MALS) was the first air lubrication system in the world to be applied to a newly built ship, and resulted in a substantial reduction in the resistance of the ship. In addition, other aspects were studied and established to apply the MALS to general commercial ships.

In this study [4] was predicted the bubble distribution around ships using CFD, the bubble coverage around the hull and the intrusion of bubbles on the area of propeller disks, which could deteriorate the performance of the hull.

The author simulated the flow around the cement carrier (Table 1.2) used for experiments, and evaluated the effects of changes in the ship posture and location of the bubble outlets on the resistance reduction ratio for the ship and the void fraction on the propeller disk area. The Nagasaki Shipyard & Machinery Works of Mitsubishi Heavy Industries, Ltd., (MHI) completed YAMATAI (figure 1.16), a module carrier belonging to the NYK-Hinode Line, Ltd., in April 2010. An air lubrication system was installed on a ship for the first time on this occasion. The ship achieved an energy-saving effect of more than 10% at sea trials prior to delivery.

Predictions utilizing CFD technology were made at the time they were installing the MALS on the cement carrier YAMATAI. Also additional test on model and actual ship were carried out. They used CFD with the same model-

scale ship to predict the distribution of the air bubble void fraction on the hull surface, which is required to predict the reduction of the hull resistance, as well as the distribution of the void fraction on the propeller area, which affects the propeller performance. Here, the void fraction is the ratio of the air volume to the air–fluid mixture.

Ship specifications belong to the cement carrier studied before in sea trials, is called YAMATAI (see table 1.2 and Figure 1.16). The ship was a twin-screw vessel characterized by its wide breadth and shallow draft. The calculation results reported are based on navigation in a straight line without considering waves on a free surface. As well all of the air bubbles were assumed to be of a uniform diameter and remain unchanged by the flow. No consideration was given to bonding of bubbles or division of a bubble into multiple bubbles. The bubble diameters are indicated in the following table.

Bubble outlets were created at three locations along the bottom of the hull, symmetrically on both sides of the centerline, as shown in the sketch of the top below the title.

	Model Ship (mm)	Actual Ship (mm)
Case 1	0.1	2.77
Case 2	0.5	13.8
Case 3	1.0	27.7

Table 1.4: Air bubble dimensions.

It is noticeable that a huge range of bubble diameter was employed to provide an approximate indication of its effect.

The calculations indicated that the influence of the air bubble diameter on air bubble distribution was limited. Therefore, the air bubble diameters can vary, the bubble effect can be roughly predicted from calculations based on bubbles with a particular uniform size.

Figure 1.21 shows the trends between predictions (picture on the left) and the experiments (picture on the right). Air bubbles flowed along the hull without escaping from the bottom of the ship and a smaller amount of them were distributed in the area near the hull centerline.

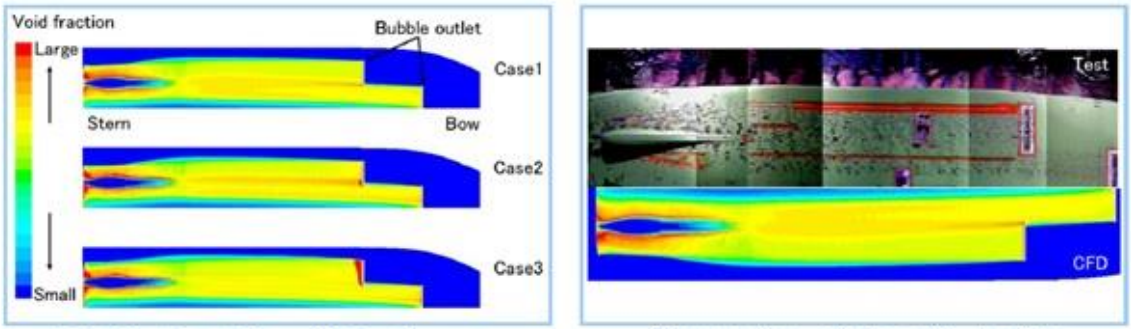

Distribution of the void fraction on the hull surface
The port side of the bottom of the ship as viewed from below. The contours indicate the void fraction.

Comparison of the void fraction distribution
Top: Experimental model test results
Bottom: CFD results

Figure 1.21: Comparison between void fraction predicted and simulated

They confirmed the loss of propulsive efficiency due to air bubbles was negligible because the air bubbles flowed along the ship bottom toward the area above the propeller. That is a good point because may cause vibration and noise on the propellers. Likewise changes in the bubble diameter vary the air bubble distribution on the ship bottom surface. This conclusion was led by qualitatively similar results of the air bubble distribution predicted by CFD and obtained experimentally.

However, the resistance reduction mechanism of the air lubrication method was not thoroughly examined, including the causes and effects of changes in fluid density and the turbulence modulation effects of air bubbles inside the boundary layer. CFD will play an important role in determining these causes by providing a detailed understanding of the physical phenomena.

1.7 Methodology for energy cost-benefit analysis

The air-lubrication is an “active” method of drag reduction, i.e. energy has to be spent on air supply, and it has to be accounted for in calculating the net energy savings.

A methodology for cost-benefit analysis is proposed in [5] that has been adapted here and will be briefly presented and applied to a sample real ship in the next chapter. The methodology concerns ALDR (Air Layer Drag Reduction) and PCDR (Partial Cavity Drag Reduction) since the mechanism and relationships of bubble lubrication are not completely clarified yet.

The basic assumptions are that air lubrication reduces the frictional drag on the area covered and the form drag is not considerably affected by the air supply or the air injector, strakes or other appendage needed to achieve air lubrication.

The possible percentage net energy savings, $\%E_{SAVED}$, can be estimated by considering the ratio of net energy savings to the total energy consumption: both for propulsion (hopefully reduced) and the energy needed for air injection.

$$\frac{\%E_{SAVED}}{100} \cong \frac{\Delta t.P_{SAVED}}{\Delta t.\frac{P_B}{\eta_D}}, \qquad \text{Eq. (1.3)}$$

where P_{SAVED} is the net power savings, P_B the brake power and η_D the propulsive efficiency.

The net energy savings can be estimated by considering the reduction in power required to overcome frictional drag and the power required to supply the gas:

$$P_{SAVED} = \frac{P_B f_{FD}}{\eta_D}\frac{A_{AC}}{A_{WET}}\left(\frac{\%D_R}{100}\right) - \frac{P_{COMP}}{\eta_{ELECT}}, \qquad \text{Eq. (1.4)}$$

where $\%D_R$ is the percentage frictional drag reduction on the air covered area, f_{FD} is the fraction of total drag due to friction, A_{AC} area covered by air, A_{WET} total wetted hull area, P_{COMP} is the power required to run the compressor or

blower, and η_{ELECT} is the efficiency of producing electricity for compressor relative to the efficiency of providing power to the shaft.

From basic thermodynamic principles the power needed to compress a given mass flow rate of gas via a polytrophic process (*i.e.* process where PV^n= constant) is given by:

$$P_{COMP} = \frac{\dot{m}_g p_1 n}{\eta_C \rho_{g,1}(n-1)} \left(\left[\frac{p_2}{p_1} \right]^{(n-1)/n} - 1 \right), \qquad \text{Eq. (1.5)}$$

For an isentropic process the exponent *n* (also called index or polytrophic index) can be replaced by *k*, the ratio of specific heats, which is 1.40 for air. $\dot{m}_g$ is the mass flow rate of gas, p_1 is the initial pressure, assumed to be 1 atm, p_2 is the pressure to which the gas needs to be compressed, which depends on the pressure beneath the hull determined by draft and piping losses, $\rho_{g,1}$ is the density of the gas to be compressed and η_C is the compressor efficiency.

The mass flow rate needed is related to the volume flow rate, *Q*, required at pressure below the hull, and assuming that the gas is cooled to 25°C after compression it can be expressed as:

$$\dot{m}_g = Q \frac{\rho_{g,1} p_3}{p_1}, \qquad \text{Eq. (1.6)}$$

For a slow moving ship the pressure under the hull is assumed to be equal to the hydrostatic pressure at the draft depth, $p3 = \rho_W.g.D$, where *D* is the ship's draft. The pressure $p_2 = p_3 + \Delta p_{los}$. In the above equation, *Q* is the volume flow rate of gas required to achieve ALDR or PCDR at pressure p_2 and it can be estimated by curve fitting the data provided by [6].

The curve fit for volumetric air flow rate per unit span, Q/W, for ALDR on a rough surface is:

$$Q \,/\, W = 0.00126U\text{^}2 - 0.00755U + 0.0391, \qquad \text{Eq. (1.7)}$$

being W the span (width) of the air-lubricated area and U the flow velocity.

The same reference gives curve-fits also for ALDR on a smooth surface and for PCDR, which are not presented here, because in the example to follow ALDR on a rough surface will be considered.

1.8 Example of cost-benefit calculations on a real ship

An objective of this thesis is to make the cost-benefit analysis using real data as much as possible. So, as no data of an own actual experiment, It is presented here an example given by the authors of reference [5].

They made some calculations for a ship navigating in the Great Lakes (inland navigation), but though it is a concrete ship, they estimated approximately much of the input data. A self-propelled river-going ship is analyzed, for which existing model test results for deep water are available.

Ships of this type are especially suitable for air lubrication because they have relatively large flat bottom; small draft, hence lower hydrostatic pressure to overcome and no navigation in waves, so, they maintain the air layer.

The main particulars of the investigated ship are given in Table 1.5, the resistance prediction from model test results in Table 1.6, the propulsive factors in Table 1.7 and the particulars of the final designed propeller in Table 1.8.

Length b/w perpendiculars	LPP, m	111,5
Length on waterline	LWL, m	112,79
Breadth	B, m	15,2
Draft	T, m	3,2
Displacement volume	DISV, m^3	4670
Block coefficient	CB	0,859
Prismatic coefficient	CP	0,865
Midship section coefficient	CM	0,993
Waterplane are coefficient	CWP	0,913
Longitudinal centre of buoyancy	LCB, m	0,19
Wetted area	S, m^2	2131,2
Area of appendages	Aapp, m^2	123,6

Table 1.5: Main particulars of the studied ship.

Vs, kn	w	t	ETAR
8,0	0,334	0,240	1
8,5	0,329	0,240	1
9,0	0,324	0,239	1
9,5	0,320	0,238	1
10,0	0,315	0,237	1
10,5	0,313	0,235	1
11,0	0,310	0,233	1
11,5	0,312	0,229	1
12,0	0,314	0,224	1

Table 1.7: Propulsive factors.

Vs, kn	Fn	CR.10^3	CFS.10^3	CTS.10^3	RTS, kN	EHP, kW
8,0	0,124	0,485	1,727	3,262	60,4	249
8,5	0,131	0,532	1,713	3,295	68,9	301
9,0	0,139	0,589	1,700	3,339	78,3	362
9,5	0,147	0,653	1,688	3,391	88,6	433
10,0	0,155	0,722	1,677	3,449	100	514
10,5	0,162	0,791	1,666	3,508	111,9	605
11,0	0,17	0,889	1,656	3,595	125,9	713
11,5	0,178	1,009	1,647	3,706	141,9	839
12,0	0,186	1,155	1,638	3,843	160,2	989

Table 1.6: Resistance prediction from model tests.

D	2.1
P/D	0.725
Ae/Ao	0.644
Z	5

Table 1.8: Final propeller data.

The following input data and assumptions were accepted:

- The bottom area covered by air layer is selected to be A_{AC} = 660 m^2, considering the bottom waterline area as shown in Figure 1.22.

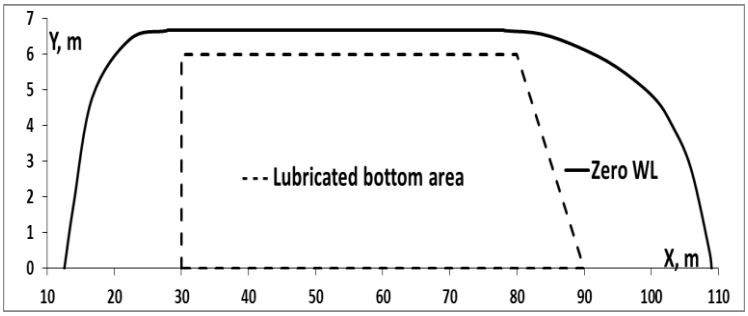

Figure 1.22: Air covered area on the bottom waterline.

- The fraction of frictional drag of total resistance, f_{FD}, was calculated for each speed from the experimental data in Table 1.9. It varied from 0.69 for the lowest speed to 0.57 for the highest tested.
- The percentage frictional drag reduction on the air covered area, $\%D_R$, was assumed as 80%, which was the lower bound based on [7].
- The propulsive efficiency, η_D, was calculated for the specific ship on the basis of data in Table 1.6.
- Efficiency of the generator providing electricity was assumed to be low, 90%.

- The compressor efficiency was assumed conservatively to be 60%, though according to manufacturers it is close to 70%.
- Pressure drop due to piping losses depends on the specific ship dimensions, structure and air lubrication system design. On the bases of reference data, it was assumed to be 1.5 atm.
- For ALDR the air layer is assumed to persist indefinitely once formed.

Vs, kn	PB, kW	f_{FD}	Q, m^3/s	Mass flow rate, kg/s	Pcomp, kW	Esave, %
8	460	0,698	0,352	1,381E-01	14,3	14,5%
9	680	0,674	0,374	1,464E-01	15,1	14,5%
10	964	0,646	0,403	1,580E-01	16,3	14,1%
11	1360	0,614	0,441	1,726E-01	17,8	13,6%
12	1900	0,569	0,486	1,904E-01	19,7	12,7%

Table 1.9: Net energy savings calculations.

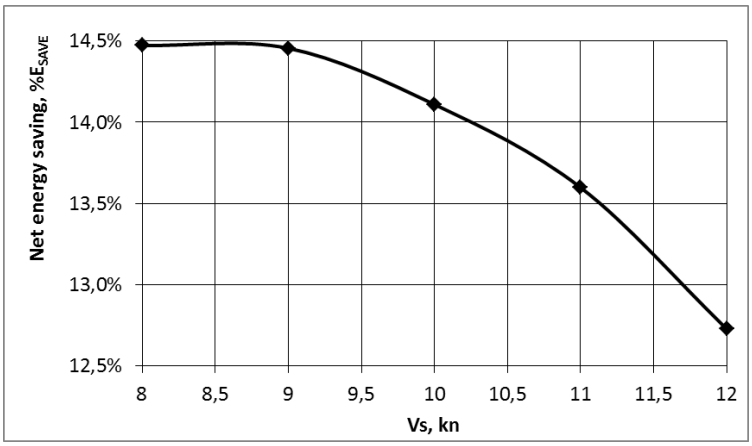

Figure 1.23: Net energy savings by air lubrication.

The basic results of the analysis for cost-benefit are summarized in Table 1.9 and in Figure 1.23.

Assuming that the propulsive factors do not change with layer lubrication the resistance reduction was deduced from the energy savings and the speed power curves compared using the Wageningen B-series propeller data. This resulted in a velocity increase of 0.5 kn as shown in Figure 1.24.

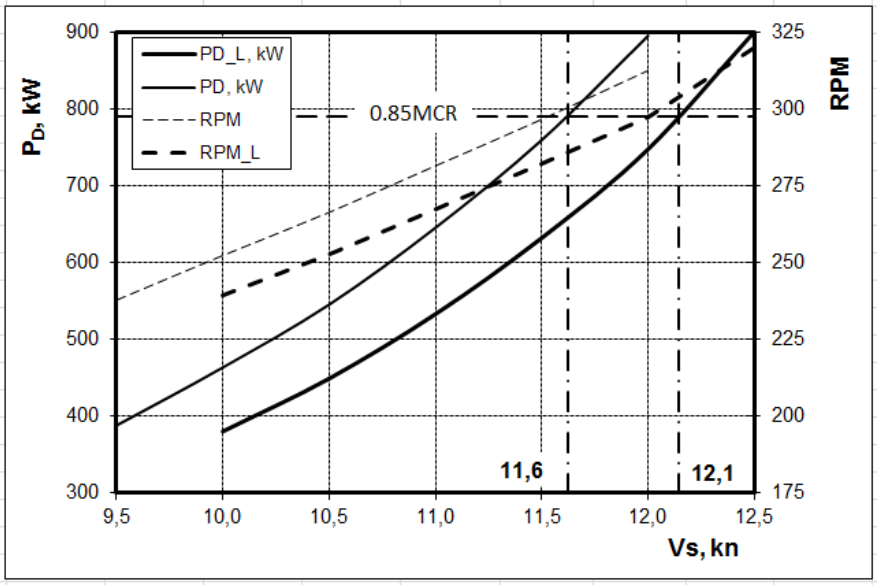

Figure 1.24: Speed-power curves for ship with and without air lubrication. It can be seen that both curves (rpm and maximum power) are below the original in the case of lubrication air (RPM_L and PD_L).

These results obviously cannot be claimed to be the ultimate truth. Many assumptions were made, the effect on the propulsive factors and on potential air entrainment in the propeller disk were ignored, some of the data used are based on model experiments and the scale effects not taken into account.

This example with a specific inland navigation ship is not the intent to make a definite quantitative statement, but rather to show qualitatively the trends of the energy economics of air lubrication. It has been proved that a considerable energy saving is feasible leading to about 0.5 kn speed increase at the same power.

Considering a possible analysis of the cost-benefit with Partial Cavity Drag Reduction system, it is noteworthy that PCDR requires more modifications to the bottom of the hull than BDR or ALDR, but could potentially offer larger frictional drag reduction with a lesser gas flux. Hence, the capital cost would probably be higher than for ALDR, but the operating cost may be lower. The tradeoff between upfront cost and operating cost will be a ship specific consideration. Also, air layers probably offer a more flexibility in the operating speed range, while PCDR may be significantly more economical for a narrow operating speed range(s). Hence the suitability of each of these techniques for a given ship or barge is also affected by the intended use of the vessel.

Furthermore, for complete assessment of the method an economic cost-benefit analysis should also be made, so that the owner/operator would know the break-even point when applying it.

The following should be taken into account in the economic cost-benefit analysis:

- The initial investment for installing the system.
- The annuity of the initial cost.
- The annual fuel savings.
- The maintenance costs and overheads.

The shipping professionals are best capable of making these estimates for a specific ship.

Section II

Model Experiments

2.1 Plan of experimentation

In this second part of the project is carried out the experimentation. It was tried to reproduce the results obtained by the previous investigations. The tests were conducted carefully and with rigor within the resources and means available. The tests were performed in the educational towing tank of the Technical University of Varna with a simple, barge shaped hull.

It is noteworthy that the flat bottom barge of these tests was developed in a previous project by another college student. That project involved the construction of the model but it was never tested in a towing tank and the construction of the barge took place two years before this thesis.

The experiment consisted of towing the barge model. First without air injection and later with a certain amount of air pressure which was supplied by an air pump through the bottom holes.

The tests covered a range of model speeds with varying air flow rate. Resistance and air flow rate were measured and registered and the air spread pattern was observed and video recorded during the runs through the transparent bottom of the model.

Also the initial model was elongated in order to increase the wetted surface. In this way the air covered a large surface and the effects were more noticeable.

The main parts of the experimentation can be summarized as:

1. Preparation the experimental set-up.
2. Carry out the tests.
3. Make visual & quantitative records.
4. Elongation of the ship model.
5. Make new visual & quantitative records.
6. Elaboration spreadsheets and graphs with results.

2.2 Preparation the experimental set-up

The towing tank of TU-Varna was unused for a long time, so it needed rehabilitation and calibration of the instrumentation before testing the flat bottom barge. It is a small towing tank intended for educational purposes with a towing carriage and computer operated system for carriage control, data acquisition and wireless transmission and processing.

Towing and measurement equipment of the channel was developed by a former college professor who worked for TU-Varna and BSHC (Bulgarian Ship Hydrodynamic Center). It was necessary to perform preliminary towing tests without any measurement to find the parameters required by the main system for making good results reading.

It is important to note that carriage could not select a specific velocity so the measure was taken just increasing the speed in every test and reading the exact speed indicated by the system. This means that speed increments were not constant but this had no importance.

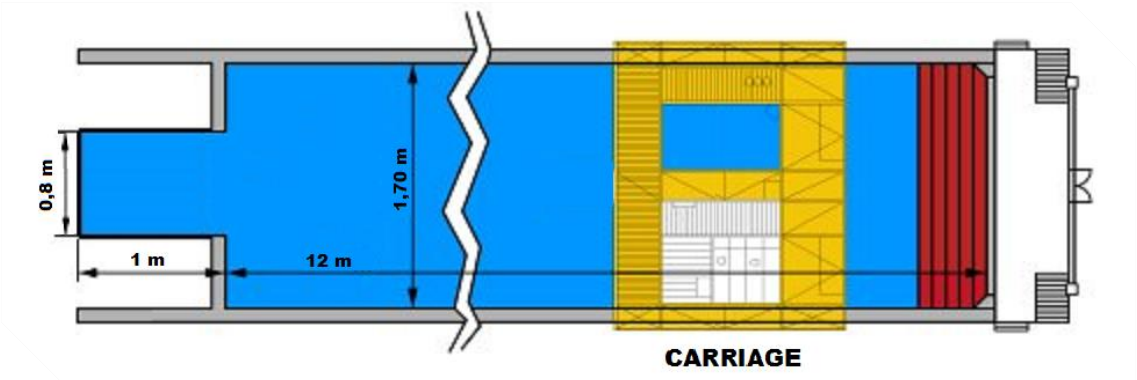

Figure 2.1: Dimensions of TU-Varna towing tank.

The sketch of the towing tank above shows the dimensions of the channel in a simple way, it had the following dimensions, 12 m length, 1,70 m beam and enough draft depending on the level of the water free surface. Anyway is illustrative to know the real appearance of towing tank of TU-Varna so the following pictures give an idea about it.

It is noteworthy that the measures were taken before the experiment to ensure the length, beam and depth of the towing tank.

Figure 2.2: Side channel view of the towing tank of the Naval Architecture Department at the Technical University of Varna.

Figure 2.3: Front channel view of the towing tank of TU-Varna.

Figure 2.4: Top channel view of the towing tank.

Concerning to the tank, water depth was increased up to 0,4 m approximately to avoid ground effects at the time of running the tests. Every component was checked, including the carriage.

The model was a simple, barge-shaped hull. This hull form was selected because of its large flat-bottom area according to the air lubrication system. The flat bottom makes easy the distribution of the air injection holes across the beam and the air layer created beneath the bottom may be smooth and uniform through the model.

The model was provided with a clear glass bottom plate which was very useful to visualize the pattern of air spread. In addition, other technologies were used. For instance, slow-motion recording helped in this goal. After shooting in 120 frames per second, the playback speed was reduced and a series of videos was checked in order to visualize the air flow distribution.

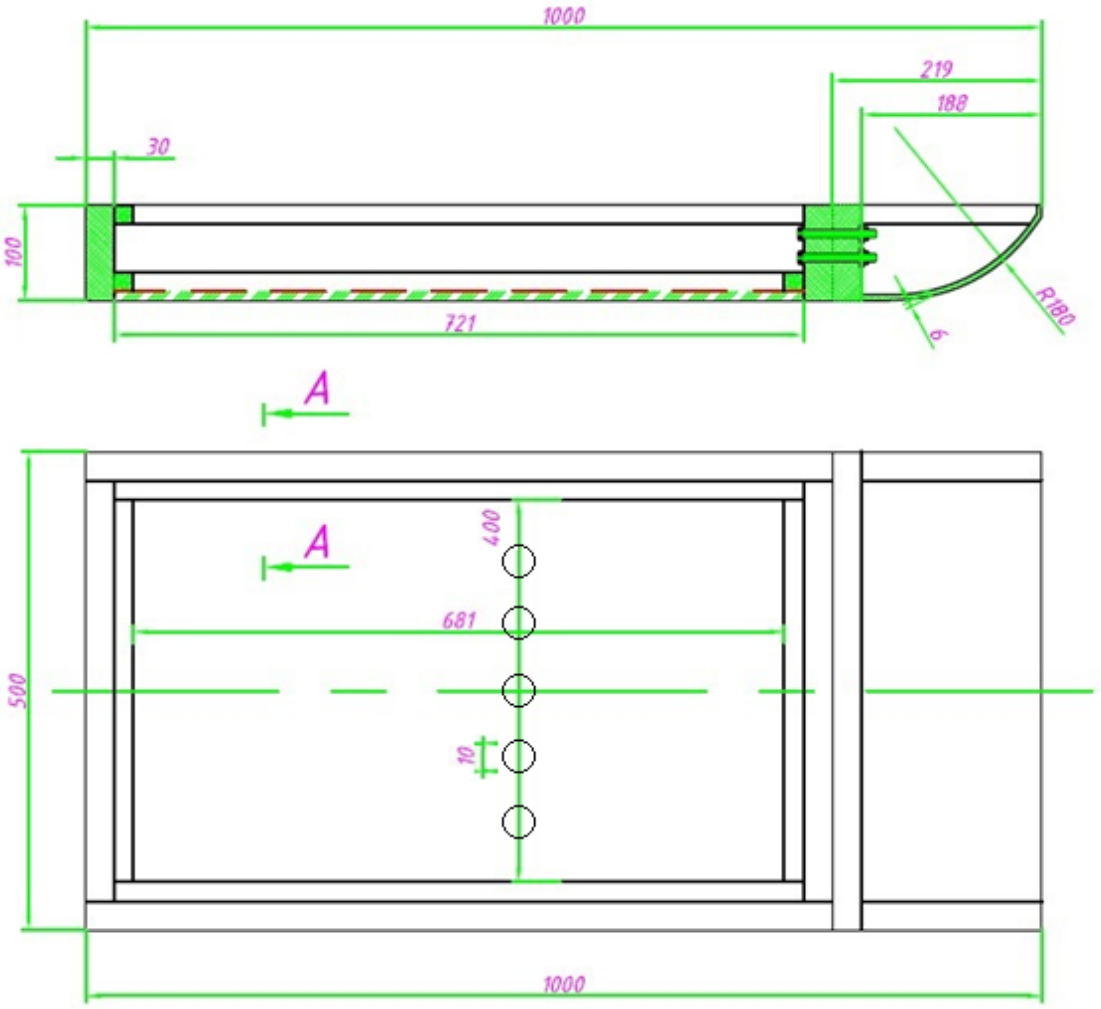

Figure 2.5: Barge dimensions.

The dimensions of the barge model are given in millimeters and the air injections holes shown in the sketch are located in the middle of the barge, it means 500 mm upstream from stern. There are 5 rounded holes with Ø 10 mm each one.

The model had around 12 meters to run but remember that the barge is carry until to reach the selected velocity and after the carriage liberates it.

Keeping in mind that the second part involves the numerical simulation with CFDs, it is necessary a digital model of the built barge. Rhinoceros 5.0 software allows work with 3D forms easily and the following picture provides to lectors a better view of the air injections position. With the dimensions of the plan, a digital model was built with the air pipes and the holes in the bottom (Figure 2.6).

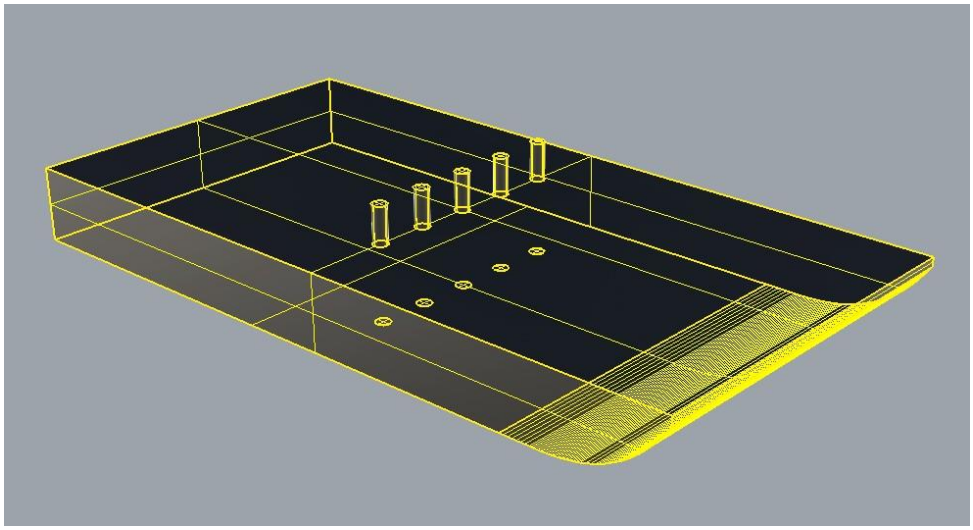

Figure 2.6: Barge model made with Rhinoceros 5.0.

The Figure 2.7 shows the different components of the real model.

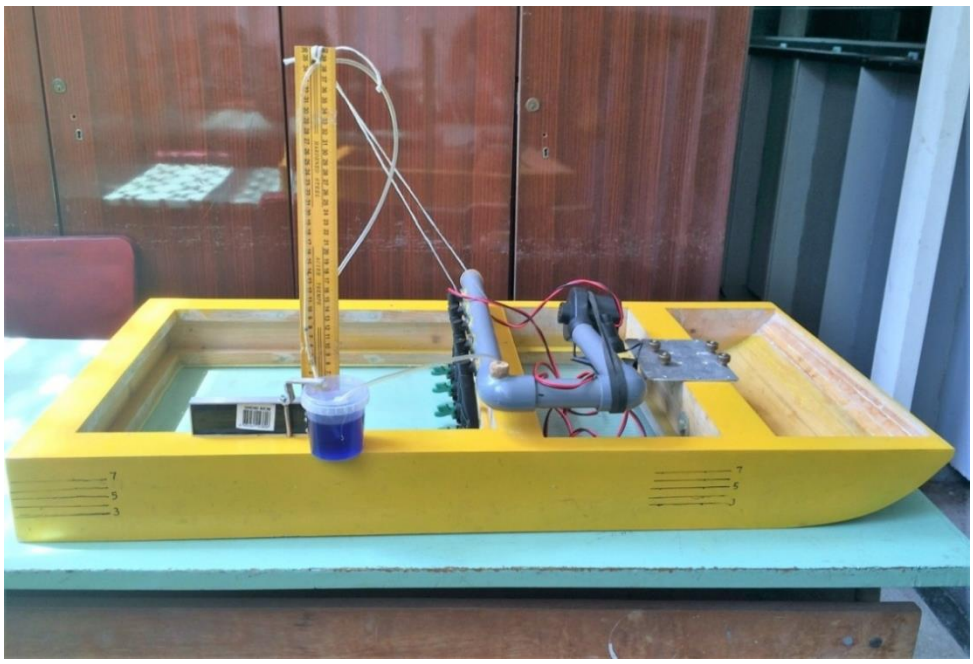

Figure 2.7: Real barge composed by an air pump which supplies the air to the bottom holes. A gauge was placed to visualize the air pressure.

The flat plate model was provided with a PVC pipe which conducts air flow supplied by the air pump. This small domestic air pump was able to give around 7 m^3/h of theoretical airflow. These five discrete air feed holes were used to supply air under the barge. The hypothesis to increase the effective air film area by the use of air injection through multiple holes was in mind at the time to build the barge model, so, the holes were arranged in the same horizontal section.

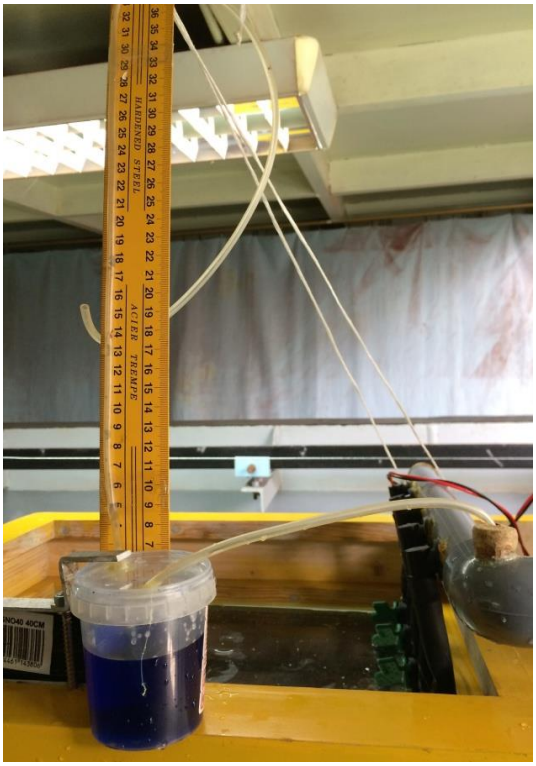

Figure 2.8: Air pressure measurement system.

Figure 2.9: Air flow-meter device.

To measure the air flow injected to the bottom, the barge was provided by a gauge with a scale in mm, including a tank with colored water and a sleeve introduced inside the PVC pipe. This system (see Figure 2.8) allows know the air pressure in mm of water column.

An easiest and direct technique to measure air flow rate would have been the use of a flow-meter, but this device was large and heavy to install onboard. The homemade device let to know the pressure inside the pipe in millimeters of water column (mm H_2O). It is easy to convert into air flow measure (m^3/h).

The air flow-meter device had a flow scale drawn in the transparent pipe, this permitted to observe the position of the ball indicator in the scale and obtain a direct reading of air flow in m^3/h. It was only necessary to connect to the main pipe and regulate the caudal of air expelled across the five secondary pipes switching on and off the opening valves.

Figure 2.10: Flow-meter onboard.

Figure 2.11: Flow-meter detail.

Different positions of the valves were tested with the aim to elaborate a graph, which gives the relationship between the pressure in mm of H_2O and the caudal Q (m^3/h). Changing the aperture position of the valves during the experiments a measure of pressure in mm of H_2O was obtained. This measure gives the required data to make a graph (see Figure 2.12).

With the stationary barge and the air pump connected to a 12v battery, it was taken six air flow points, in mmH_2O and m^3/h, just playing with the valves aperture. The indicator rises according to the pressure inside the pipe. The Figure 2.11 shows an enlarged image of the moment when was taken the measure of airflow.

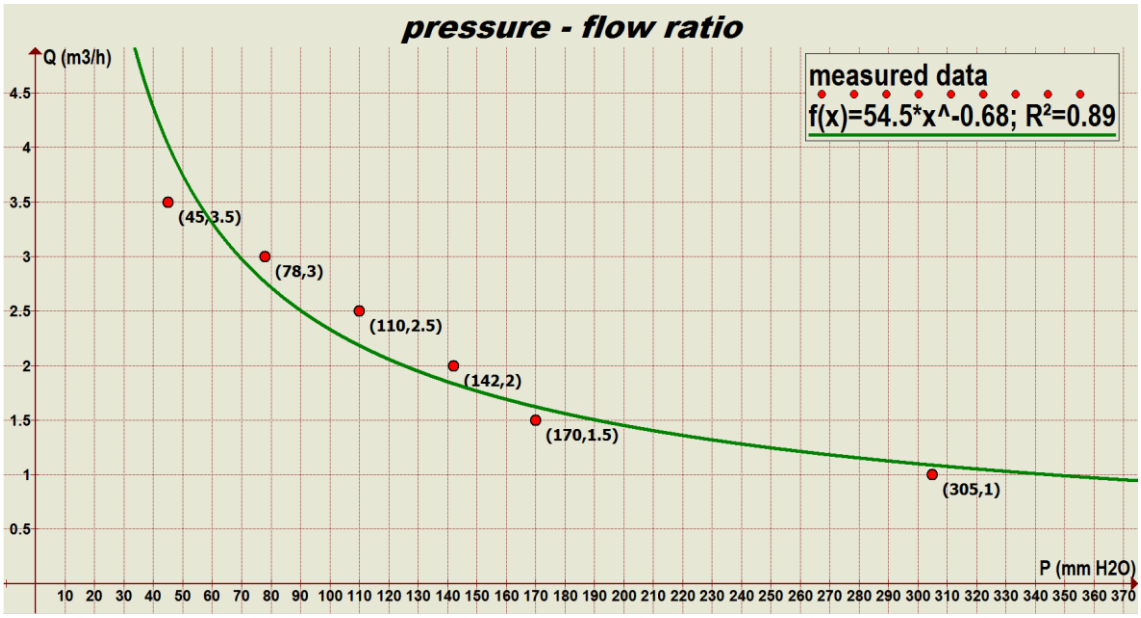

Figure 2.12: Pressure – flow rate calibration curve.

It can be seen that the correlation (R^2) between the function and the measured points is strong ($R^2 \approx 0.9$). The function relating the pressure with the flow is formulated as follow:

$$Q = 54.5 \cdot P^{-0.68}, \qquad \text{Eq. (2.1)}$$

where P is the independent variable (in mm of H_2O) and the flow Q (m^3/h) is the dependent variable which is drawn on ordinate axis.

Up to this point the amount of air expelled trough the holes was well known, the following step consisted of place the barge inside the tank and connect every element. Linking the barge to the carriage, connecting the air pump with the battery and to ballast the barge with weights were some of the tasks previous to begin the towing tank tests.

2.3 Towing experiment

First of all, the model was carefully placed inside the channel and joined to the carriage as shown in Figure 2.13. Also by using a sponge, the bottom window was cleaned because usually some water drops inside. Furthermore, to fix the draft and stabilized the barge, ballast weight was placed strategically inside the barge.

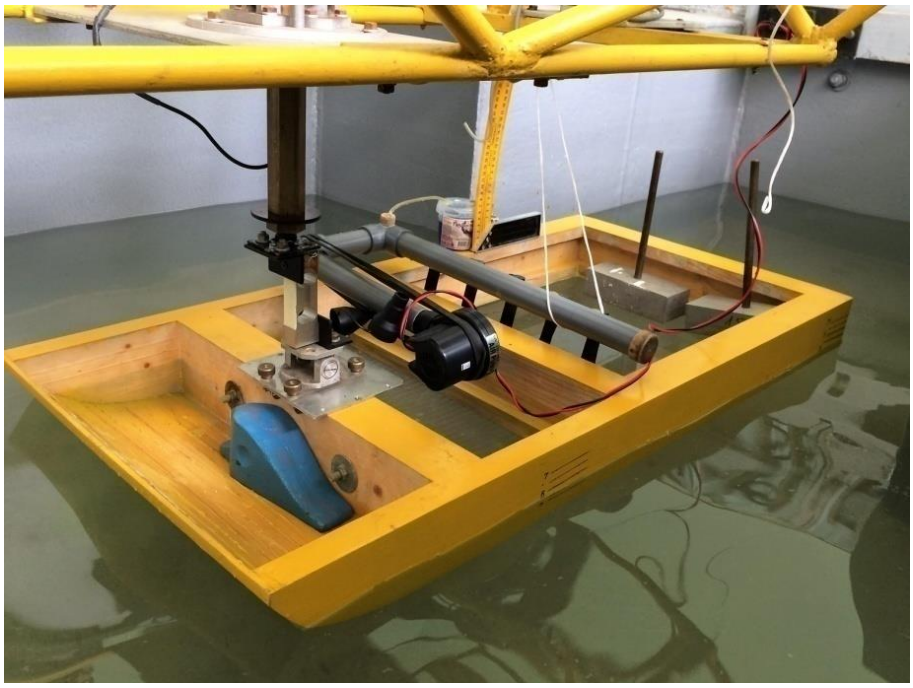

Figure 2.13: Fixation the barge to the carriage. Three ballast pieces were distributed along the length.

Thanks to the transparent bottom plate, it could be seen easily the air path. With the different mounting available in the market, the camera was placed at a suitable angle for viewing thanks to the carriage structure. This gave a qualitative visualization of the airflow distribution along the bottom.

Figure 2.14: GoPro mounted on carriage structure.

It was used an action camera, concretely the model of GoPro Hero 3. Slow-motion technology was used and videos of 120 fps were recorded in 720p quality. This was suitable to make a huge idea of what was happening during the towing test. The complete experimental set-up is depicted in Figure 2.15 which gives an overview with the entire set-up ready to start the test.

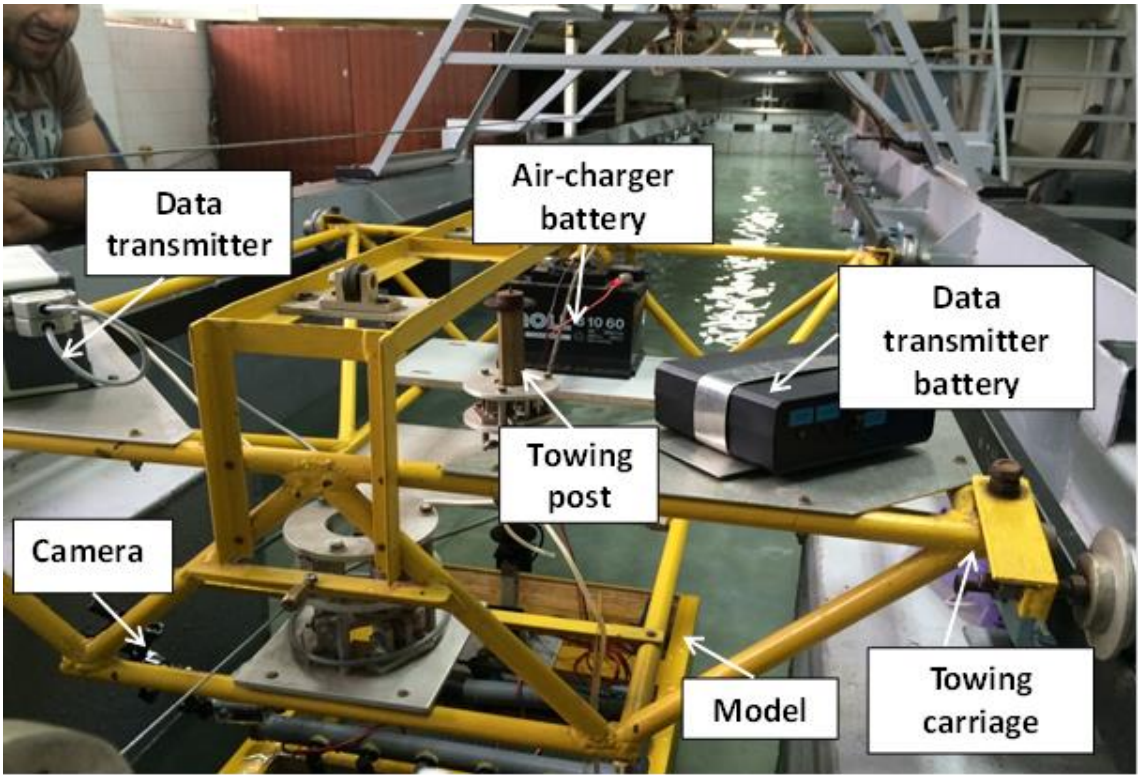

Figure 2.15: General view of the experimental set-up.

The data transmitter sends dynamometer data to the computer which returns them processed. Black device is the one that supply of energy for Data transmitter. Air-charger battery is connected and towing tests are carried out.

At first place, the model was experimented without air injection and after with air. Different positions of the opening valves are tested while the pressured in water column is read.

Figures 2.16 and 2.17 show different shots of the experiment. Moreover, it was taken a film footage where is visible how the bubbles flux escapes from free surface, how the waves are created by the movement of the model.

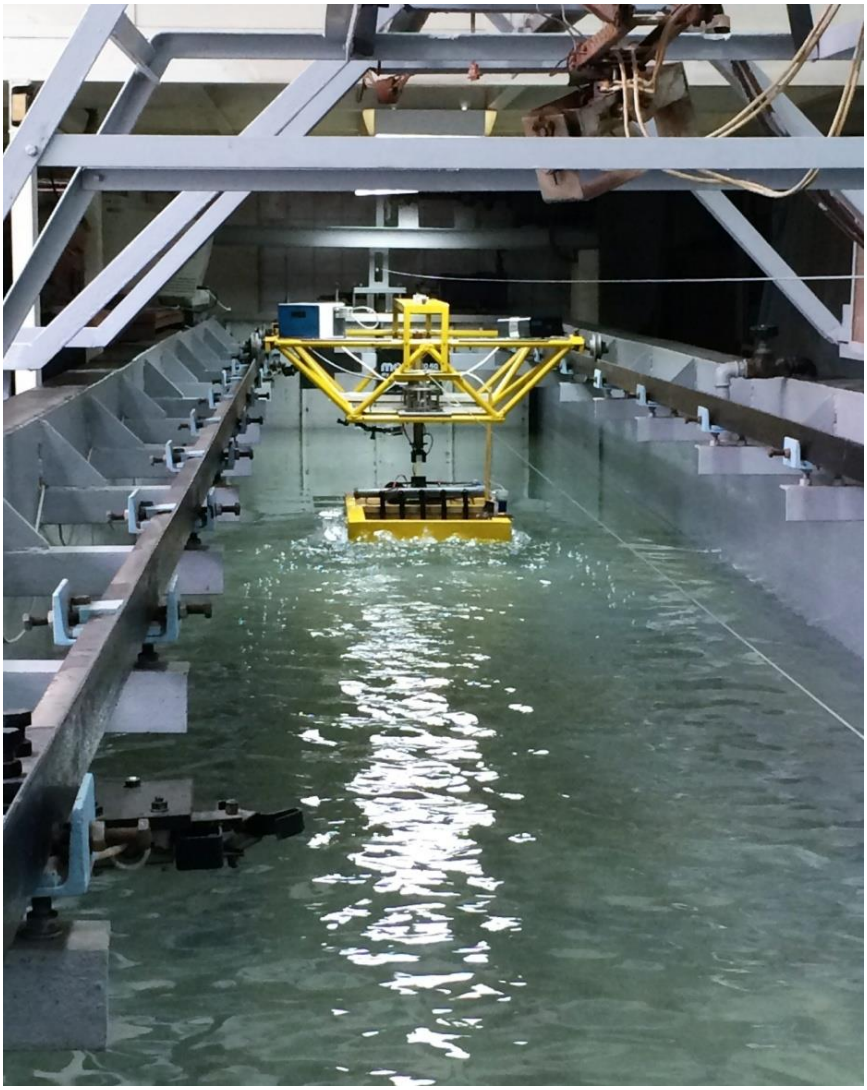

Figure 2.16: Model test with air lubrication.

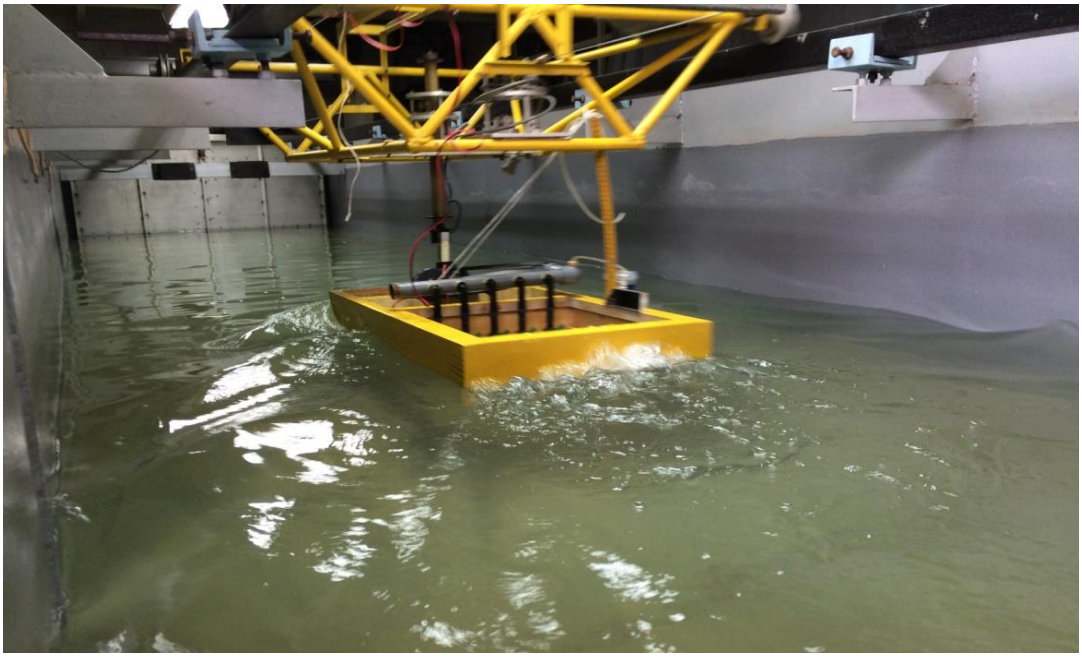

Figure 2.17: Bubble flux escaping from the free surface.

Air fed through the holes separates into two arms forming V sections with an angle depending on water flow speed and air feed quantity. Once V arms merge together, an area filled with an unstable air film is obtained (figure 2.18).

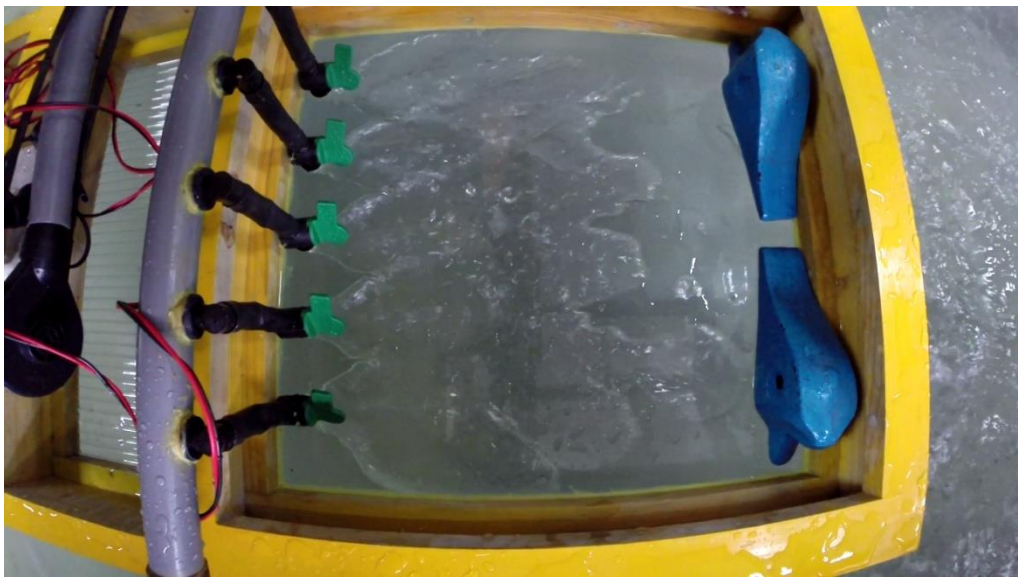

Figure 2.18: The air spread pattern was observed and video recorded during the runs with a Gopro camera. This footage belongs to a short barge test.

It is subsequently checked that the V air distribution found in the tests corresponds to results found in simulations with CFD codes. So until now, there is a match between the actual test and simulation.

It should be noted that the first results of drag resistance with air lubrication system had no consistency. The explanation was very simple; the turn on of air pump has to be done after the model start running. In this way, free surface is not disturbed before starting the test by reflection of the waves generated in the channel walls.

Following the completion of all tests, arose the idea of extending the initial model with an aft plate. The reason was there was not big effect on drag reduction by mean of air lubrication. The hypothesis that an increase in wetted surface can lead better results was obvious, so it proceeded to build a long barge model.

2.4 Ship model elongation

Starting from a short version it was later decided to elongate the hull with a box-shaped part in the stern to increase the bottom area. The aim was to increase the wetted surface and hopefully make the effects more noticeable. It was used a 1 m length plate for the bottom, and was flanked with a metallic plate. The reason for using a sheet metal responds to the malleability, thanks to a clamp the plates were easily bended. Previously two long strips were cut from a big griddle. Below pictures of the process:

Fig. 2.19: 1 m added length.

Fig. 2.20: Bending side plates.

Another idea was to make two rails which keep the air inside the beam of the model, so with the same side plates they were made. The metallic sheet was previously drilled and fixed with screws to the added bottom plate and

alongside the initial barge, thus the assembly is stiffened. Finally, the bottom was coated with the aim to have a smooth bottom.

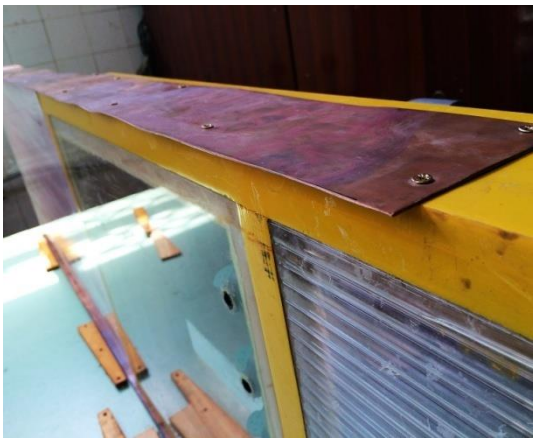

Fig. 2.21: Bottom rail.

Fig. 2.22: Bottom coating.

After waiting enough hours the coating was dried so everything was ready to start new tests with this long barge. The final appearance of the model is presented in Figure 2.23.

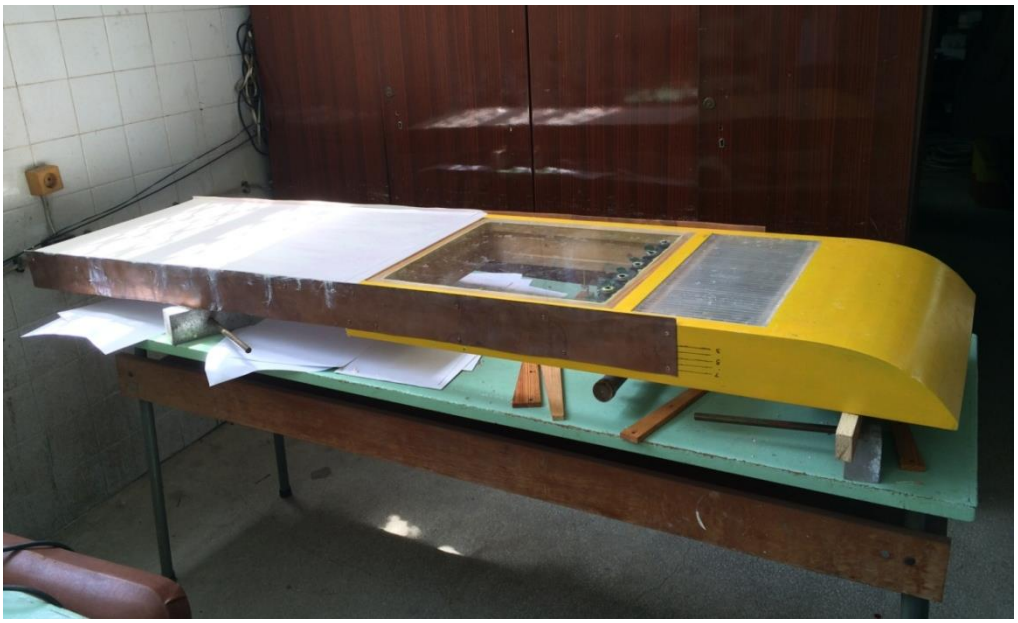

Figure 2.23: Long barge model.

The model was correctly placed again in the tank keeping in mind this new length and the tests were carried out. The methodology was the same than in the short model tests, by varying the position of the opening valves and towing with different velocities, different points of water and air flow are obtained whereby it will elaborate graphs. These graphs allow to see clearly whether any drag reduction is found, in what percentage, and if is worth all this system.

2.5 Experimental results and observations

In this section the results obtained in tests with the short model (initial) and the long one (posterior elongation) are reviewed. The results of the short model drag resistance in Newton correspond to the green column. All the results can be reviewed in the spreadsheet attached to this thesis called "Summary results".

Element	Symbol	Unit	Value
Wet surface	S	m^2	0,55
Length waterline	L_{WL}	m	0,95
Density of water	ρ	kg/m^3	1000
Kinematic viscosity	ν	m^2/s	1,14E-06

Figure 2.24: Short barge experiment data.

No Air

Vm, m/s	Fn	Rn	Read	R, N	CTm	CFm	CR
0,246	0,081	2,052E+05	20,006	0,1630	9,795E-03	6,121E-03	3,674E-03
0,248	0,081	2,068E+05	19,98	0,1370	8,100E-03	6,110E-03	1,990E-03
0,515	0,169	4,295E+05	20,263	0,4200	5,758E-03	5,261E-03	4,970E-04
0,779	0,255	6,497E+05	20,79	0,9470	5,675E-03	4,852E-03	8,228E-04
1,034	0,339	8,624E+05	21,641	1,7980	6,115E-03	4,597E-03	1,519E-03
1,295	0,424	1,080E+06	23,165	3,3220	7,203E-03	4,407E-03	2,796E-03
1,289	0,422	1,075E+06	23,152	3,3090	7,242E-03	4,411E-03	2,831E-03
1,293	0,424	1,078E+06	22,966	3,1230	6,793E-03	4,408E-03	2,384E-03

285 mm H_2O

Vm, m/s	Fn	Rn	Read	R, N	CTm	CFm	CR
0,242	0,079	2,02E+05	19,971	0,128	7,948E-03	6,142E-03	1,81E-03
0,511	0,167	4,26E+05	20,277	0,434	6,044E-03	5,270E-03	7,74E-04
0,774	0,254	6,46E+05	20,777	0,934	5,669E-03	4,858E-03	8,11E-04
1,032	0,338	8,61E+05	21,704	1,861	6,354E-03	4,598E-03	1,76E-03
1,288	0,422	1,07E+06	22,906	3,063	6,714E-03	4,411E-03	2,30E-03

210 mm H_2O

Vm, m/s	Fn	Rn	Read	R, N	CTm	CFm	CR
0,24	0,079	2,00E+05	19,944	0,101	6,376E-03	6,153E-03	2,2334E-04
0,508	0,166	4,24E+05	20,245	0,402	5,665E-03	5,276E-03	3,8881E-04
0,772	0,253	6,44E+05	20,854	1,011	6,169E-03	4,860E-03	1,3082E-03
1,029	0,337	8,58E+05	21,482	1,639	5,629E-03	4,601E-03	1,0278E-03
1,286	0,421	1,07E+06	22,878	3,035	6,673E-03	4,413E-03	2,2606E-03
1,285	0,421	1,07E+06	22,763	2,920	6,430E-03	4,413E-03	2,0171E-03

125 mm H_2O

Vm, m/s	Fn	Rn	Read	R, N	CTm	CFm	CR
0,239	0,078	1,99E+05	19,907	0,064	4,074E-03	6,158E-03	-2,084E-03
0,508	0,166	4,24E+05	20,172	0,329	4,636E-03	5,276E-03	-6,398E-04
0,772	0,253	6,44E+05	20,763	0,920	5,613E-03	4,860E-03	7,530E-04
1,029	0,337	8,58E+05	21,459	1,616	5,550E-03	4,601E-03	9,489E-04
1,287	0,422	1,07E+06	22,9	3,057	6,711E-03	4,412E-03	2,299E-03

Figure 2.25: Short barge test results.

The charts below summarize the measurements of resistance in two aspects: as a function of speed and as a function of air flow rate. This is the better way to find if there is a relationship between the drag reduction, air flow rate and towing velocity.

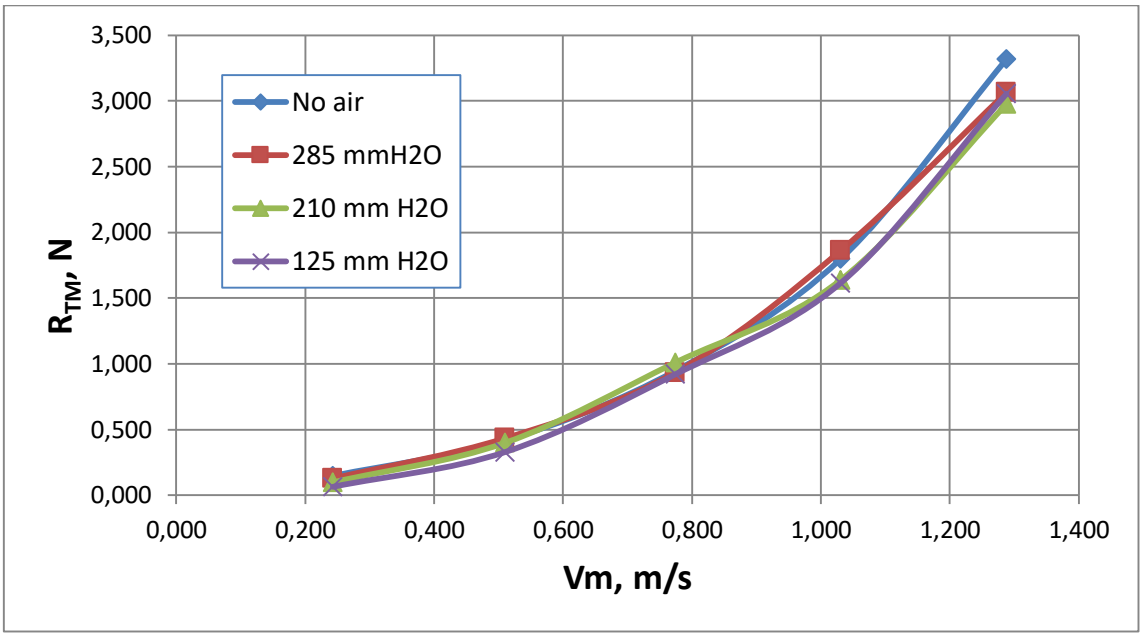

Figure 2.26: Resistance vs. speed, Short barge.

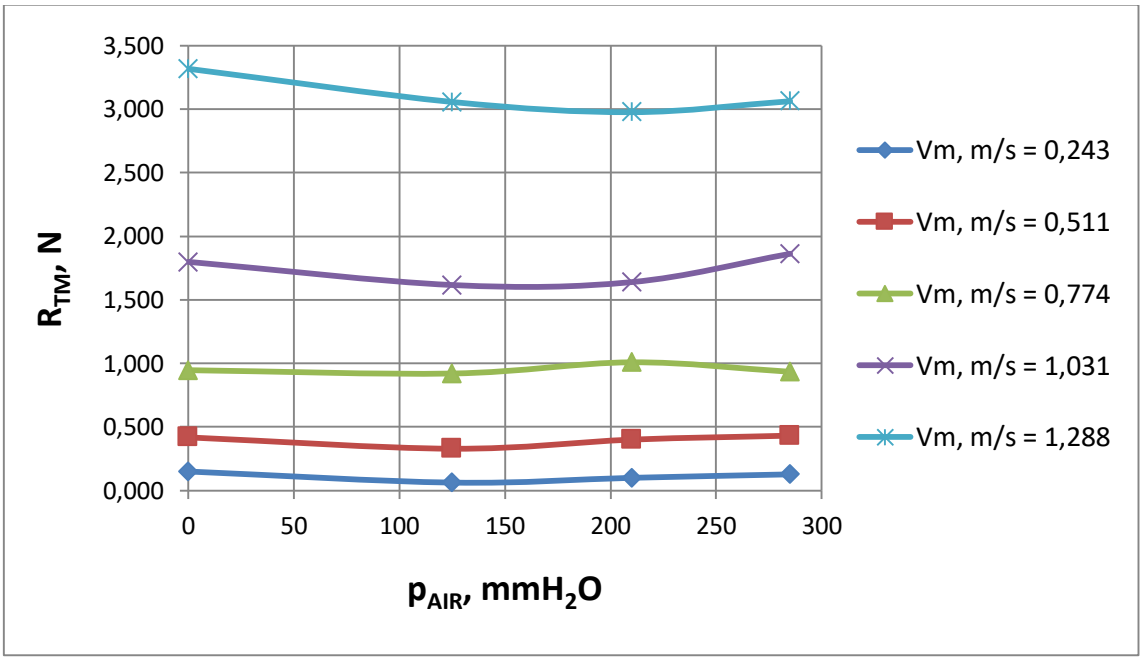

Figure 2.27: Resistance vs. air pressure, Short barge.

Now is time to show the results of the long model. In this case is noticeable an improvement in drag resistance as well as a specific ideal value for the air flow injection.

Element	Symbol	Unit	Value
Wet surface	S	m^2	1,04
Length waterline	L_{WL}	m	1,85
Density of water &	ρ	kg/m^3	1000
Kinematic viscosity	ν	m^2/s	1,14E-06
Density of air &	ρ	kg/m^3	1,23
Kinematic viscosity	ν	m^2/s	1,46E-06

Figure 2.28: Long barge experiment data.

No Air

Vm, m/s	Fn	Rn	RTm, N	CTm	CF_Pr-Schl	CR
0,25	0,0587	4,06E+05	0,2	6,15E-03	5,32E-03	8,331E-04
0,5	0,1174	8,12E+05	0,592	4,80E-03	4,65E-03	1,507E-04
0,75	0,1761	1,22E+06	1,459	4,99E-03	4,31E-03	6,779E-04
1	0,2347	1,62E+06	2,777	5,34E-03	4,09E-03	1,250E-03
1,25	0,2934	2,03E+06	5,155	6,34E-03	3,93E-03	2,415E-03
1,5	0,3521	2,44E+06	8,589	7,34E-03	3,81E-03	3,536E-03

120 mm H_2O

No air (f=0)

Vm, m/s	Fn	Rn	RTm, N	CTm	CFm	CR
0,25	0,0587	4,06E+05	0,208	6,40E-03	5,32E-03	1,08E-03
0,5	0,1174	8,12E+05	0,337	3,10E-03	4,65E-03	-1,55E-03
0,75	0,1761	1,22E+06	0,686	3,00E-03	4,31E-03	-1,31E-03
1	0,2347	1,62E+06	2,001	3,85E-03	4,09E-03	-2,42E-04
1,25	0,2934	2,03E+06	3,606	4,44E-03	3,93E-03	5,08E-04
1,5	0,3521	2,44E+06	6,919	5,91E-03	3,81E-03	2,11E-03

180 mm H_2O

Vm, m/s	Fn	Rn	RTm, N	CTm	CFm	CR
0,5	0,1174	8,12E+05	0,22	2,95E-03	4,65E-03	-1,70E-03
1	0,2347	1,62E+06	1,89	3,63E-03	4,09E-03	-4,55E-04
1,5	0,3521	2,44E+06	6,65	5,68E-03	3,81E-03	1,88E-03

260 mm H_2O

Vm, m/s	Fn	Rn	RTm, N	CTm	CFm	CR
0,25	0,0587	4,06E+05	0,304	9,35E-03	5,32E-03	4,03E-03
0,5	0,1174	8,12E+05	0,296	3,95E-03	4,65E-03	-6,99E-04
0,75	0,1761	1,22E+06	1,106	3,78E-03	4,31E-03	-5,29E-04
1	0,2347	1,62E+06	2,176	4,18E-03	4,09E-03	9,47E-05
1,25	0,2934	2,03E+06	3,979	4,90E-03	3,93E-03	9,67E-04
1,5	0,3521	2,44E+06	7,406	6,33E-03	3,81E-03	2,52E-03

Figure 2.29: Long barge test results.

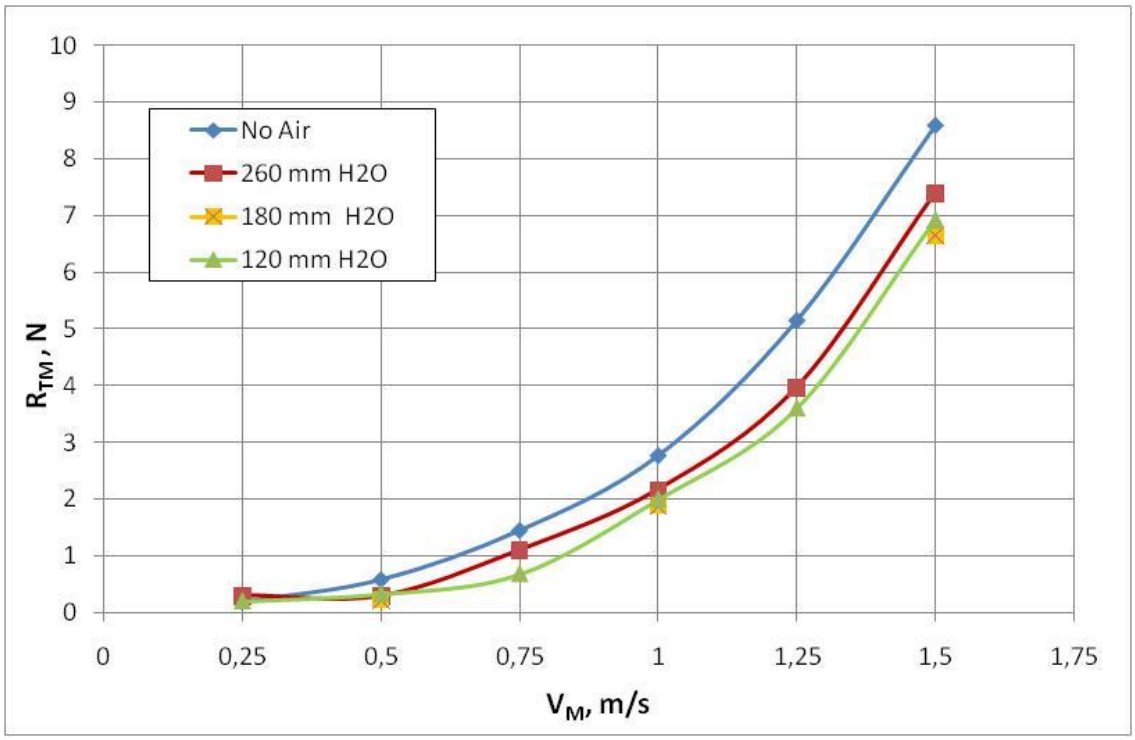

Figure 2.30: Resistance vs. speed, Long barge.

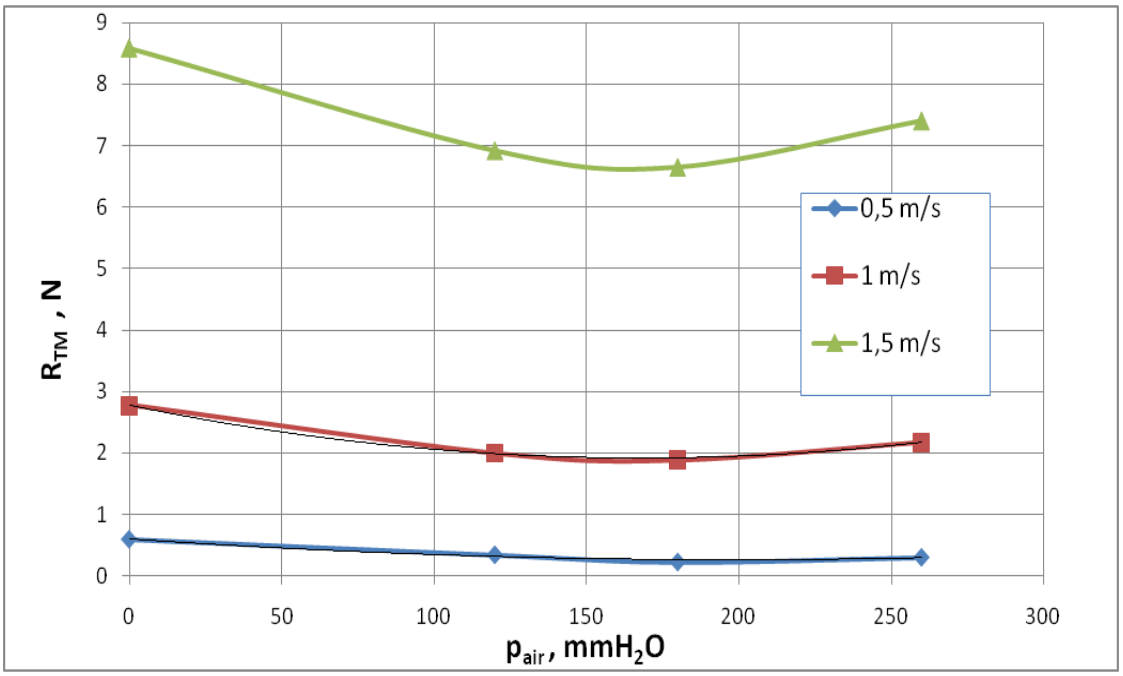

Figure 2.31: Resistance vs. air pressure, Long barge.

In both cases (short and long barge) there is resistance reduction effect of the air discharge in the whole investigated range of speed and air flow rate values. Of course, the effect is bigger in the case of the Long barge. Moreover, there is a noticeable optimum of air pressure in the range of 150 to 200 mm H_2O for all tested speeds.

Figure 2.32 shows samples of the observations of air spread pattern for the case of long barge and the “optimum” air pressure of 180 mm H_2O.

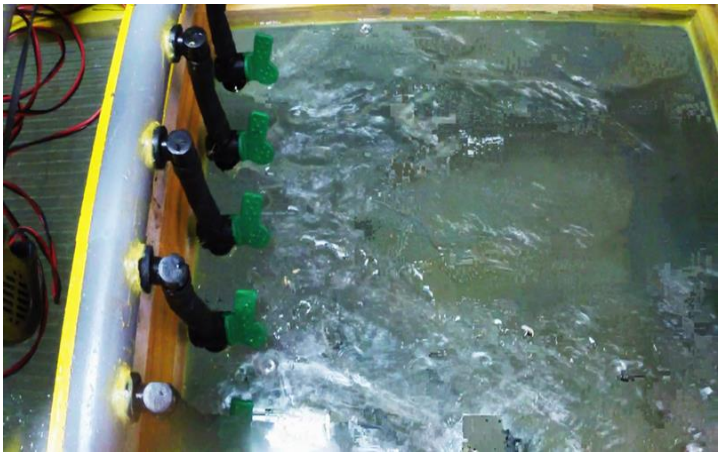

Vm = 0.5 m/s, Rn = 8.12x10^5

At low speed the air covers randomly shaped spots of the surface but only in the upstream part close to the holes.

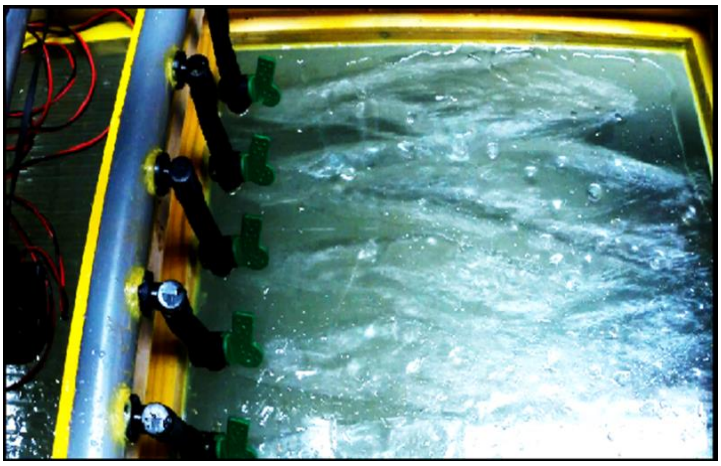

Vm = 1.0m/s, Rn = 1.62x10^6

At higher speed, rather speed – airflow combination, the air forms V-shaped traces interfering with each other, propagating farther downstream and (in this case) reflected by the end-plates. In this model the air is still attached to the bottom surface. This pattern has been observed in other experimental investigation [9] and CFD simulation of this thesis.

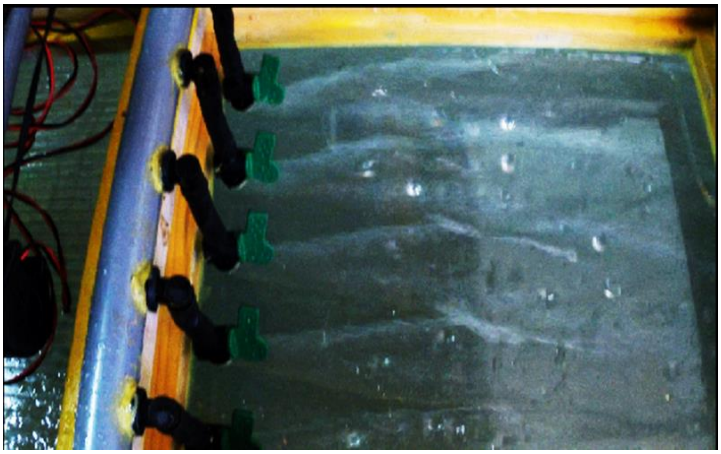

Vm = 1.5 m/s, Rn = 2.44x10^6

At still higher speeds and/or air flowrate the V-shaped pattern is still preserved but the air volumes seem detached from the surface.

Figure 2.32: Patterns of the air phase distribution along the bottom surface.

Similar trends are observed with increasing the air flow rate. These observations indicate the possible reasons for the presence of optimum in the air lubrication effect on resistance with respect to the air flow rate.

The first obvious reason might be the part of the bottom area covered with air attached to the surface. At low flow rate a smaller air layer is formed on the bottom surface; at an “optimum” flow rate the air streams, interfering and reflecting, cover the maximal area of the bottom surface; at higher flow rates part of the air streams detach from the surface and the air-washed area is smaller.

Secondly, the mode of the air phase distribution along the surface changes with speed and air flow rate. The experimental set-up implemented in this research does not provide any of the basic types of air lubrication described in Figure 1.2. It is just a set of discrete air-injection points. That means all observations and results concluded cannot be considered universal for all types of air lubrication.

2.6 Extrapolation to full scale

Air lubrication is one of the methods for resistance reduction requiring consumption of additional power for air pumping. A reasonable question in such cases is about the cost-benefit analysis, i.e. evaluation of the net gain of power. This issue has been considered in *Section I, 1.7 Methodology for energy cost-benefit analysis* using assumptions proposed in [5] and resistance data for an inland-navigation ship based on model testing. Here this assessment is not discussed because it can be realistic only if full scale data are used. That raises the problem about extrapolation of model test results as those presented above to full scale.

Since frictional resistance is the main target of air lubrication, the first question is how to calculate frictional resistance coefficient. The ITTC-57 friction line, commonly used in ship hydrodynamics practice, is not exactly a scientifically derived flat-plate frictional resistance coefficient but rather empirically adjusted curve for ship-model to full-scale extrapolation.

$$CF_{ITTC} = \frac{0.075}{(lg\ Rn - 2)^2}, \qquad \text{ITTC-57 friction line} \qquad \text{Eq. (2.2)}$$

$$CF_{\mathrm{Pr}\_Sch} = \frac{0.455}{lg\ Rn^{2.58}}, \qquad \text{Prandtl – Schlichting flat plate Frictional resistance coefficient} \qquad \text{Eq. (2.3)}$$

On the other hand, the friction line proposed by Prandtl – Schlichting (Eq. 2.3) is a formula for flat plate frictional resistance coefficient based on boundary layer theory and experiments (like those of Prandtl-Schlichting, Schönherr, etc.). The largest differences between this line and the ITTC-57 are in the low Reynolds number range, with ITTC-57 giving higher values.

Since in the tests presented here the Reynolds number covers such range (from 4.10^5 to 3.10^6) the higher ITTC-57 values may lead to negative values of the residual resistance coefficient in the lower part of range. The wave resistance has an important part in the total resistance of the model, in any case, residual resistance can never give negative values. These values are demonstrated in Figure 2.33 for the case of no air injection. So, Prandtl – Schlichting line is used in the further analyses.

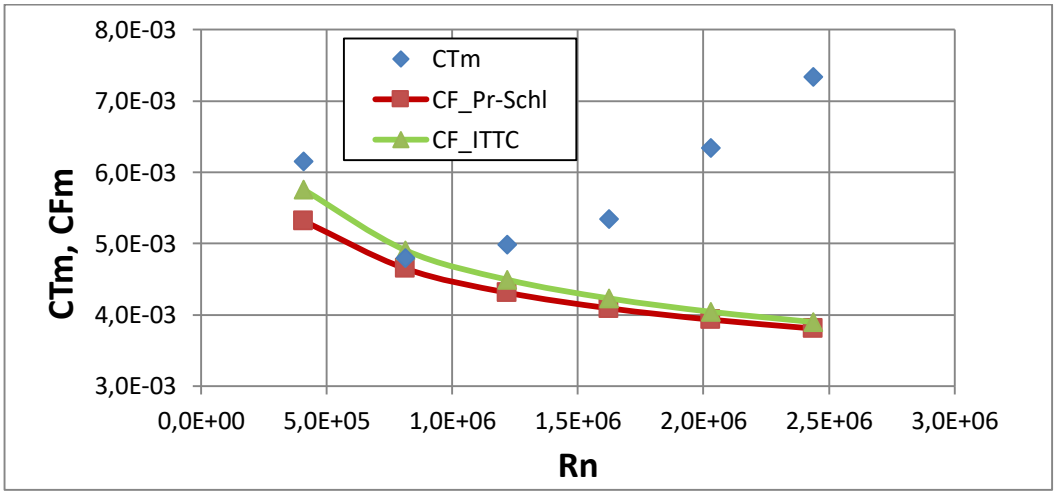

Figure 2.33: Friction lines applicability in the case of the long barge.

For the case of no air injection the C_T-C_F relationship is reasonable for both barge lengths using Prandtl - Schlichting friction line (see Figure 2.34).

For all cases with air injection, however, there are velocity ranges where $C_T < C_F$, i.e. $C_R < 0$ (Figures 2.35, 2.36, 2.37). In these figures the frictional resistance coefficient is calculated with the Rn for water viscosity assuming the whole bottom surface is covered with water.

The situation is summarized in Figure 2.38 showing residual resistance coefficient determined with C_F calculated under the above conditions. This shows that the Prandtl- Schlichting line need some considerations.

To avoid these problems is necessary to change the way of calculating frictional resistance depending on the areas covered by water or air. Obviously the frictional resistance with air injection is lower than that in entirely water flow predicted by the friction line.

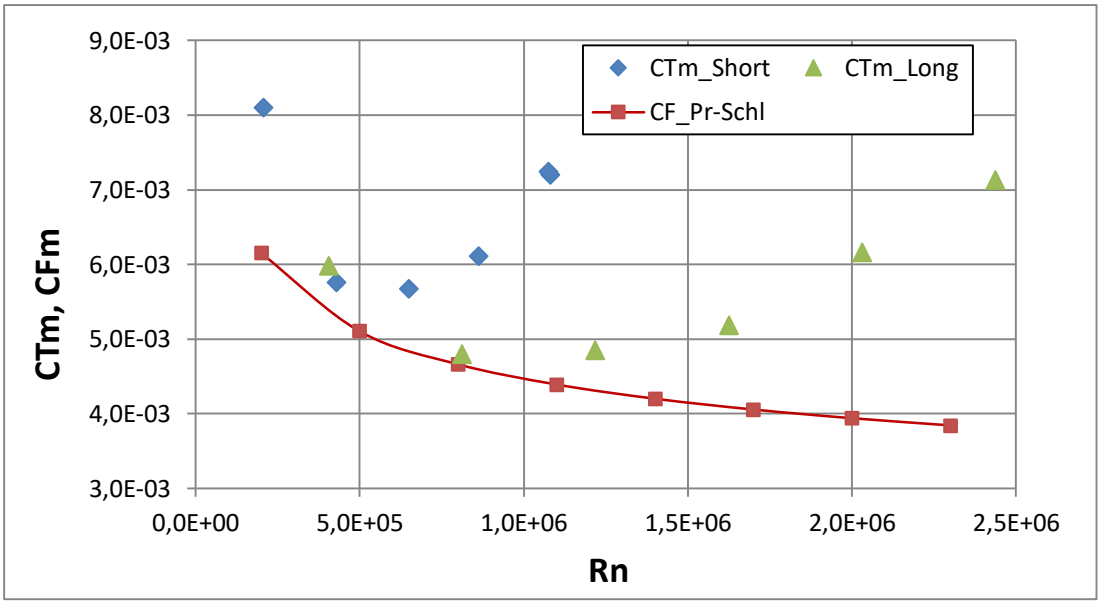

Figure 2.34: C_T (Rn), C_F (Rn) with no air injection.

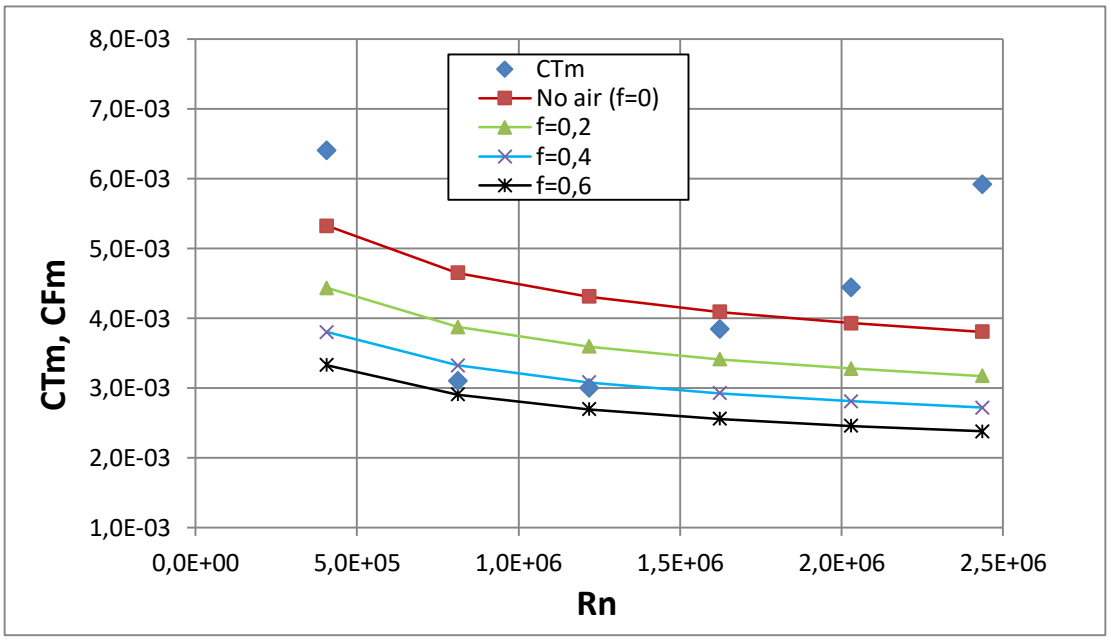

Figure 2.35: C_T (Rn), C_F (Rn) with air pressure 120 mm H_20 for different "f" coefficients which establish the percentage of area covered by water and air.

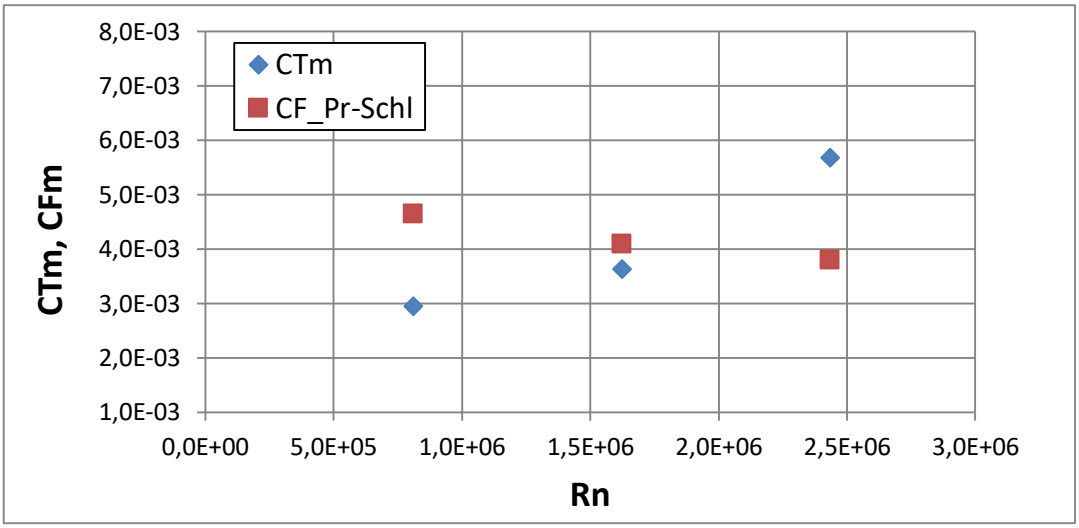

Figure 2.36: C_T (Rn), C_F (Rn) with air pressure 180 mm H_20.

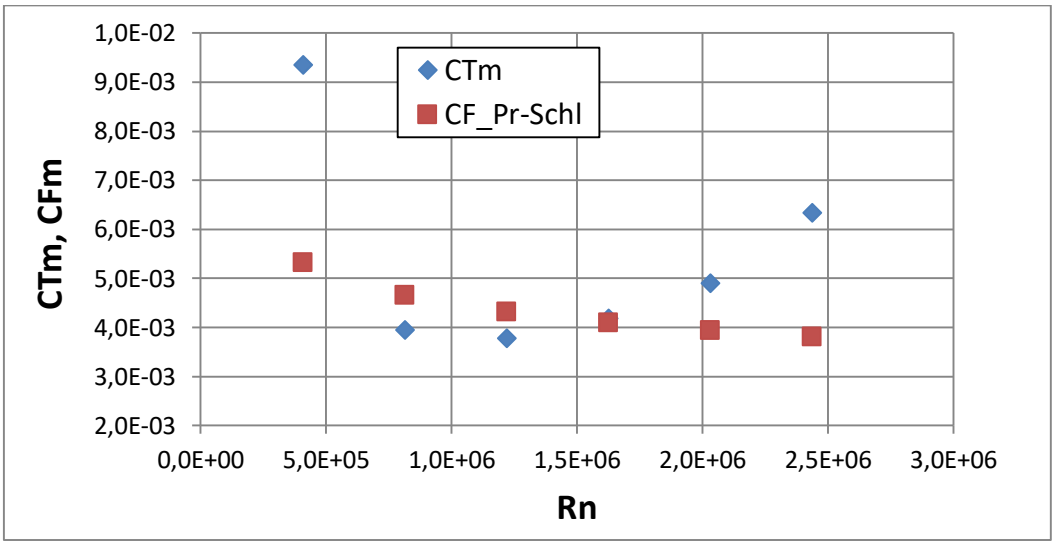

Figure 2.37: C_T (Rn), C_F (Rn) with air pressure 260 mm H_20.

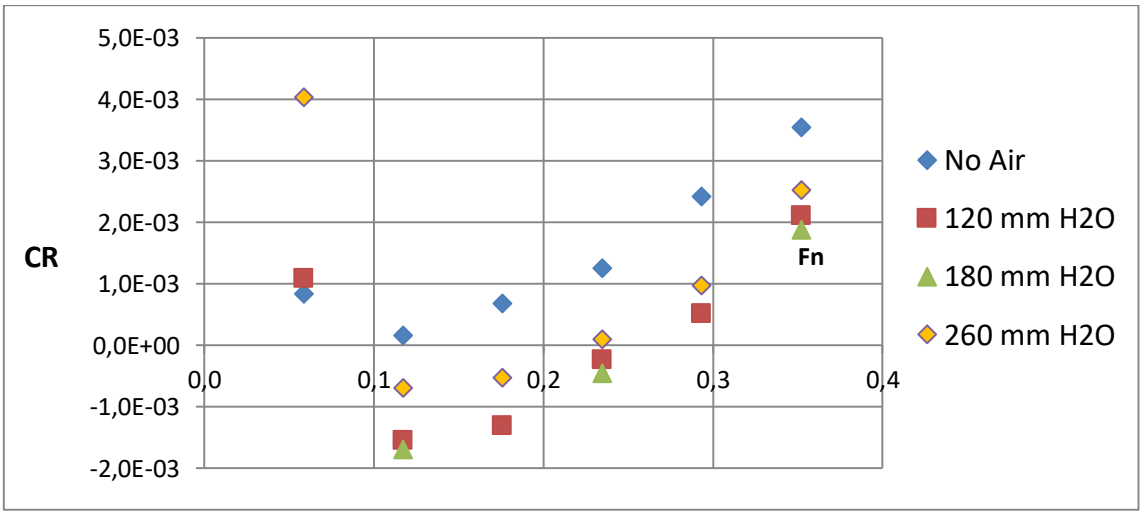

Figure 2.38: Residual resistance coefficient at different air pressures.

It is presented in the following calculus a way to reduce the frictional resistance coefficient using a new coefficient "f" which responds to the real case of air lubrication. This coefficient represents the percentage of bottom surface lubricated or covered by air with a range between 20 ($f = 0{,}2$) and 60 ($f = 0{,}6$).

Let's assume the frictional resistance with air injection is a simple sum of water and air frictional resistance:

$$R_{Fmix} = \frac{1}{2} v^2 (\rho_{water} \cdot S_{water} \cdot C_{Fwater} + \rho_{air} \cdot S_{air} \cdot C_{Fair}) \qquad \text{Eq. (2.4)}$$

Than the frictional resistance coefficient normalized with the water density and the total wetted area (to be comparable with total resistance coefficient) will be:

$$C_{Fmix} = \frac{R_{Fmix}}{1/2 \, \rho_{water} . v^2 . S_{tot}} \qquad \text{Eq. (2.5)}$$

denoting the ratios of air-to-water wetted areas and densities by:

$$f = \frac{S_{air}}{S_{water}} \quad \text{and} \quad d = \frac{\rho_{air}}{\rho_{water}} \qquad \text{Eq. (2.6)}$$

substituting them in Eq. (2.5) and rearranging it:

$$C_{Fmix} = \frac{C_{Fwater} + d \cdot f \cdot C_{Fair}}{1+f} \qquad \text{Eq. (2.7)}$$

here the frictional resistance coefficients C_{Fwater} and C_{Fair} are calculated with the kinematic viscosities of water and air, respectively.

Figure 2.35 contains, as an example, several lines of C_{Fmix} according to Eq. (2.7) for different values of *f*. It can be seen that at some value of *f* ($f = 0{,}6$) the curves of C_T and C_F "get to normal", i.e. the total resistance coefficient approaches the frictional resistance coefficient at low Reynolds numbers.

In this example the factor *f* was taken constant for all speeds. As is shown in the observations of Section 2.5, the area covered by air is speed dependent. This suggests that in tests like these there must be a way of registering and using the actual area covered by the air layer.

For the sake of completeness of the analysis it should be mentioned that the focus was on frictional resistance but there was a factor not taken into account. This is the wave making by the discharged air after leaving the hull.

Conclusions

- Model tests were carried out to estimate the effect of air lubrication on ship resistance. The tests covered a range of model speeds with varying air flow rate.
- The tests proved that there is resistance reduction effect of air discharge in the whole investigated range of speed and air flow rate values.
- It was established that there is a noticeable optimum of air flow rate for all tested speeds.
- The frictional resistance with air injection turned out to be lower than that in entirely water flow predicted by the popular friction lines.
- That raises the question about extrapolation of model test results to full scale.
- For the extrapolation to full scale it would be useful a way of registering and using the actual area covered by air layer in tests with air lubrication.

Section III

Numerical Simulations

3.1 Introduction

Computer Fluid Dynamics are nowadays a valuable tool for Naval Architects during the ship design process. In particular, they are widely used in several areas such as power prediction, propeller design, seakeeping and even time-accurate flood analysis.

Experimental methods, although highly valuable, have the drawback of being unable to satisfy the dynamical similarity of gravitational and frictional forces between the model and the full scale ship. As a result, there are significant scale effects in the transformation of the flow obtained from the model, for example in the wake of full hulls with considerable flow separation. These limitations, in addition to the increased accuracy of the models and the codes developed and associated with the enormous growth in available computational power have finally convinced almost every designer about the benefits of the CFD methods. Even if building a model test is still necessary, the use of CFD saves time and money by identifying, among different possibilities, the most promising design.

In this section is carried out a prediction of drag resistance of the barge models by mean of the use of CFD codes. The real model and the digital one have the same dimensions, so, no scales effects will be found here. At the same time, the numerical simulation can be validated with the experiment results to form a judgment about air-lubrication effects.

The hull resistance of a vessel moving through the water can be broken down into two components according to the Froude approach:

- **Friction resistance (R_F):** It is the sum of all components of the longitudinal shear stresses acting on the hull surface. It is due to the viscosity. The friction resistance influenced by the viscosity depends only on the nº of Reynolds:

$$Rn = \frac{\rho \cdot v \cdot L_{WL}}{\mu}, \qquad \text{Eq. (3.1)}$$

where ρ is the density of the fluid, v is the ship velocity, L_{WL} is length on the waterline and μ the dynamic viscosity.

- **Residuary resistance (R_R):** Is the sum of the pressures developed by the water push during the advance. It is due to the viscous origin pressure (hull shape) and the wave formation. The resistance produced by the waves formation depends only on the nº of Froude:

$$Fn = \frac{v}{\sqrt{g \cdot L_{WL}}}\,, \qquad \text{Eq. (3.2)}$$

where v is the ship velocity, g is the acceleration of gravity and L_{WL} is the length on the waterline.

According to the Froude approach any type of resistance depends on a fixed parameters and its own dimensionless coefficient, so, the total resistance would be:

$$R_T = R_F + R_R \quad \rightarrow \quad R_T = 0{,}5 \cdot \rho \cdot S \cdot v^2 \cdot C_T \qquad \text{Eq. (3.3)}$$

From a towing test it would be obtained the total resistant and the friction one would be obtained by empirical formulation from the ITTC regression curve (which was made from a study with flat plates). Then, working with the dimensionless coefficients, the residual coefficient would be the subtraction ($C_R = C_T - C_F$). Residual resistance for a full scale ship it will be scaled from the residual coefficient and friction resistance calculated empirically, the total resistance of the real hull would be the results of the sum.

The high cost of a towing test has contributed to the rapid evolution of numerical models to be able to predict the drag resistance with the same solvency as a scale model test. In recent years, hundreds of studies have been published comparing numerical simulations results with test in channels.

This investigation is intended to find out the effects governed by the air-lubrication system. It is a new phenomenon that has not been studied in depth yet so there is no numerical model established for it. To achieve appropriate results is very important to capture the effect of the air layer created beneath the hull. For that purpose, it should be established a suitable turbulence model as well as a physical model and contour conditions that resemble the reality of the experiment as much as possible.

3.2 Used software

The codes ANSYS Fluent and Tdyn CFD will be the used tools; they divide the total resistance into viscous resistance (tangential forces) and pressure resistance (normal forces). An overview of both is exposed below:

- **ANSYS Fluent ®**

  It will be briefly explained the different calculation options of the module Fluent (v.14) which is included inside the ANSYS package. The company behind this program is ANSYS Inc. and was founded in 1970 (Swanson Analysis System, Inc.). This simulation software contains the broad physical modeling capabilities needed to model flow, turbulence, heat transfer, and reactions for industrial applications.

- **Tdyn CFD ®**

  This software developed by COMPASS includes a complete set of simulation tools that allows give solution to almost any engineering calculation need. The product offers a unique solution for structural calculation problems, fluid dynamics, heat transfer, coupled problems, multi-physics and behavior of the sea, in a single integrated package.

  Tdyn integrates three analysis packages: Tdyn CFD + HT, Ram Series and Sea FEM, which offer 12 simulation modules to solve any need of analysis. Tdyn CFD is the used module that allows working with free surfaces.

3.3 History of CFD

It can be said that science called "Computational Fluid Dynamics" (CFD) began its development in the 60s. In 1966, Moretti and Abbett developed a finite difference numerical model that solved the problem of steady supersonic flow around a blunt body, giving solution to a problem that had occupied many researchers of the 50s and 60s. This example is the first sign of importance of CFD: a problem that was unsolvable happens to have a practical solution.

Historically, perhaps the first major work in CFD is the work of Kopal, who showed in 1947 the tables that solved the supersonic flow over sharp cones, solving numerically the differential equations of conservation (the calculations were performed on a primitive digital computer in the 'Massachusetts Institute of Technology', MIT).

It has subsequently been developed the CFD, successive generations have appeared, characterized each of them by a progress. With the appearance of modern digital computers, the CFD has become the third method of analysis problems of Fluid Mechanics, with the same importance as the other two methods, experimental research and theoretical development by analytical methods. The three methods are closely related and complement each other (see Figure 3.1).

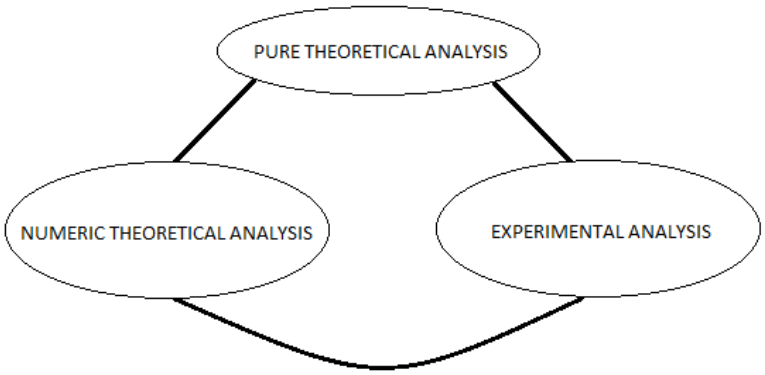

Figure 3.1: Methods of analysis of problems in fluid mechanics.

In recent years, it has been solved many problems of Fluid Mechanics with CFD tools; it has advanced, for example, in the investigation of supersonic flows around bodies, the problems of detachment of the boundary layer, in turbulent flows simulation, in flows inside hydraulic machinery, in flows with chemical reactions and combustion or multiphase flows.

Any problem of Fluid Mechanics is solved from the equations of mass conservation, momentum and energy, which are expressed in the form of partial differential equations of second order, strongly coupled to each other. It can be said that the science of CFD is the art of bringing these differential equations to algebraic equations that will eventually become relationships between numbers. This is especially attractive for engineering, where a quantitative description of the problems is required, that is, numbers. Of course, the numerical solution of

any problems involved in handling many numbers, so the development of CFD market requires computers with a capacity of calculation increasing.

As just indicated, the flow of any fluid is subject to general conservation equations obtained from the application to a fluid particle of the following principles:

- Principle of mass conservation → equation of continuity.
- Newton's second law → Navier-Stokes equations (if the viscous energy dissipation terms are included) or Euler equations (if these terms are not included).
- Principle of energy conservation → equation of energy.
- Equation of state or behavior of the fluid, along with the constitutive equations of the medium.

Solving differential equations of conservation (with corresponding initial and boundary conditions and necessary behavioral equations), It provides as a result the three velocity components at any point and for any time t, u (x, y, z, t), v (x, y, z, t) and w (x, y, z, t), together with the distributions of pressure p (x, y, z, t), density ρ (x, y, z, t), and temperature T (x, y, z, t).

Numerical simulation may be focused on determining phenomena such as separation and flow recirculation, or more elaborate practical results, such as mass flows incoming and outgoing heat transfer between solid surfaces and the fluid forces on surfaces, yields in hydraulic machinery, etc.

It should be emphasized, however, that the numerical simulation cannot successfully solve problems in which their physical principles have not been formulated correctly. This occurs, for example, in turbulence flows; in the simulation of turbulent flows, approximate models including empirical constants are used. The numerical results are subject to the accuracy of the turbulence model used, as well as the appropriateness of applying the model to the specific problem to be solved. This is the case of this thesis; the Reynolds number of the barge is high so the flow is turbulent. In addition, the air injection phenomenon implies an added difficulty because it is a need to select a suitable model which is able to capture the effect of the air layer beneath the hull.

3.4 Use of CFD

These tools have application in almost all fields, from medicine to engineering. It also occurs in hydrodynamics where appears in the following fields:

- **Resistance and propulsion:** The CFD applications focus primarily on this field. Here especially, until the end of the 90s was typical to ignore the viscosity effects and waves formation on free surface. This provided simple, fast and more or less accurate calculations. However, with time and since the late 90s, all these effects began to be considered and nowadays are the greatest problems.

- **Maneuverability:** This aspect, is continually gaining in importance with the new IMO regulations after maritime accidents of tankers. Therefore, analysis with CFD tools of flows around the ship appendixes allows calculate the different moments produced in order to evaluate the maneuverability of the vessel.

- **Seakeeping:** there are commercial codes that allow the calculation of ship motions in a particular state of the sea. However, this problem presents a great difficulty since it is necessary to have a mesh of different sizes depending on the wave height and the different characteristics of the sea. As well as a large computational domain that can represent the sea states and wave diffraction phenomena, water aboard deck, etc. Another application in this field is the "Offshore", field with great vision; here the study of wave and wind loads on structures is extremely important in order to get a good design.

- **Design of propellers:** In the field of CFD are used viscous techniques because they allow better performance calculation of propeller for a better approximation to the results of real experiments. Here BEM techniques ("Boundary Element Methods") or other like airfoils are used.

- **Flows within pipes and ducts.**

3.5 Advantages and disadvantages of CFD

The advantages of CFD analysis techniques can be summarized basically in:

- Substantial reduction in time and costs in new designs.
- Ability to analyze systems and conditions that are difficult to simulate experimentally.
- Ability to study systems under dangerous conditions or beyond their operating limits, for example, accidents with toxic substances.
- Detail level practically unlimited. The experimental methods are more expensive as the higher are the number of measuring points, while CFD programs can generate lots of information at no extra cost and with the possibility of parametric studies.
- Added product value. There are graphics generation capacities that allow a better understanding of the results and thank to it stimulate the purchase of the product.

However, all may not be advantages. As the main disadvantages it can be mentioned:

- It requires a great knowledge of the equations that model the physical phenomena; it is needed personal with great knowledge in the field.
- Another disadvantage is that it is not always possible to achieve sufficiently accurate results, leading to large errors in basic issues.
- Simplification of the phenomenon studied with the aim that hardware and software can deal with it. The accurate of result depend on the assumptions and simplifications made.
- The existence of insufficient and incomplete models to simulate the effect of turbulence, multiphase or combustion phenomena, among others.
- Last but not least, the human tendency to believe everything from the computer, especially when results are presented attractively.

Ultimately it can be summarized that the CFD still continue being an aid to other tools of analysis and experimentation, such as wind tunnels or hydrodynamic channels and should therefore be used together with these.

3.6 Classification of CFD tools

Within the naval field, CFD tools can be classified into two groups:

- Those that consider **potential flow**; this means, those flows without take into account the fluid viscosity. It is found here those with and without free surface.

- In the other group it is considered **viscous flow**. Are those flows that consider the viscosity of fluid, this group is divided in those with and without free surface.

3.7 Basic features of CFD programs

Currently, there are a huge variety of programs intended to CFD calculation from free codes to great powerful commercial codes. Nowadays it is possible to group them into several blocks:

- **General codes:** These may include those codes which has tools available at the user's service to: generate the geometry, applying boundary conditions, discretization of the spatial domain (it means, geometry meshing), problem solver, and post process of the results. Examples of this are Tdyn, CFX, Fluent, Phoenix, Open FOAM...

- **Specific codes:** these are destined to every concrete part of the application process of a CFD code. It can be divided in: codes for geometry generation and application of the boundary conditions, codes for geometry meshing, codes for specific calculations and codes for results visualization. There are a huge variety of theses codes as Paraview, ezVIZ, VTK, FieldView...

The general codes are usually divided into three fundamental parts: a preprocessor, a calculation module and a postprocessor. The preprocessor is the part of the program which is responsible of performing all necessary work for a correct calculation of the equations to solve the specific problem.

The calculation module is the part of the program whose function is to solve numerically by certain parts of the equations raised by the preprocessor.

Finally, the post-processor, is the other part of the program which once solved the problem, it is responsible for displaying in a graphical or similar way, the results of the calculation.

3.8 Initial considerations

As previously stated, CFDs are a tool that helps to solve the equations that describe the movements of the fluid, which, for the most part, cannot be solved analytically. Therefore, its objective is searching for an approximate solution of the equations that govern the movements of fluids, discretizing the calculus domain and solving the equations there.

For that reason, any numerical scheme must have a number of factors in order to reach results: convergence, consistency, stability; these properties however do not guarantee that the final solution obtained is the closest to the real. Anyway during the numerical simulations both in ANSYS and Tdyn code will be taken into account all these factors.

Moreover, it should be noted that the progress made in mesh generation, from classical regular grids of finite difference to unstructured meshes, to local mesh refinements, to the mesh body adjusted, or adaptive meshing. All of them contribute to the improvement of numerical methods and increasing approximation of the solutions obtained. The grid resolution must be quite higher at and near the interface, i.e., close to the holes, the bottom of the barge and free surface. It consequently requires more computational time for the calculations but it is indispensable to catch the effect of air spreading beneath the hull.

Regarding the turbulence model, it may have a dramatic influence, as shown later, in the accuracy of the results obtained. So, next points show an introduction to turbulent flow and suitable turbulence models for this case.

3.9 Introduction to turbulent flow

Apart from care about setting the turbulent flow boundary conditions required by the simulation software used, a good physical understanding about what turbulent flow is has vital importance to understand the problem.

Actually most of the processes around life are turbulent, from airflow around vehicles to water running from a tap. Everything is surrounded by turbulent flows. But, what does turbulence mean? since most flows are invisible, this makes it difficult to see a turbulent flow. However, some turbulent flows are visible like the one shown below.

Figure 3.2: A smoke plume rising from a candle in a room where the ambient airflow is completely still.

Figure 3.2 is an example of visible turbulent flow. Smoke rises from the candle flame due to buoyancy. The smoke rises upward in a straight line, but its behavior changes at a certain point when the flow becomes turbulent. If the movement of the plume at this transition point is closely inspected, some eddies (regions where the plume recirculates upon itself) will be seen starting where the flow becomes turbulent. These movements occur because the momentum of a flow (inertia force) is larger than the force acting against the flow (viscosity).

When the inertia forces of the fluid moving are very low, the viscosity is the dominant force and the flow is laminar. In the other side when the inertial forces dominate, the flow is turbulent. Reynolds established a relationship that sets the type of flow that has a particular problem. Turbulence is a regime in which the properties of a fluid in a stationary state manifest in a random and

chaotic way. Even in fluids where main pressures and speeds occur in a 2-D space, fluctuations troubled always have a three-dimensional character.

With respect to turbulence models, no method can be considered better than the rest so it will be proven various turbulence models in order to produce better and more reliable results in relation with the ones obtained during experimentation test.

3.10 Turbulence models

It is not surprising that the methods to study the turbulence are still today being investigated. There are three methods to predict this turbulent flow which are based on different applicable models:

1. **RANS-based turbulence models.** The objective of the turbulence models for the RANS equations is to compute the Reynolds stresses. The best known are $\kappa - \varepsilon$ and $\kappa - \omega$. This method requires modest calculation capabilities. Even if this approximation is not as exact as the following two methods, it is the most used by engineers.

   It is noticeable that are used for this case two models bases on this method.

2. **Large eddy simulation (LES).** Is a mathematical model for turbulence used in computational fluid dynamics. This would be like the intermediate term of the turbulence calculation of which represents behavior of larger scale eddies. The domain mesh must be much smaller than models based on RANSs, it requires short time intervals. Also it is required much memory and computational cost but nowadays this method is gaining importance, overall in the case of complex geometries.

3. **Direct Numerical Simulation (DNS)**. This technique is able to solve all types of fluctuations in addition to the main flow. However, is computationally expensive, and its cost is prohibitive for simulation of practical engineering systems with complex geometry or flow

configurations, such as turbulent jets, pumps, vehicles, and landing gear. The use of this model is reserved only to research with high capacity computers.

Boussinesq's approximation for RANSs

In 1877, Boussineq proposed that Reynolds stresses could be proportional to the main deformation ranges. Using this approximation, the 6 known stresses became two unknown variables, μ_t and k. These two unknown variables used for the resolution of turbulence models are the Eddy viscosity and the turbulent kinetic energy.

The number of equations necessary to determine these two unknown variables depends on the type of model chosen.

No. of equations	Model
1	Spalart Allmaras
2	κ – ε (Standard, RNG and Realizable)
	κ – ω (Standard, SST)
7	Reynolds Stress

Table 3.1: Examples of turbulence models according to the number of additional equations.

To summarize, Spalart Allmaras, ILES and κ – ε are the turbulence models chosen to simulate the barge. The choice was made according to the appropriate behavior of the equations that govern the physical model.

The advantage of a two equation model (κ – ε) over the one equation model (Spalart Allmaras) is that it allows to determine independently the fluctuations and length scale of eddies.

3.11 Introduction to VOF model

The problem of free surface is one of the main obstacles in the computation with CFD in marine hydrodynamics. These flows are encountered in many different applications but the most important here is the flow around a ship. This problem can be studied from several points of view: potential flow and viscous flow.

The free surface problem can be considered as a particular case of a more general problem, the prediction of the interface between two immiscible fluids: a flowing liquid (usually water) and air. The calculation of the interface between two immiscible fluids is difficult because neither the shape nor the position of the interface is known a priori.

To solve the free surface problem, the most common method used in CFD programs based on the finite volume method (see 3.12 FVM) is the volume-of-fluid (VOF) model. From the point of view of viscous flow is found the methods of tracking the interface (Figure 3.3) and those which capture the interface (Figure 3.4). The most common representatives of the last one class of approaches are the level set and the volume of fluid method.

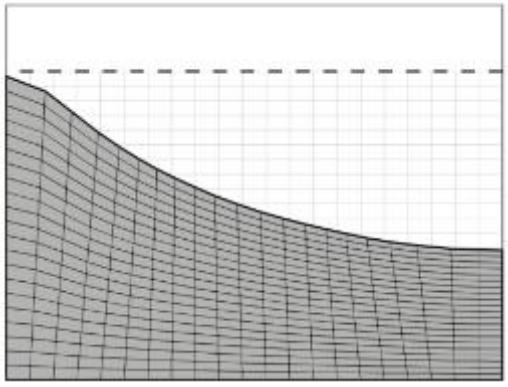

Figure 3.3: In interface tracking the moving interface is explicitly described by the computational mesh.

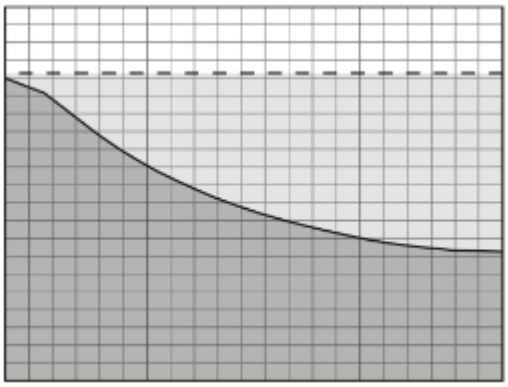

Figure 3.4: Interface capturing methods use an artificial scalar field for an implicit description of the interface.

VOF method belong to interface capturing method where the fluids are considered as one and the position of each phase of the fluid is described by the assigning a fraction of the total volume with a number between 0 and 1.

The Volume of Fluid (VOF) model is a free surface modeling technique. It is a direct method of predicting interface shape between immiscible phases. It can model two or more immiscible fluids by solving a single set of momentum equations and tracking the volume fraction of each of the fluids throughout the domain. An application of this model includes the motion of large bubbles in a liquid and the steady or transient tracking of any liquid-gas interface.

This Eulerian method has some restrictions in the code ANSYS Fluent:

- The VOF model uses only the pressure-based solver.
- All control volumes must be filled with either a single fluid phase or a combination of phases. The VOF model does not allow for void regions where no fluid of any type is present.
- Only one of the phases can be defined as a compressible ideal gas. There is no limitation on using compressible liquids using user-defined functions.
- Streamwise periodic flow (either specified mass flow rate or specified pressure drop) cannot be modeled when the VOF model is used.
- The second-order implicit time-stepping formulation cannot be used with the VOF explicit scheme.

The VOF formulation in Fluent is generally used to compute a time-dependent solution, but for problems in which is concerned only with a steady-state solution, it is possible to perform a steady-state calculation. A steady-state VOF calculation is sensible only when the solution is independent of the initial conditions and there are distinct inflow boundaries for the individual phases. For example, the flow of water in a channel with a region of air on top and a separate air inlet can be solved with the steady-state formulation.

The VOF formulation relies on the fact that two or more fluids (or phases) are not interpenetrating. For each additional phase added to the model, a variable is introduced: the volume fraction of the phase in the computational cell. In each control volume, the volume fractions of all phases sum to unity. The fields for all variables and properties are shared by the phases and represent volume-averaged values, as long as the volume fraction of each of the phases is known at each location. Thus the variables and properties in any

given cell are either purely representative of one of the phases, or representative of a mixture of the phases, depending upon the volume fraction values. In other words, if the q^{th} fluid's volume fraction in the cell is denoted as α_q, then the following three conditions are possible:

- $\alpha_q = 0$ → The cell is empty (of the q^{th} fluid).
- $\alpha_q = 1$ → The cell is full (of the q^{th} fluid).
- $0 < \alpha_q < 1$ → The cell contains the interface between the q^{th} fluid and one or more other fluids.

Based on the local value of α_q, the appropriate properties and variables will be assigned to each control volume within the domain.

Multiphase flows can be numerically calculated using either Euler-Lagrange approach or Euler-Euler approach. VOF is a type of Euler-Euler approach; it is basically a surface tracking technique. Usually used if there are more than two immiscible fluids, where interface position is of importance.

It has only one set of momentum equations, shared by all fluids and volume fraction of each of the fluid in each computational cell is tracked.

To summarize, VOF method is an advection scheme, it will be useful for the study focused on interface tracking, i.e., to study the shape and the location of the interface between the air layer and surrounding water, but it is not a standalone flow solving algorithm. Otherwise mixing study can be modeled using a mixture model.

3.12 FVM (Finite Volume Methods)

This method is used for both temporal and spatial discretization of the problem in question. The continuum is divided, by imaginary lines or surfaces, into a number of elements connected to each other by nodes. However, they integrate the conservation of mass and momentum equations over the entire cell before approaching the value in the central node. In this way, the error committed on the output side is allowed to be canceled with the error of the neighboring face, allowing the conservation of mass and momentum. For this reason, many commercial codes (ANSYS Fluent) use this method for the resolution of the equations.

3.13 ANSYS

In this part, the software ANSYS Fluent (v.14 & v.15) is used to calculate the drag resistance of the model. Fluent is a module included inside the ANSYS package. This software suite is one of the most attractive general purpose codes on the market and also results in one of the most widely used application codes worldwide, in companies, universities and research centers. Nowadays ANSYS is the reference in the world of numerical simulation of fluid flows, mechanical problems and resistance of materials, and electromagnetic fields.

Fluent uses the Finite Volume Method (FVM) which is one of the most versatile discretization techniques used in CFD. Firstly, in this method based on the control volume formulation of analytical fluid dynamics, the domain is divided into a number of control volumes (aka cells, elements) where the variable of interest is located at the centroid of the control volume.

In the next step, the differential form of the governing equations is integrated (very similar to the control volume approach) over each control volume. Interpolation profiles are then assumed in order to describe the variation of the concerned variable between cell centroids. The resulting equation is called the discretized or discretization equation. In this manner, the discretization equation expresses the conservation principle for the variable inside the control volume.

The resulting solution with this method satisfies the conservation of quantities such as mass, momentum, energy, and species.

It is carried out the simulation of flow filed with free surface near the short barge model in the case without air lubrication due to the difficulties encountered in implementing the phenomenon of air injection below the hull.

This software was studied from the beginning of the thesis in a self-taught way. But it has not been enough to get results because of the extensive knowledge of the software needed. So the second CFD code will solve this problem because is already known thanks to subjects taught at UPCT.

3.13.1 Pre – processing

- **ANSYS Workbench**

This is a project-management tool. It can be considered as the top-level interface linking all the software tools. Thanks to this interface is easy to handle the passing of data between the different applications to develop the towing analysis.

Once ANSYS Software is open, it is found a sidebar where can be chosen the module, in this case, FLUENT is selected for working with fluid flow. Also it would be possible to use the module CFX or POLYFLOW.

After choosing the module, a chart box appears with different applications: Geometry, Mesh, Setup, Solution and Results. The following figure shows an overview of the workbench chart.

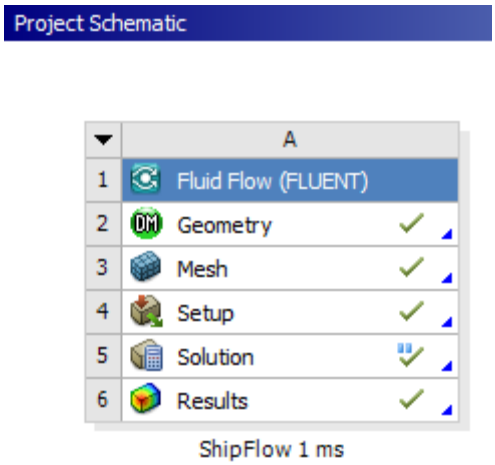

Figure 3.5: Workbench of ANSYS FLUENT.

- **ANSYS Design Modeler – Geometry editor**

The next step is to import the geometry created in Rhinoceros software. It has the peculiarity of being a solid instead of a surface which allows making a Boolean subtraction to the parallelepiped and creating a hole in the prism, in that way the control volume is created (see Figure 3.6). Previously it has to be defined the dimension of parallelepiped and these are the same in width and depth that the towing tank used for the experimental tests. Upstream and downstream is large enough to allow the flow development.

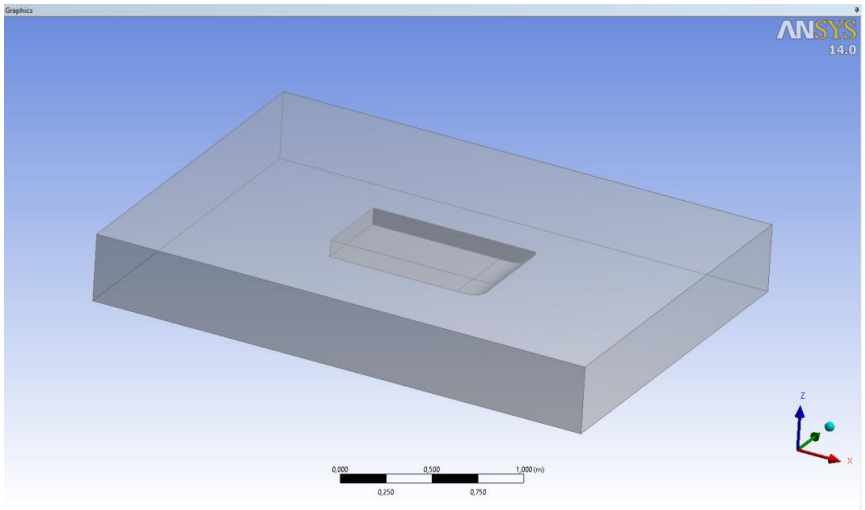

Figure 3.6: Geometry and control volume after the Boolean subtraction.

➢ ANSYS Meshing

Basically a mesh is the discretized representation of the geometry in question. To this case it was opted by test both meshing options, a structured and unstructured meshing and try which one best adjust to reasonable results. It is not necessary to perform a study of the convergence of the meshes because the barge shape is simple and there are no large requirements to adjust the mesh. Finally, it was chosen the second meshing because this type of meshing is an advantage in the cost of working time because is automatically generated using tetrahedrons and triangles surfaces and it produces good results as well.

Below there are details of the mesh around the outline of the barge where the difference between the two types is evident and easily visible:

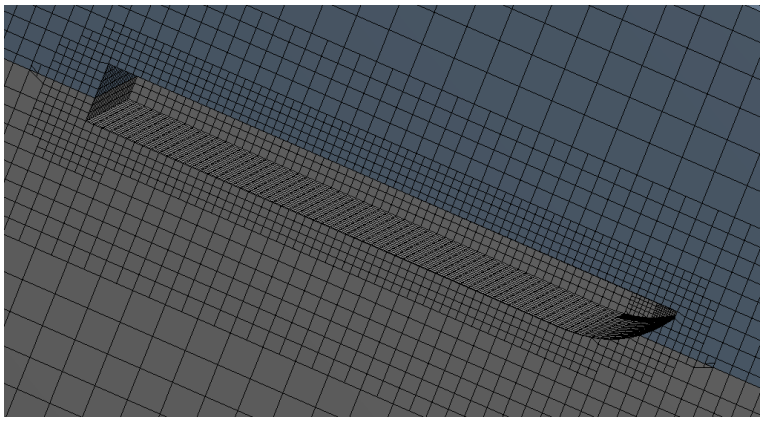

Figure 3.7: Detail of assembly meshing with CutCell method.

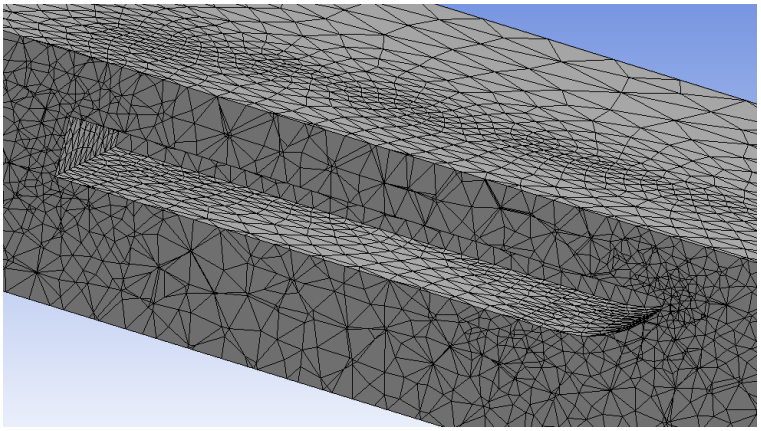

Figure 3.8: Detail of assembly meshing with Tetrahedrons method.

The meshing process is the one that have the greatest influence on the result, so a quality mesh is required. A compromise solution for the case studied here would be the mesh of Figure 3.9, as it is not too tedious to work and get quick results.

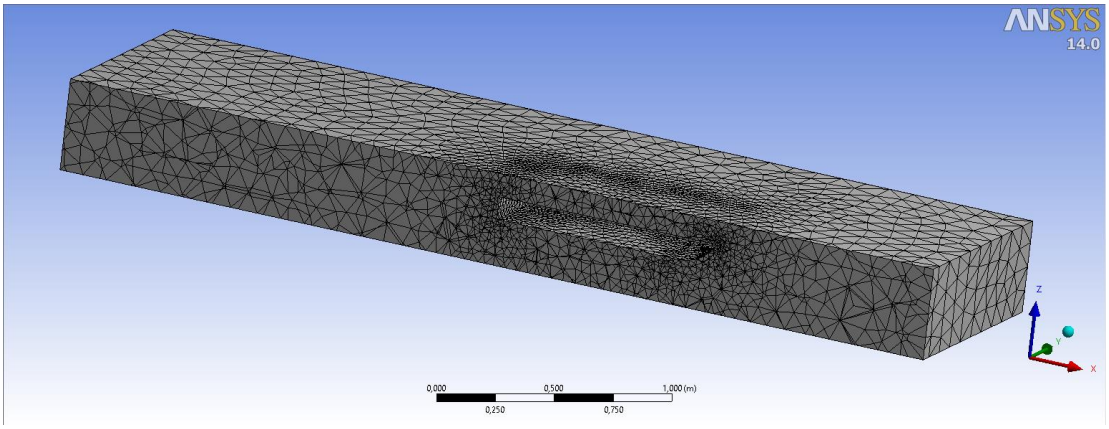

Figure 3.9: Cut of the control volume by the symmetry plane.

Previously to the mesh generation, in the control volume was defined all the relevant surfaces such as mass flow inlet, outlet, symmetry condition and ship surface.

The fact of having simple hull geometry was not considered for making a structured mesh because during the use of the second software, it will work with unstructured meshes. In this way the preparation of the simulations is equalized as much as possible to compare them.

3.13.2 Calculation

- **ANSYS Setup**

Fluent requires solver settings which tell it how to calculate the solution. The purpose of these settings is to achieve the accuracy, stability and convergence of the problem.

Within the problem setup, different options are found in the sidebar. This towing analysis is a problem with two phases so it is chosen the *Volume of Fluid* model for multiphase. It is important to check the gravity option because is an external influencing force.

Besides it was used an implicit discretization scheme with time steady for the resolution of the volume fraction equation. The equation of the volume fraction in this scheme requires that its values be in the current time interval (unlike the explicit scheme, which needs the previous time interval). Because of this, a scalar transport equation is solved iteratively for the volume fractions of the secondary phase at each time interval. Spatial discretization for free surface representation has been set as BGM (Bounded Gradient Maximization), in order to accurately recreate the interface between phases, From the maximization of the local volume fraction gradient. Since this method is only applicable for steady state simulations, the Modified HRIC (High Resolution Interface Capturing) has been used for real-time simulation.

The turbulence model chosen is an improvement of the Standard k-epsilon viscous model. The choice was the Realizable $\kappa - \varepsilon$ model because it produces reasonable results as has been demonstrated in the simulations carried out with Tdyn CFD. These simulations are available in the Section 3.14. This model offers several treatments, being the "Standard Wall Functions" the designated in this work.

The materials involved in the calculation were then assigned, such as the air and water phases, as well as their relative positions with respect to the Z axis, i.e. free surface position, density and other properties. The air is fixed like the primary phase for being the material of lower density. The draft of the barge is fixed with to the position of the free surface.

The boundary conditions are set in the wall of control volume. In the inlet surface, mass flow of water and air are established according to the towing velocities considered for the calculus which obviously are the same than in the experiments. Intensity and length scale for turbulence are assigned also.

With the aim to facilitate the convergence of the calculations made, some other specific parameters are established such as limits for the turbulence viscosity ratio, open channel initialization method, body force weighted for spatial discretization, high order term relaxation, pressure-velocity coupled with volume fractions, etc.

Before running the calculation some initialization Parameters related to velocity and pressure as fluid settings for air and water are set.

The calculation process was limited to 11000 iterations with a time step of 0.01 s. It was added monitors (like mass flow rate,) by means of control points to evaluate the convergence of the forces acting on the barge.

When it was decided that convergence was good enough, the iterative process was stopped to obtain the final answer. In this way time was saved and it was not necessary to reach the 11000 iterations fixed.

The Figures 3.10 and 3.11 show details of one calculation process where is visible how it ends with around just 3000 iterations.

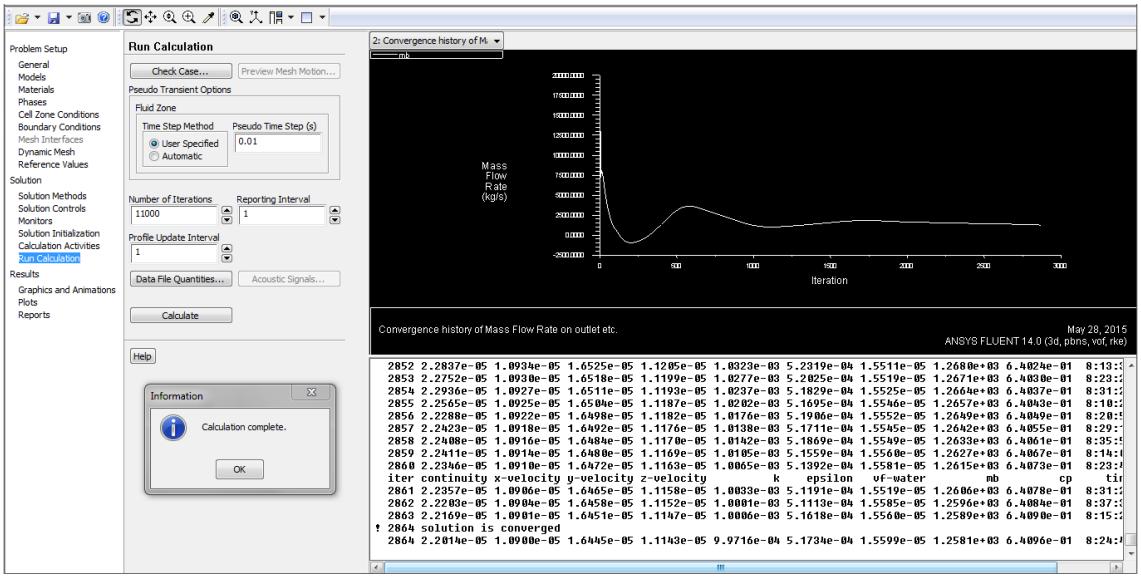

Figure 3.10: Convergence history of Mass Flow Rate on outlet.

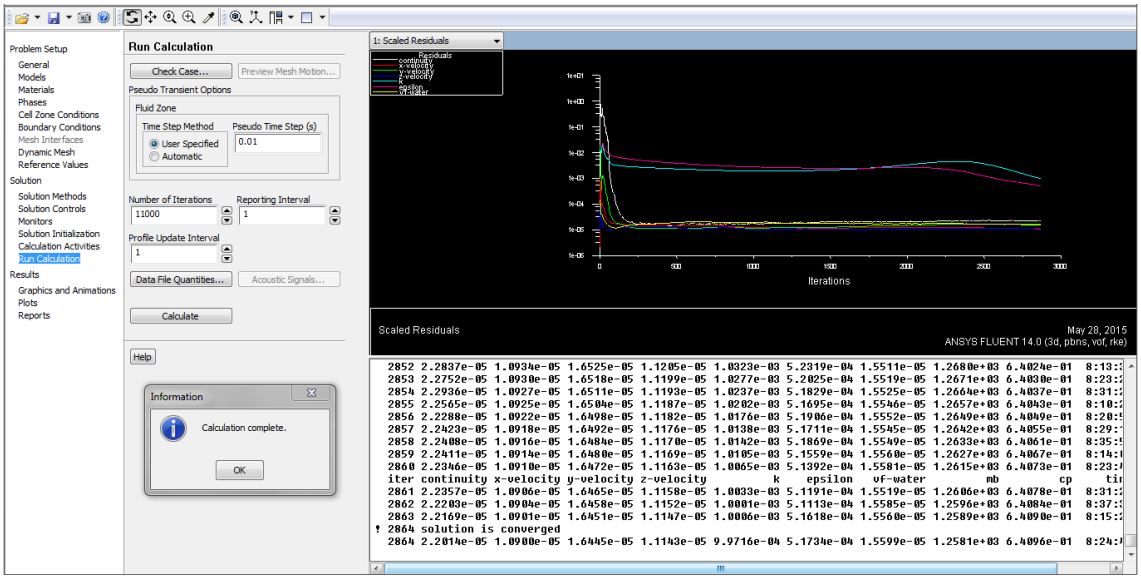

Figure 3.11: Scaled residuals where is visible the continuity and convergence of the calculation.

The solution was reviewed in order to validate the results and be able to obtain useful information. For that purpose, these results are compared to those obtained during experimentation.

Different simulations were developed, each raised in the same way but with the different towing speeds.

3.13.3 Post – processing

- **ANSYS Results**

The last application is referred to the results of the calculus. Here can be seen the values of the flow velocity, the pressures on the surface of the hull, the profile of waves and other visualizations.

The most interesting here are the values of the drag resistance, so this information is obtained reading the report created after the simulation (in the tab "forces and torques"). The values of the tangential and normal forces on the surface of the hull are given for all directions of the Cartesian axes (X, Y, Z), but only have interest those of the X axis. The flow pattern around the barge for one case of the simulations can be seen in the Figures 3.12 and 3.13.

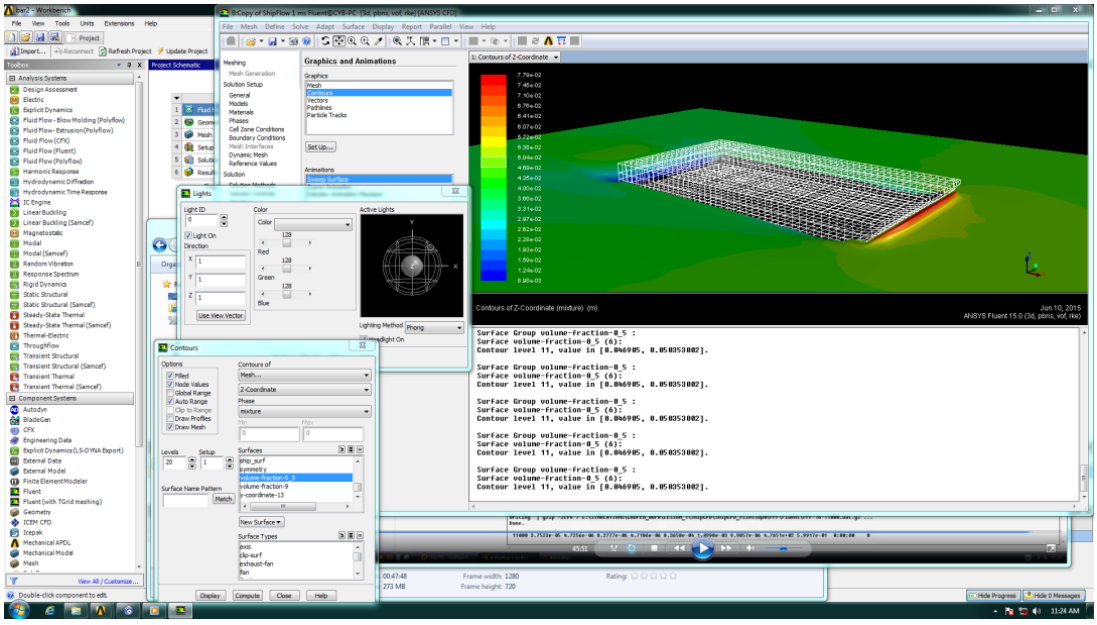

Figure 3.12: Contours of the multiphase between air and water.

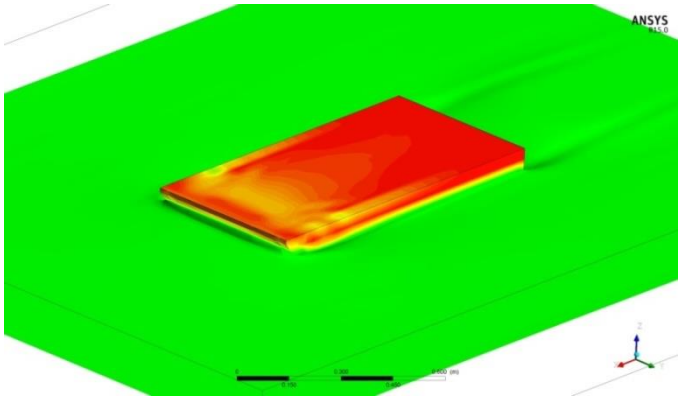

Figure 3.13: Display shows the flow pattern around the barge.

Finally, is remarkable that, parallel to the experimental tests, was investigated the simulation of the air injection through the bottom holes of the barge.

The flow around an air injection at the hull bottom was conducted using FLUENT 6.3 because was the first version of this software installed on the PC lab. A cylindrical hole is defined in right angle to the flow as shown in the figures below; the grid was made with the meshing program Gambit. These were the software on which was begun to study the simulation of this phenomenon. Fluent was at that version a separated module from ANSYS, afterward thank to

the complete package of version v.14 and later, all the tools are available in the workbench.

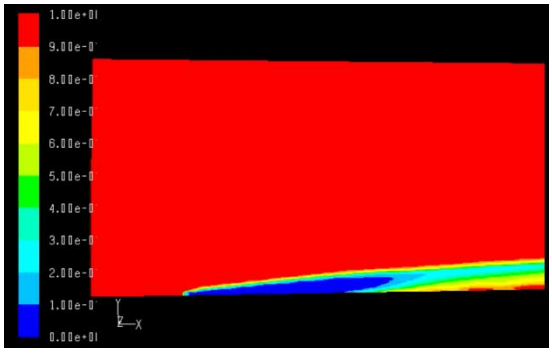

Figure 3.14: Top view of air spread flow in water from a single air injection.

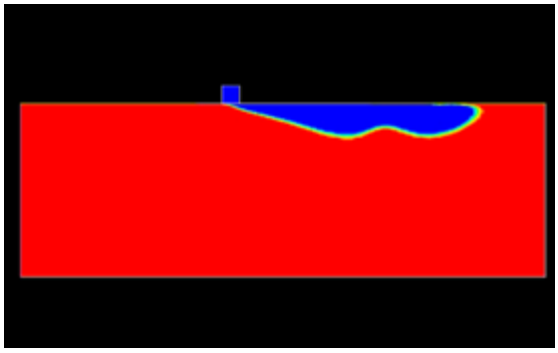

Figure 3.15: Side view of air spread flow in water from a single air injection.

These screenshots allow visualizing pressure and velocity contours of the air layer giving an idea of the spreading in a V shape as it happened in the experiments.

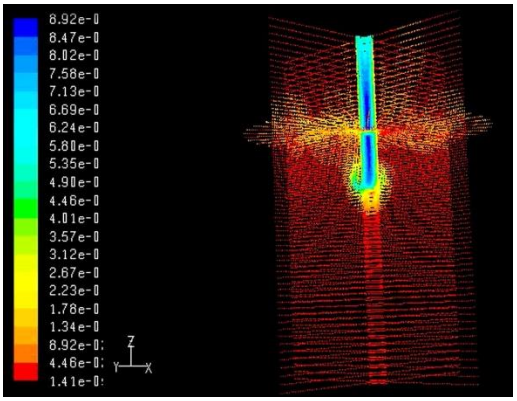

Figure 3.16: Velocity vectors of the mixture.

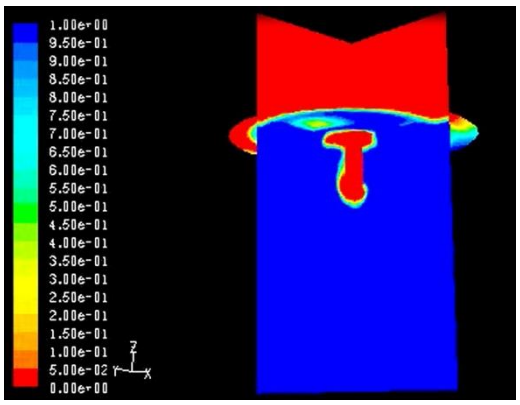

Figure 3.17: Contours of volume fraction.

As has already been mentioned, due to the difficulties encountered in implementing the phenomenon of air injection, this was conducted with a single pipe in a qualitative way without getting any relevant result, just trying to find a way of simulate the air-lubrication case but without success, so Tdyn code will help in this goal.

The final results of drag resistance calculated by ANSYS Fluent are shown in the Section IV – Results comparison where these are well organized to contrast them with those from experimental tests and Tdyn CFD software.

3.14 Tdyn CFD

This general code software has been chosen to calculate the drag resistance of the model because it was used in the subject of hydrodynamics taught at UPCT as part of the master program. In addition, it has specific naval modules and it allows enjoying the full features with a free license of 3 months.

Tdyn CFD is an environment for multi physics simulation that uses a stabilized finite element method. It includes different modules that allow solving problems of Heat Transfer in both solids and fluids, Turbulence, Advection of Species in fluids and solids and Free Surface (Transpiration or Odd Level Set method) using the same stabilized scheme mentioned above. Also includes a complete environment for geometry and data definition, and post-processing of the analysis results, based in the Custom GiD system.

The analysis of a problem by means of Tdyn CFD consists of the following basic steps (see Figure 3.18):

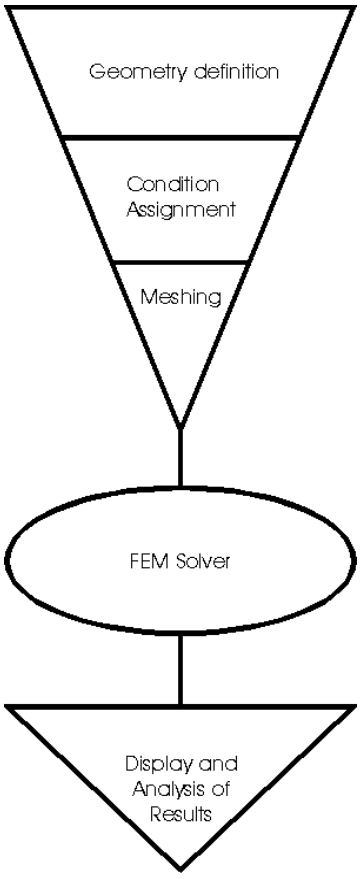

1. Pre – processing

- Creation (or importation) of the geometry to be analyzed.
- Assignment of the material properties as well as the boundary conditions and definition of general data.
- Mesh generation.

2. Calculation

3. Post – processing

Fig. 3.18: Steps in any FEM problem.

Basically will take place in this part of the thesis a towing tank test using the NAVAL capabilities of the Compass FEM suite. A brief review of the simulation process would be the one shown below:

On the one hand, it will be necessary to have a model that describes the physical phenomenon, so that the computer is able to solve the equations in the different elements in which the continuum will be divided. The geometry is divided in order to facilitate the resolution of the model because it is not possible to work with the continuous fluid field so it should be spatially discretized.

On the other hand, when the phenomenon is governed by equations that depend on the time, it is not possible either to study the phenomenon continuously, so it will be required a time discretization.

Finally, from the equations of government it will be eliminated those terms that are not necessary, so another level of approximation is added called dynamic approximation.

It is shown in the following points the process step by step and full explanations to predict the drag resistance of the barge models with the software Tdyn. The results will be exposed at the end and compared with the experimental results.

3.14.1 Modeling of the physical phenomenon

The first step is to take into account some initial considerations. Getting a good estimation of drag resistance using CFD tools is a time-consuming process of computing; besides the treatment way of the air-lubrication phenomenon will have consequences in the results obtained. Hence, it is vital to make the necessary assumptions and simplifications for get a stable and computationally feasible calculation.

The calculation of the interface between two immiscible fluids (water and air in this case) is difficult because neither the shape nor the position of the interface is known a priori. Therefore, the air layer created beneath the hull by

the air flow injected through the bottom holes will be simplified in a biphasic mixture between the air flow and surrounding water.

It has incorporated to this case the transport problem resolution associated with the partial air density which is the independent variable of the biphasic mixture model employed for modeling the air flow injected through the barge. In that way, the air-lubrication phenomenon is supposed like a diffusion of the air injected in the water flow and thanks to the available modules within Tdyn CFD package is possible to work with the advection of the air in the fluid. To go deeper into the mixture model used, a summary is available in the section **3.14.2 Mixture model.**

As usually, one of the main issues is to adjust turbulence initial parameters as these have considerable influence both on the results as in convergence of the model. Alike, is noteworthy analyze what is the most suitable value for the diffusion coefficient (k).

Normally the more practical turbulence model is chosen, but in this case it will be chosen the one that generates more accurate predictions. To study which model best fits the problem, simulations will be performed with the three models chosen (Spalart Allmaras, ILES and κ – ε). The results of each model of turbulence can be compared to the experimental results, so it will be a great help to make the choice.

Coming back to diffusion coefficient (k), it will be proved several values with the aim of doing a fair judgment. These values are shown in Table 3.2 next to the turbulence models tested. They are quite bigger compared to the real value of the air diffusion in water (around $1 \cdot 10^{-5}$) but the problem is that if these values go down quite, the convergence is lost.

Turbulence models	Spalart Allmaras - ILES - κ – ε
Diffusion coefficient -> k	0,01 - 0,05 - 0,1

Table 3.2: Turbulence models and Diffusion coefficients tested.

Up to this point, it is considered an air diffusion phenomenon for the experiment during numerical simulations. Through experimentation can be seen that real case consists of an air layer with random and dispersed air bubbles transported by the inlet water flow. So, the value of this coefficient is an open discussion since the actual process does not respond to a process of pure diffusion. In consequence, in this case may be a bit arbitrary because is not a pure diffusion phenomenon, so these values of the coefficients have been chosen because the results are reasonable.

Once the diffusion coefficient parameter is set, the turbulence models will be tested to choose the appropriate one. Spalart Allmaras was chosen in the first tests because it is usually more robust. However, it may not be the most suitable for this problem since the injection of air through the holes will resemble a jet and it is well known that the model of Spalart Allmaras is not the most suitable to solve the turbulence in jets. Anyway, all of these questions will be clarified along the following points.

3.14.2 Mixture model

Here the mixture model used to simulate the process of air discharge in water is described. For this purpose, it is considered that the problem to solve responds to a two-phase flow. In this context, the mixture density is defined as:

$$\rho_m = \frac{m_A + m_B}{V} \qquad \text{Eq. (3.4)}$$

being m_A the mass of A specie (air in this case) and m_B the mass of B specie (water in this case). The partial densities of the two mixture components are defined in turn as:

$$\rho'_A = \frac{m_A}{V};\ \ \rho'_B = \frac{m_B}{V} \qquad \text{Eq. (3.5)}$$

so that the mixture density can be expressed in terms of the partial densities:

$$\rho_m = \rho_A{}' + \rho_B{}' \qquad \text{Eq. (3.6)}$$

Such partial densities are not independent of one another but are related as follows:

$$\rho_B' = \rho_B \left(1 - \frac{\rho_A{}'}{\rho_A}\right) \qquad \text{Eq. (3.7)}$$

so it can be taken $\rho_A{}'$ as an independent variable of the problem. In fact, it will identify the partial density of the mixture secondary component $\rho_A{}'$ as variable or ϕ specie whose transport equation must be solved together with the Navier-Stokes equations for mixing. Such transport equation takes the form:

$$\frac{d\rho_A'}{dt} + (v \cdot \nabla)\rho_A' - \nabla \cdot (k \cdot \nabla \rho_A') = 0 \qquad \text{Eq. (3.8)}$$

where v is the mixture velocity and k is the total diffusion coefficient of air in the water.

From the above definitions it can be developed the expression of the mixture density as follows:

$$\rho_m = \rho_A' + \rho_B' = \rho_A' + \rho_B \left(1 - \frac{\rho_A{}'}{\rho_A}\right) = \frac{m_A}{V} + \frac{m_B}{V_B}\left(1 - \frac{m_A/V}{m_A/V_A}\right) = \qquad \text{Eq. (3.9)}$$

$$= \rho_A \frac{V_A}{V} + \rho_B \left(1 - \frac{V_A}{V}\right)$$

from where it finally follows the following mixture law for the density:

$$\rho_m = \rho_A \cdot a_v + \rho_B \cdot (1 - a_v) \qquad \text{Eq. (3.10)}$$

being $a_v = V_A/V$ the volume fraction of the mixture secondary component.

On the other hand, it can be defined the mass fraction of the secondary component as:

$$a_w = \frac{m_A}{m_A + m_B} = \frac{\rho_A' \cdot V}{\rho_A' \cdot V + \rho_B' \cdot V} = \frac{\rho_A{}'}{\rho_A' + \rho_B{}'} = \frac{\rho_A{}'}{\rho_A' + \rho_B \left(1 - \frac{\rho_A{}'}{\rho_A}\right)} \qquad \text{Eq. (3.11)}$$

the mass fraction is defined once the transport equation for $\rho_A{}'$ is solved.

Finally, the volume fraction a_v can also be associated directly with the weight fraction thus being also determined by the solution of $\rho_A{}'$.

$$a_v = \frac{V_A}{V_A + V_B} = \frac{m_A \cdot \rho_B}{m_A \cdot \rho_B + m_B \cdot \rho_A} = \frac{\rho_B}{\rho_B + \left(\frac{1-a_w}{a_w}\right)\rho_A} = \frac{1}{1 + \left(\frac{1-a_w}{a_w}\right)\frac{\rho_A}{\rho_B}} \quad \text{Eq. (3.12)}$$

Once known the volume fractions, all the physical properties of the mixture (density, viscosity, and thermal properties if necessary) can be expressed by the same mixture rules:

$$\rho_m = \rho_A \cdot a_v + \rho_B \cdot (1 - a_v)$$

$$\mu_m = \mu_A \cdot a_v + \mu_B \cdot (1 - a_v) \quad \text{Eq. (3.13)}$$

The resolution of the problem will then be as follows:

1. Solving the transport equation Eq. (5) for the partial density of air

$$\frac{d\rho_A'}{dt} + (v \cdot \nabla)\rho_A' - \nabla \cdot (k \cdot \nabla \rho_A') = 0$$

2. Calculate the partial density of water and the weight and volume fraction of air Eq. (4), Eq. (8) and Eq. (9)

$$\rho_B' = \rho_B \left(1 - \frac{\rho_A'}{\rho_A}\right)$$

$$a_w = \frac{\rho_A'}{\rho_A' + \rho_B'} = \frac{\rho_A'}{\rho_A' + \rho_B \left(1 - \frac{\rho_A'}{\rho_A}\right)}$$

$$a_v = \frac{1}{1 + \left(\frac{1-a_w}{a_w}\right)\frac{\rho_A}{\rho_B}}$$

3. Calculate the velocity field by solving the Navier-Stokes equations for a fluid with properties corresponding to a biphasic mixture given by:

$$\varphi = a_v \cdot \varphi_A + (1 - a_v) \cdot \varphi_B$$

being a_v the volume fraction of air.

3.14.3 Pre – processing

This stage of the simulation includes the preparation of the geometry; basically the barge models will be imported from another specific program of computer aided drawings. Thereafter, properties are assigned: material, boundary conditions and definition of the general data of the case to be studied. The last step concerns the meshing of the domain.

- **Input data**

A summary of input data with the main dimension of the barge models (short and long) is found in Table 3.3. Moreover, the characteristics of the fluids (air and water) are shown, in this case the simulation was carried out under the conditions of towing tests, i.e. the fluid is fresh water (15 ºC). Likewise, towing velocities and air flow injected are the same than in model experiments.

Input data	Short Barge	Long Barge	Unit
Length waterline	0,95	1,85	m
Wet surface	0,55	1,04	m^2
Density of water	1000		kg/m^3
Kinematic viscosity of water	1,14E-06		m^2/s
Density of air	1,23		kg/m^3
Kinematic viscosity of air	1,46E-06		m^2/s
Gravity	9,81		m/s^2

Table 3.3: Input data for both barge models.

- **Initial data**

Once the software is open, a window appears in order to choose the type of problem required within the fluid dynamics simulation. Between all available modules, a fluid flow analysis in 3D is chosen in addition to others (see Figure 3.19). Fluid flow is able to solve incompressible or slightly compressible fluid flow problems, including turbulence effects (RANS equations).

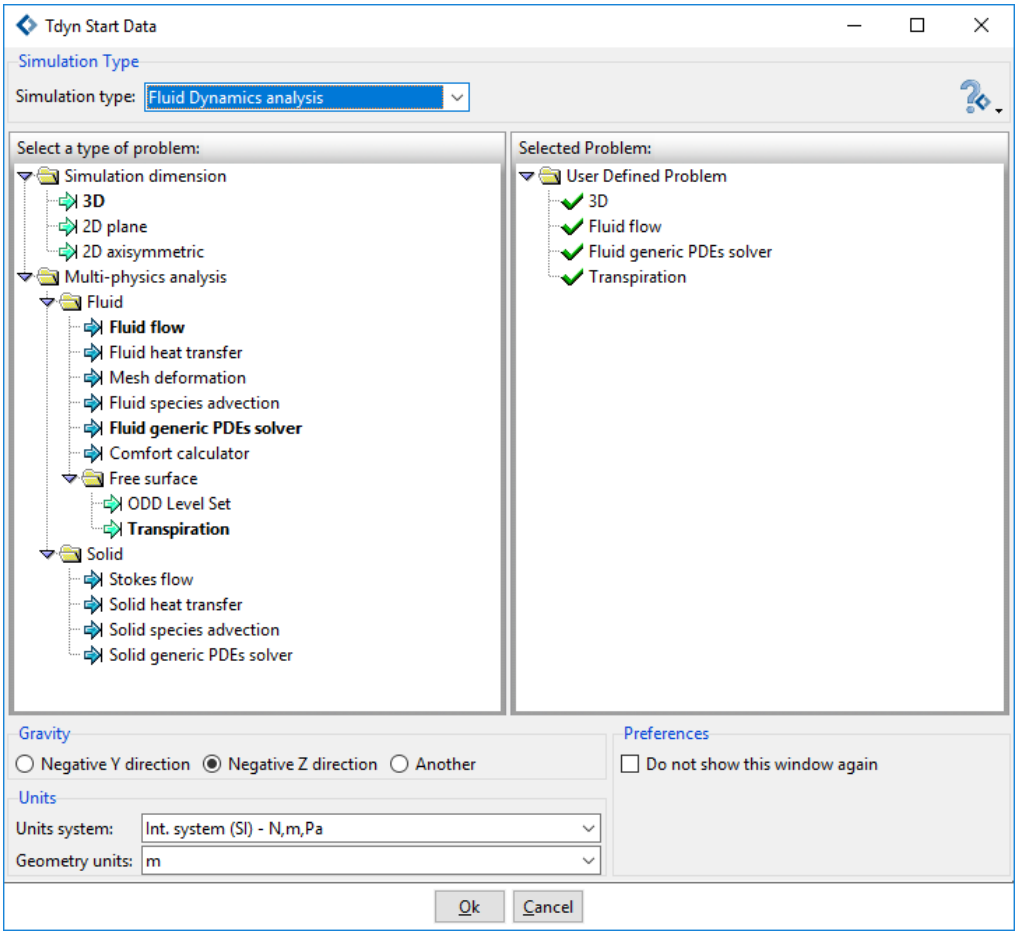

Figure 3.19: Definition of the problem within start data window of Tdyn.

The Transpiration Free Surface Analysis of Tdyn CFD+HT were specially designed for the simulation of the towing test of ships. This module is able to solve free surface equations, based on the transpiration technique and is especially adequate to solve naval hydrodynamics problems like the one that is going to take place here.

By using Tdyn CFD it is also possible to work with a PDE's solver module which is able to solve user defined partial differential equations (PDE) problems. This module allows defining a number of new variables (called φ-phi problems) and specifying and solving the differential equation that governs its behavior. New user-defined problems can be coupled among them or with any other variable (i.e. velocity, pressure, temperature …) used in Tdyn CFD+HT. So, this module was chosen to work with the transport equation for the partial density of air.

- **Creating or importing the geometry**

There are two options for introducing the geometry to work on:

1. To create the geometry with Tdyn.
2. To import the geometry from other platforms.

Tdyn allows creating lines and surfaces to build the model, although is also possible working in other CAD design programs such as Rhinoceros or SolidWorks. In this case, a digital model of the short barge was created with Rhinoceros 5.0. It allowed save time because these programs are more productive than the solution available in Tdyn.

Moreover, Tdyn supports a lot of file formats so there is no problem importing the geometry, only a few considerations will be taken into account at the time of import the geometry. Design programs often duplicate lines and surfaces so the model must be checked before it is imported. Once the file ".igs" from Rhinoceros is imported, all these duplicated surfaces, lines or layers can be eliminated with the tools available in Tdyn interface. Also is recommendable to collapse all the necessary points, lines and surfaces, this option is available both in the CAD programs and Tdyn CFD.

- **Control volume**

The control volume where the software solves the equations has the same dimensions in width and depth that the towing tank of TUV Varna in order to keep the numerical simulations as similar as possible to model experiments. This also contemplates the free surface and has to be large enough for the flow to develop freely. An appropriate control surface size would be as follows:

Control volume	Short Barge	Long Barge
Length waterline	0,95	1,85
Upstream (afore) - 70% L	0,7	1,3
Downstream (astern) - 140% L	1,4	2,6
Width	1,70	
Depth	0,41	

Table 3.4: Control volume dimensions in meters.

The distance downstream of the control volume is greater to allow the wake left by the vehicle to develop freely. After introducing the points that form the vertices of the control volume and joining these by means of lines, it was created the surfaces and finally the control volume taking into account the interior volume of the barge as is visible in the Figure 3.20. This construction process is required for both barge models.

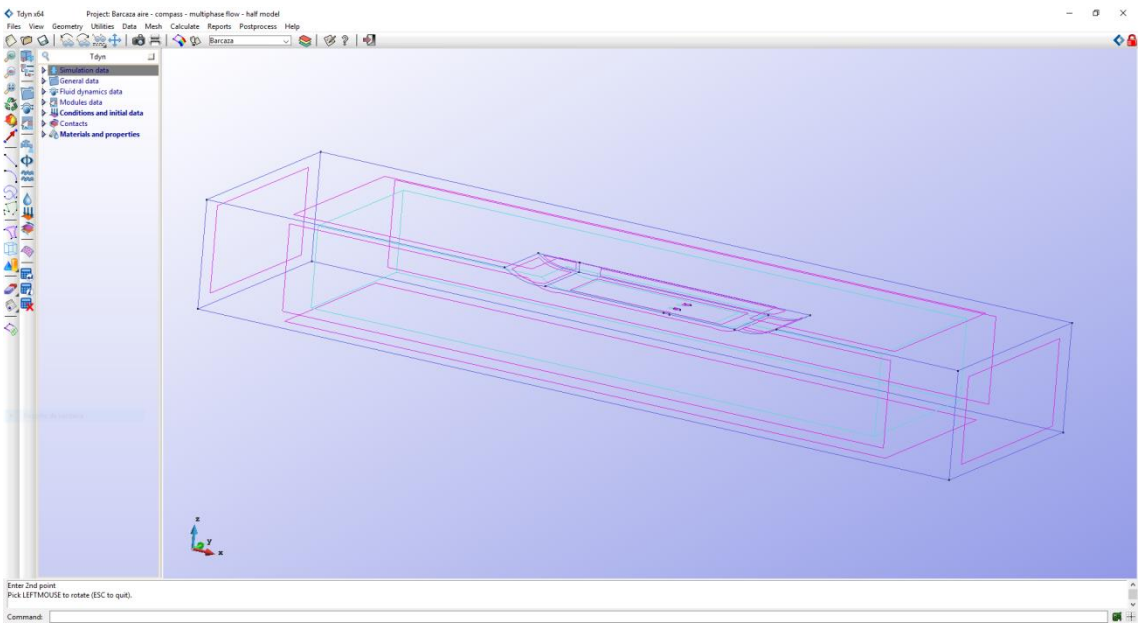

Figure 3.20: Short barge model with associated surfaces and control volume.

The model prepared to execute the numerical simulation in Tdyn finally considers a suitable symmetry condition. In this way, simulation time is reduced significantly because size model is now the half.

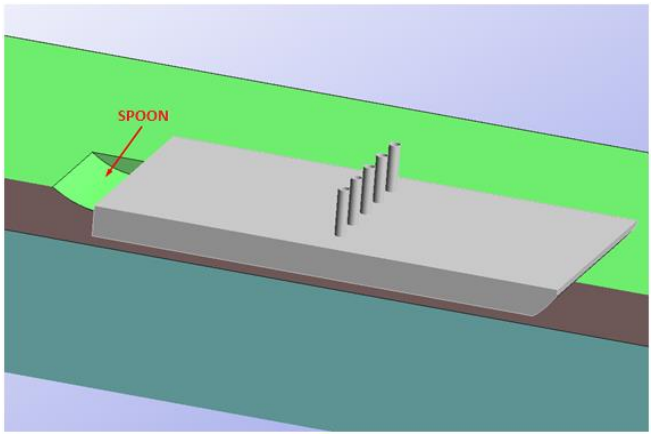

In this case, due to the barge shape hull, a transom stern flow demand the creation of a spoon of a certain length, so, it was also opted to keep the stern spoon because calculus converges well and most reasonable results are obtained.

Figure 3.21: Detail of the shape of the spoon which responds to a tangent surface to lower part of stern. The view is rendered to give a better idea of the spoon surface.

➢ Identification of geometric entities

The different surfaces of the geometry were assigned to different layers as shown in the Figure 3.22. Thanks to that division is possible to make groups which can be treated separately. These groups allow setting the boundary conditions such as velocity and pressure fields which will be explained in the next point. A better view of the groups appears in the dialog box of the Figure 3.23 after establishing the boundary conditions of the following step.

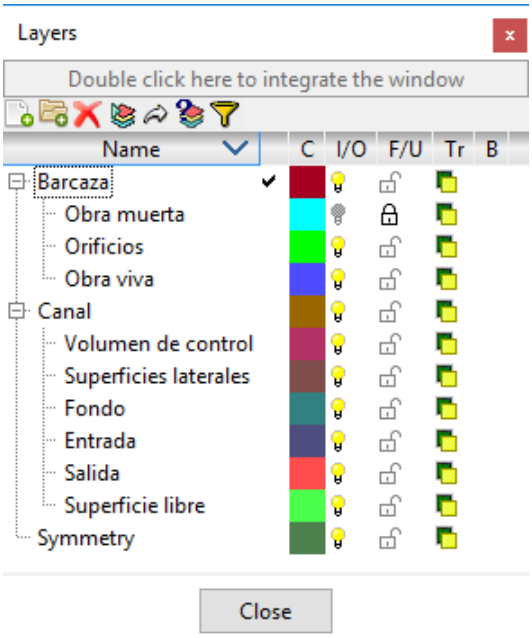

Fig. 3.22: Layers of the different surfaces that form the model and the volume of control.

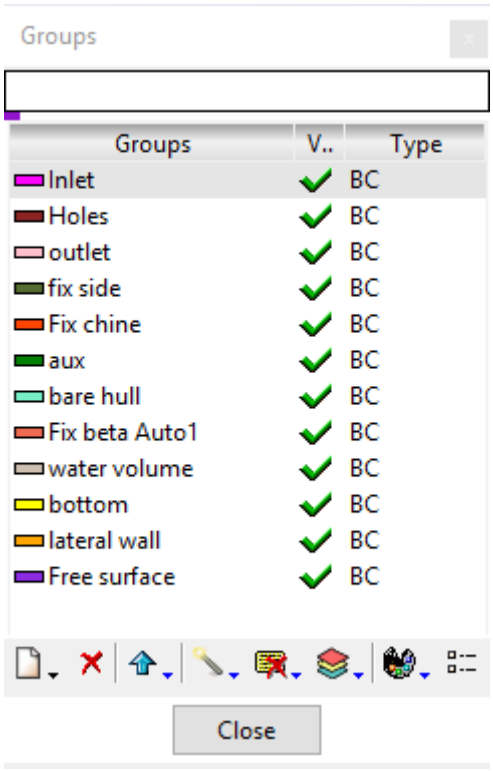

Fig. 3.23: Tdyn groups allow to show the geometric entities of the model.

➢ Initial data & Boundary conditions

Once the geometry has been defined together with its control volume, the necessary boundary conditions for the resolution of the problem were set. These conditions are the velocity of the fluid (barge speed), velocity of the injected air, boundary layer, velocity and pressure fields, wall type, etc.

The main areas where special mention is required are the representation of the free surface, the turbulence models and the grid requirements to accurately capture the flow characteristics.

A simple scheme of the simulation is exposed in Figure 3.24 in which the inlet is the surface afore of the control volume. The barge goes forwards the direction of X axis, but for the simulation in Tdyn the barge is stationary and it is the fluid that will move in the opposite direction to the advance of the model.

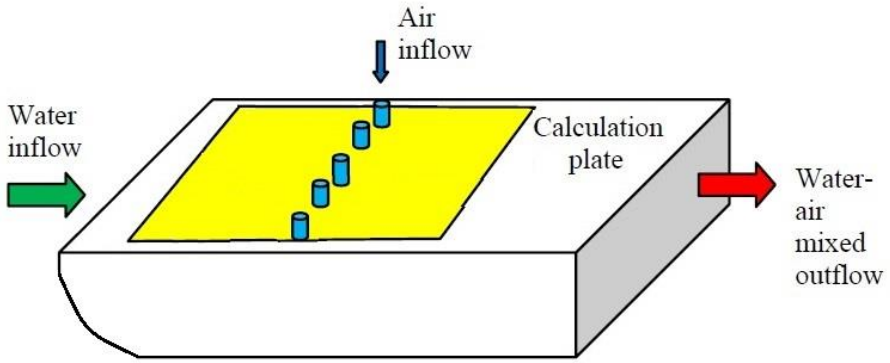

Figure 3.24: Scheme of the simulation. Water flow through the inlet extends downstream; at the place of the holes the water mixes with air and exits by stern.

Same air inflow quantities and water speeds were simulated to generate validation with the experiments. But first, the velocity fields must be set.

The velocity field condition is used to fix the velocity (during all the simulation process) to the initial value of the function given in the *Initial and Field* window of Tdyn. To do this, the corresponding *Fix Initial* flag has to be marked. For the water flow velocity in the inlet the activation is set in the three axis direction X, Y and Z. For the rest of the surfaces, the direction is always perpendicular to them. For example, in the bottom is Z axis and in the symmetry plane, lateral wall and auxiliary surface of the spoon is the direction of Y axis. Also the velocity in the chine of the barge is set as 0 in the three directions in order to avoid some calculation problems that might appear. The velocity in Y field is always fixed as 0 m/s and in the X field is negative as the water flow goes against the X axis positive direction.

The pressure field condition is applied to the outlet surface of the domain, i.e. the surface downstream of the control volume. In this case the relative pressure will be 0 Pa, which means that the atmospheric pressure value 101325 Pa is being set.

The air flow injected through the holes is indicated to the software in the form of air velocity, so a transcription is required knowing the dimension of the hole's surface (10 mm as shown in Figure 2.5). The Table 3.5 shows the final air inlet velocities, for both cases, short and long barge models. It was considered the same velocities for a range of the air flow pressure in mm H_2O because practically there is no variation in them.

mm H_2O	0	120-125	180-210	260-285
air flow - m^3/h	0	2,044	1,436	1,167
air flow - m/s	0	1,446	1,016	0,825

Table 3.5: Input data air inlet velocities in the holes.

The air velocities above in m/s are fixed in negative because the air flow goes against the direction Z of the axis as shown in Figure 3.25.

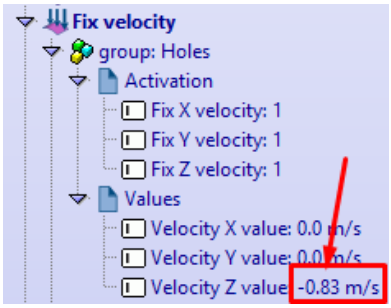

Figure 3.25: Air velocity corresponding to a pressure of 285 mm H_2O.

The boundary layer is the area of the fluid field near a solid contour in which the viscous effects are manifested especially. The type of boundary layer assigned to the bare hull and the holes is the ITTC Wall which corrects the wall stresses taking into account the ITTC 57 friction line. The parameters (Yplus) were fixed correctly with the aim to obtain suitable results.

The properties of the free surface (which is being solved by the transpiration method) must be prescribed for the top surface of the control volume. All data keeps their default values, except the length parameter which is set with the length value of the barge models. Besides, the condition of variable flux can be applied. This is intended to capture the diffusion effect of air through the free surface into the atmosphere. However, the effect is negligible, so is not necessary to activate it. It is also important to fix beta in the spoon.

Another point to take into account in order to capture the effect of diffusion and advection in the simulations is the activation of the option "density buoyancy".

The air lubrication phenomenon considers two fluid materials, the air injected and the surrounding water. At the outlet of the bottom holes the air undergoes a phenomenon of diffusion and later with its contact with the water flow takes place the phenomenon of transport or advection. This is indicated to the program thanks to the PDEs solver incorporated and the function introduced for the resolution of the transport problem of the air injected is the following:

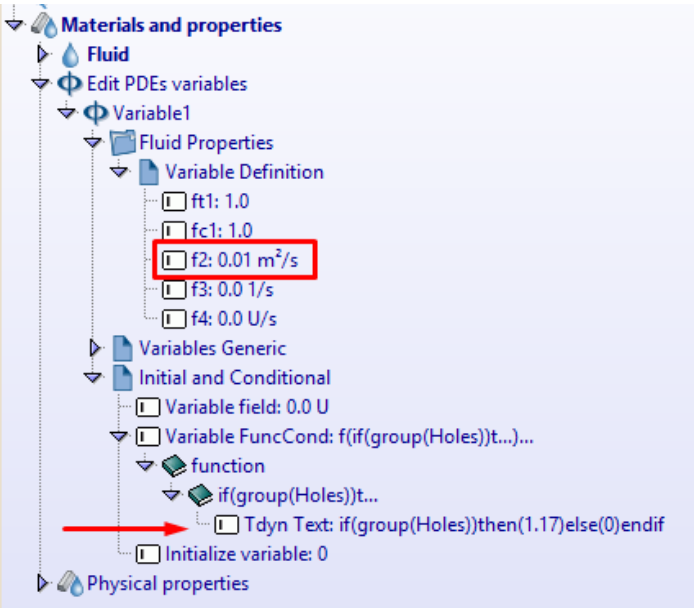

Figure 3.26: Conditional function for establishing the density in the holes and in the mixture.

The value for the pure air density (independent variable of the mixture model) at the exit of the holes is 1.17 without dimension because it has solved the transport equation for a generic variable, but it can be considered kg/m^3 as units.

The diffusion coefficient corresponds to the variable definition “f2” shown in Figure 3.26. From the first simulations it was verified that 0.01 is the value more suitable because the shape of the wake follows better the V shape discovered during experiments.

As this value is slightly arbitrary, since the phenomenon does not really consist of a pure diffusion process, it is chosen according to the qualitative

results found during the post-process. Moreover, this value does not have strong influence in the resistance obtained and is the minimum value that most approximates to the real value before the calculation has difficulties of convergence, so this value will be finally adopted for all the simulations.

The shape of the wake for 0,1 and 0,01 values of the diffusion coefficient are shown in the Figures 3.27 and 3.28. It was also checked for 0,05, but with these two limits values is enough to make a visual judgment of what is trying to explain.

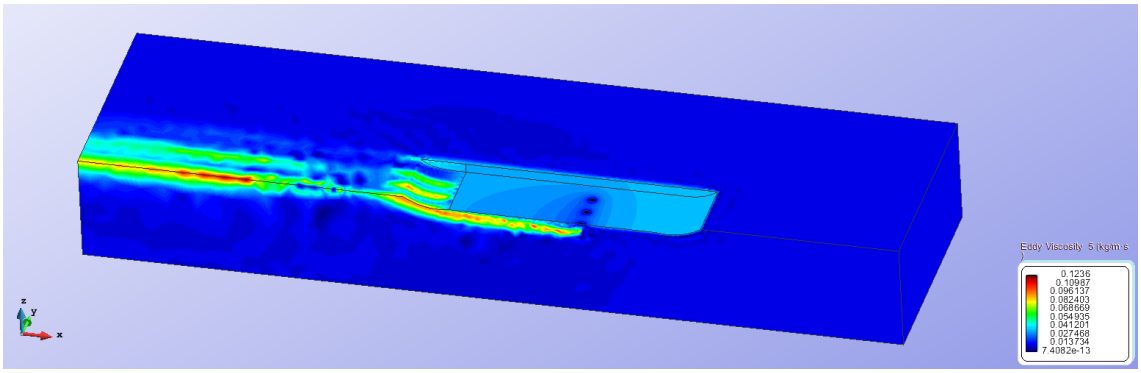

Figure 3.27: Eddy viscosity for the short barge model where the transport of the injected air is linear and do not spread in the bottom. K = 0,1 and Spalart Allmaras turbulence model.

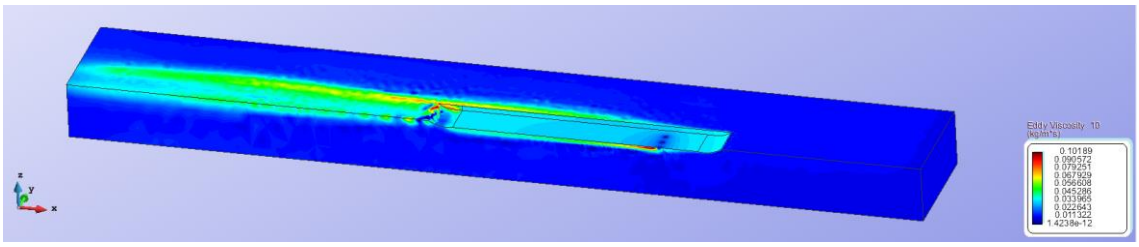

Figure 3.28: Eddy viscosity for the long barge model where the injected air spreads and covers the hull bottom. K = 0,01 and Spalart Allmaras turbulence model.

The figures above are the result of the post-processing of the calculation but they are exposed in this point in order to explain the choice of the diffusion coefficient.

Next step concerns to the establishment of turbulence models and the initial parameters of turbulence. The method used by Tdyn calculates the shape of the flow from an initial estimate of the fluid field. This initial estimate marks how quickly the convergence of the problem is reached and in some cases

marks that the system can converge or not. So it is necessary to correctly estimate these parameters in the initial steps.

As the Reynolds number of the simulated problem is high, the flow is fully developed.

The κ – ε turbulence model is suitable for the case of flow fully developed and this is checked with the results obtained. This model has 2-additional equations to represent the properties of turbulent flow, allowing the model a report of transient effects such as convection and diffusion of turbulent energy. As mentioned before, the variables, "k" is the turbulent kinetic energy, and the second variable, ε, is the dissipation of the turbulence. The latter determines the scaling of the turbulence, while the first determines the energy in the turbulence. These variables were calculated for every simulation.

The behavior of the equations is adequate. However due to the simplifications used, the solution not represents exactly the real system in the case with air injection. The effects are not caught and this is easily visible in the post-processing stage as shown the Figure 3.29. So this model was used for the case without air lubrication only.

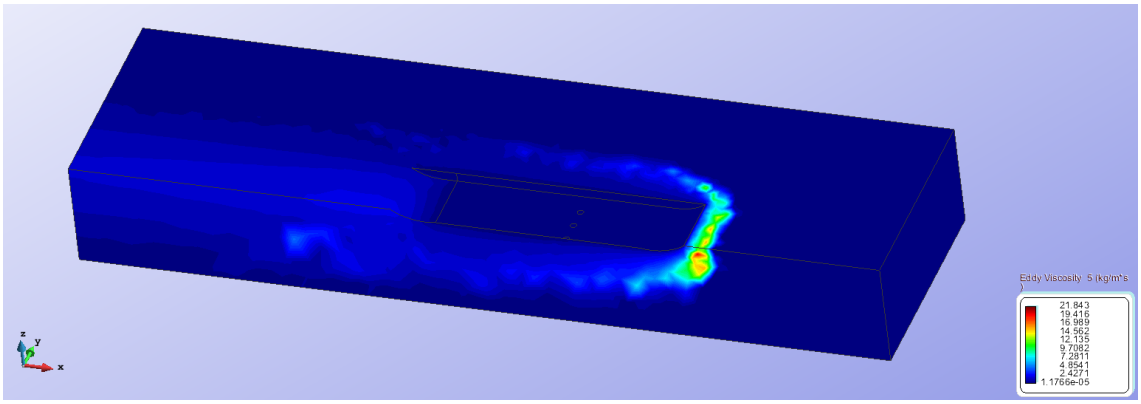

Figure 3.29: Eddy viscosity for the case of the short barge running at 0.75 m/s and 0.83 m/s of air flow. This κ – ε turbulence model for High Reynolds cases do not capture the air injected through the bottom holes.

For the case of ILES turbulence modes (Large Eddy Simulations), the initial boundary conditions are not into account these initial boundary conditions and therefore do not require the user to define the initial turbulence parameters

or turbulence contour conditions. But this model finally was rejected due to the long calculation process and its results far from the experimental test.

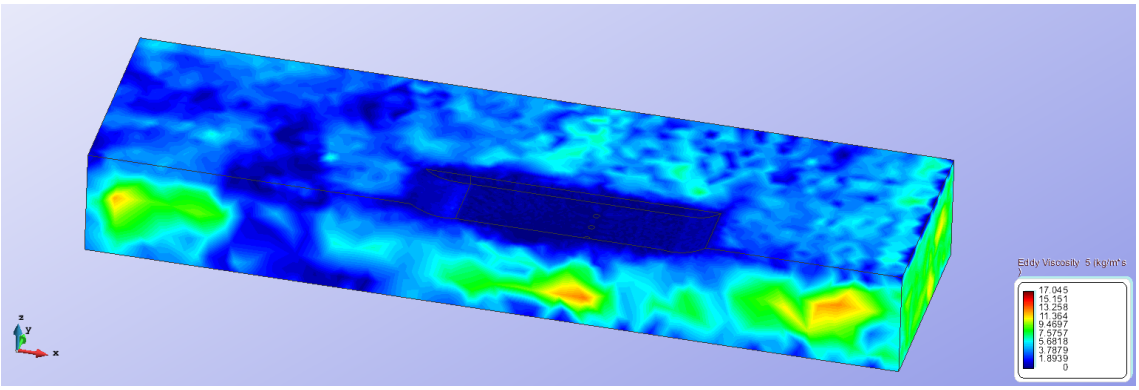

Figure 3.30: Eddy viscosity for the same case shown in Figure 3.29. The ILES turbulence model did not work properly for the condition of air lubrication.

The third chosen model, Spalart Allmaras, is a model of a single closing equation and only uses the Eddy Kinetic Energy variable to initialize the turbulence fields. The other variable Eddy Length has no effect in this model. The fact of setting the Eddy Kinetic Energy variable (See Figure 3.31) by a conditional function is because the formation of the jet is very different from the flow generated by the advancement of the barge. For that reason, it must set the value of that variable in the jets output to a different value from the rest. Actually, it is used a different TIL (Turbulence Intensity Level) value in the two zones. Details of how the TIL is related with K can be found in the turbulence manual available at [21].

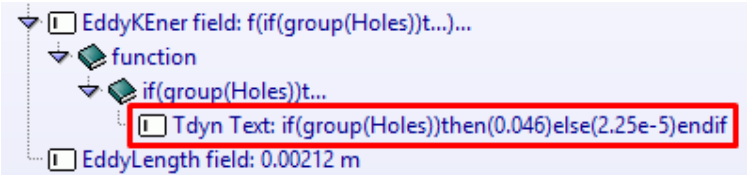

Figure 3.31: Conditional function for establishing the Eddy Kinetic Energy in the holes and in the mixture for the Spallart Allmaras turbulence model.

Spalart Allmaras proved to be the one that best represented during the post-processing the effect of diffusion and transport of the air layer created, for that reason it was chosen to simulate the cases with air lubrication. Figures 3.27 and 3.28 are referred to this model.

The last point before mesh generation concerns to the temporal discretization. It is necessary to establish in the program an adequate simulation time. The time step is a function of the Courant number (C), but in this case it was proven several Number Of Steps (NOS) between 10.000, 15.000 and 20.000 depending on the case. The case without air lubrication requires less computation time so it was possible to increase the time step and reduce the steps. For the case with air lubrication, 20.000 steps and 0.0005 s or also 0.001 with 5 iterations was enough for the convergence of the calculus. Also it was checked that the time step was compatible with the mesh size and checked at the end of the calculation that converged without incident.

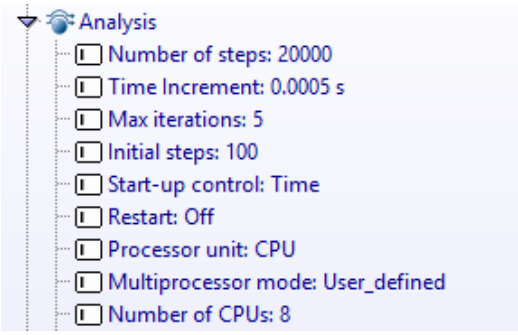

Figure 3.32: Time discretization analysis where is visible the number of CPUs employed for the simulations. Thanks to the workstation used which was equipped with Intel Xeon inside, it was possible to use the multithreading of its 8 cores.

- **Mesh generation**

The following step has vital importance in results accuracy. The previous geometry will be meshed as thin as possible taking into account the limitations of RAM.

The higher density of the mesh should be located where the spatial variations of the solution is expected. This is the surrounding area of the bottom holes, hull surface and free surface.

It was chosen a non-structured mesh because the automatic generation is easier and adaptability higher than in structured mesh.

It was tested different mesh sizes to check the sensitivity of the results to this change. Finally, were chosen the sizes shown in Figure 3.33 because results were appropriate and the calculus took a reasonable time.

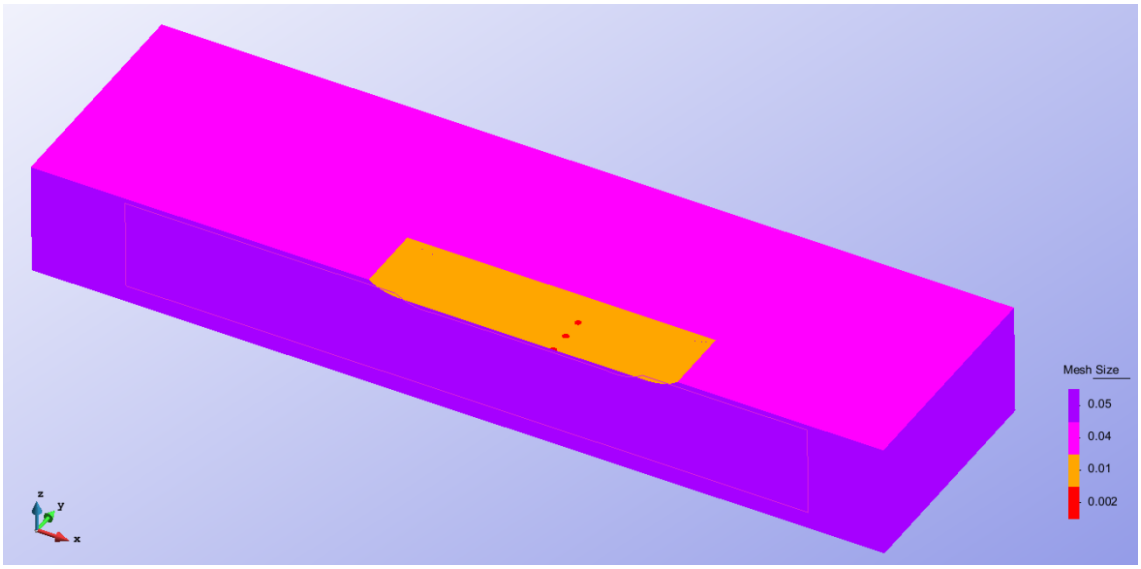

Figure 3.33: Mesh sizes on surfaces. The holes have 2 mm of element size, bare hull 10 mm, free surface 40 mm and the rest of the control volume surfaces have 50 mm.

Once the mesh is generated the results can be viewed in Figures 3.34 and 3.35. The different elements sizes are visible for every surface of the control volume and also is shown a mesh refinement on the model surfaces.

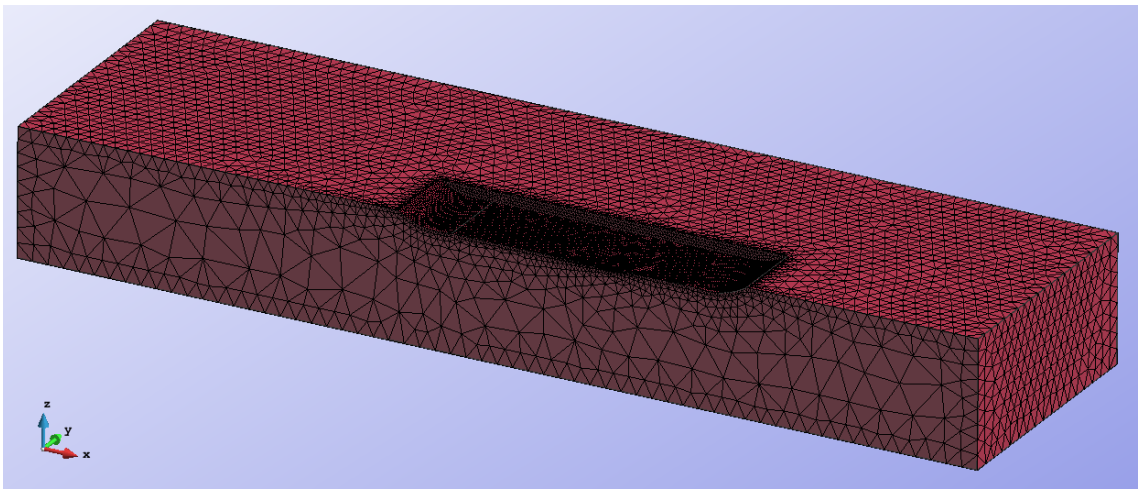

Figure 3.34: Mesh generated for the case of the short barge.

As is visible in the figure above, the density of the mesh is concentrated in the layers contiguous to the free surface where is interesting to capture the effect of the air lubrication.

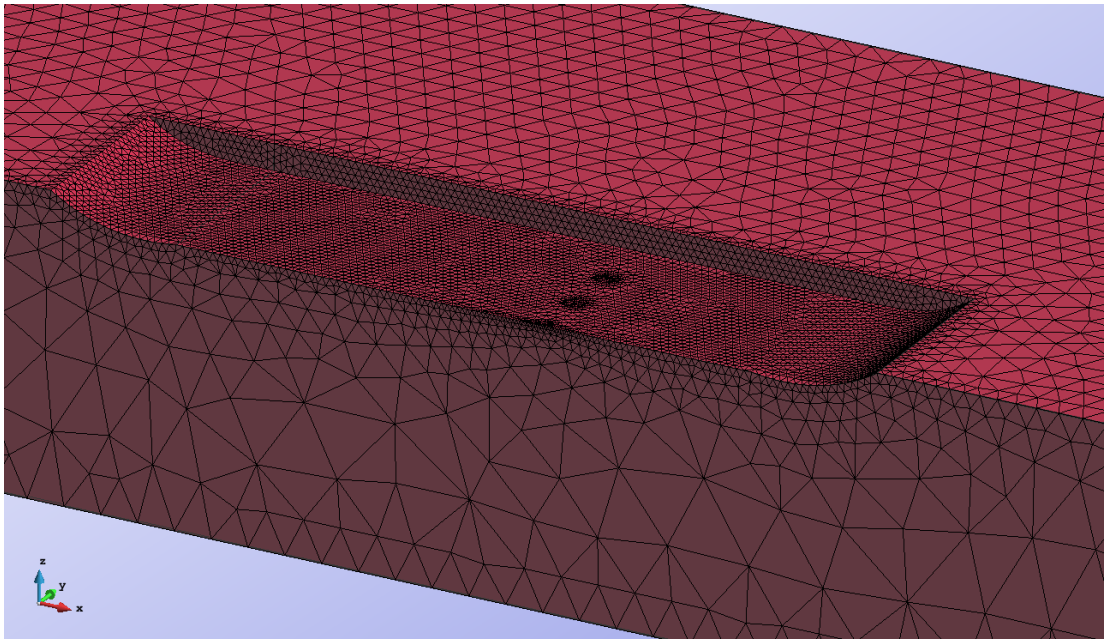

Figure 3.35: Detail of the surrounding meshing of the short barge hull.

3.14.4 Calculation

Once the problem has been meshed, it is proceeding to its calculation and finally with the visualization of the results. After the process is finalized it should be checked the Forces Graph to determine the convergence of the calculus as shown in Figure 3.36. It shows the evolution of the forces and moments acting on the hull depending on the simulation time.

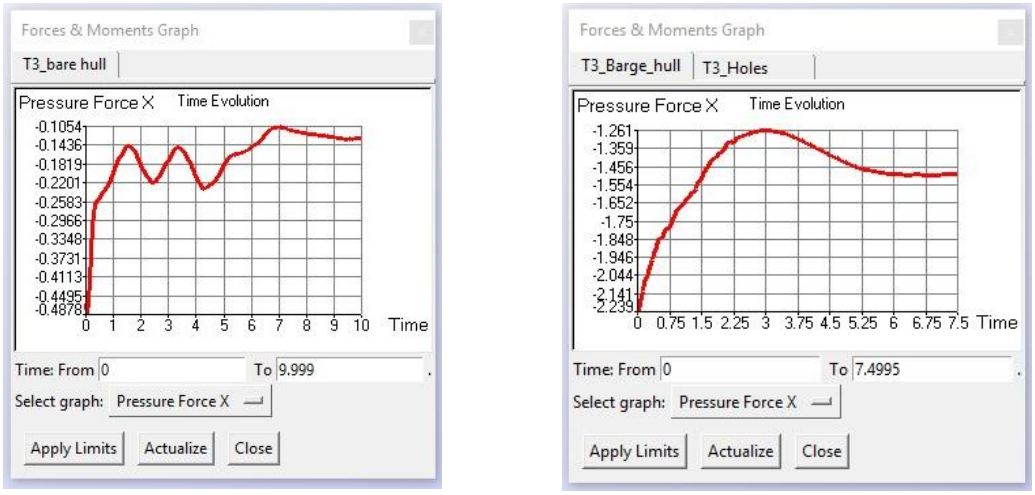

Figure 3.36: Convergence of two simulations processes which can be checked with the Forces & Moments Graph. The graphs are asymptotic so the calculus is fine.

3.14.5 Post – processing

In this part of the simulation is possible to get a variety of graphic results, from current lines to videos of the problem in motion. The used CFD codes allow the export of these, so that the user can work on other platforms.

After checking the convergence of the calculus, the resistance values obtained were analyzed and verified.

The value of the drag resistance is the sum of the pressure and viscous forces in the X direction. Opening the tab utilities > Forces on Boundaries appears the chart shown in Figure 3.37.

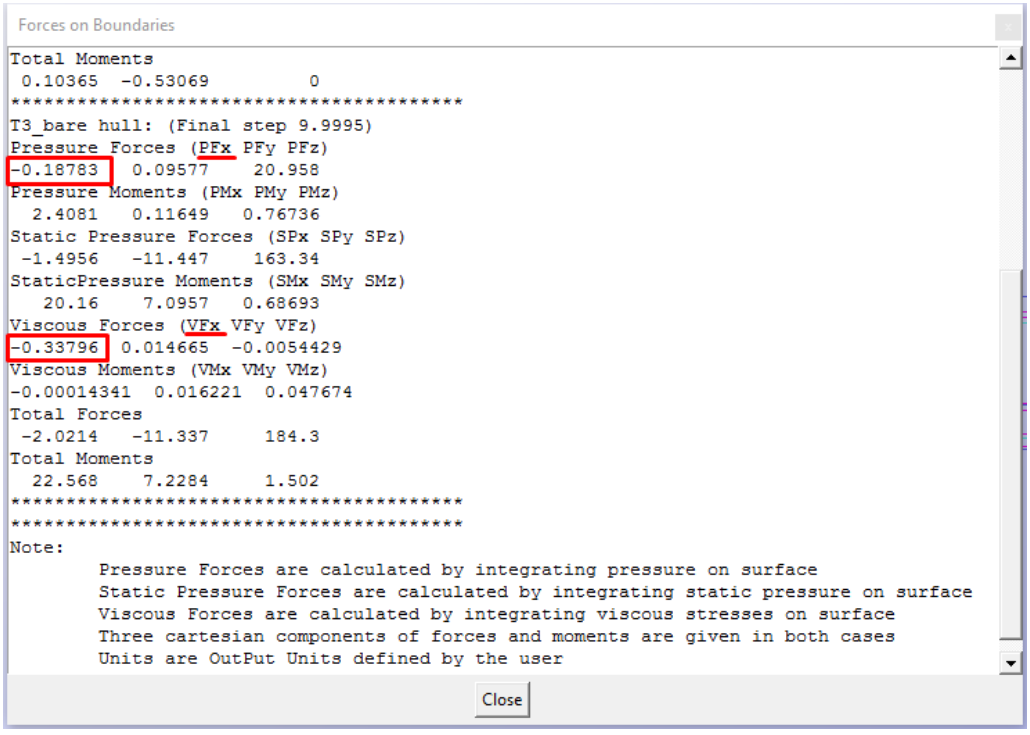

Figure 3.37: Forces on Boundaries for the case of long barge with a speed 0,5 m/s and 1,02 m/s of injected air flow.

In the figure above the sum of the red numbers is the half of the drag resistance because all the simulations were made with the symmetry condition to reduce the simulation time. So multiplying by 2 gives the total resistance in Newton.

$$2 \cdot (PFx + VFx) = 2 \cdot (0.1878 + 0.3380) \approx \mathbf{1.052\ N.}$$

All this analysis must be applied for each speed of the model in which the resistance is looked for and in that way is possible to obtain the resistance-speed curve.

The results will be validated by comparing them with the experimental results. Before starting the section of results comparison is interesting to view some screenshot of the pressure and speed distribution, wave profile among others. Figures 3.38, 3.39 and 3.40 show these visualizations.

An example of the distribution of the waves is the one shown in the Figure 3.38 for the case of the short barge running at 1, 29 m/s and 0,83 m/s of injected air. The screenshot made during the post-processing makes visible how the main waves are generated downstream of the model due to the hull shape, the flow does not exit smoothly so a relative high waves are visible as shown in the figure.

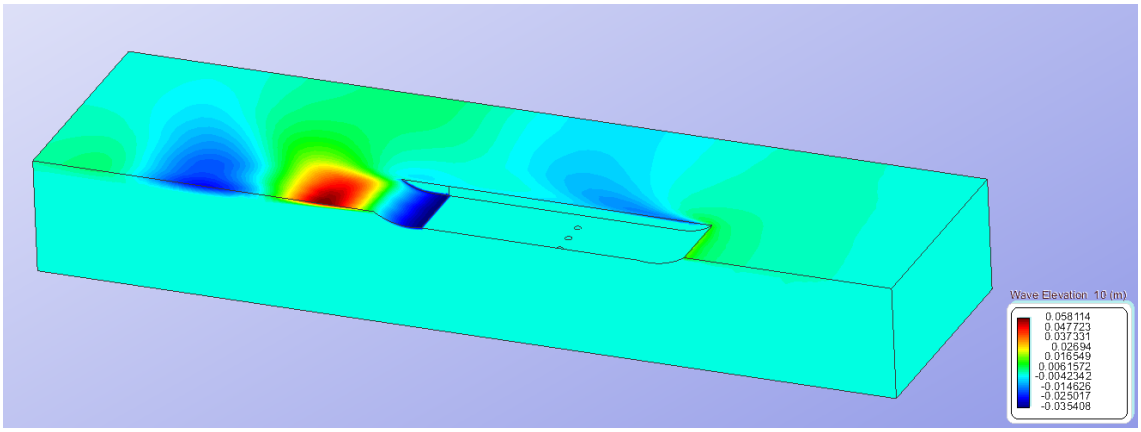

Figure3.38: Example of wave distribution on the short barge.

➢ **Pressure distribution:** The pressure must be higher at the bow of the barge, as the latter advances forward and the water will strike there first, then the pressure must be reduced in the curves of the barge, as these will accelerate the flow and this acceleration of the flow leads to a loss of pressure. This pressure must increase again in the stern because due to the wake the water moves with slower speed, and a lower speed carries greater pressure. The Figure 3.39 gives an idea of how the pressure field looks like.

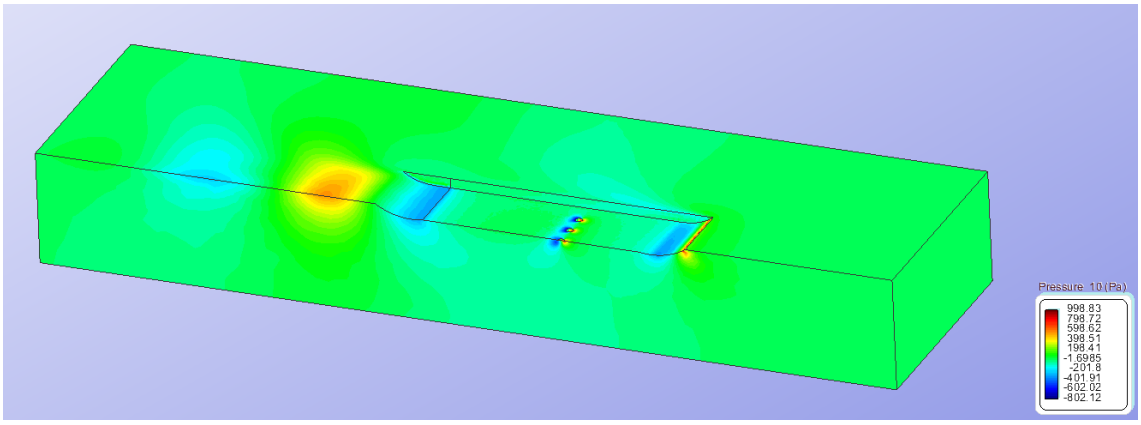

Figure 3.39: Example of pressure field distribution on the short barge.

➢ **Distribution of velocities:** As already explained above, what moves is the water and not the model, so in the areas farthest from the vehicle the flow velocity must be that of the vehicle. The velocity distribution is expected to be contrary to the pressure, that is, lower in the bow and stern and higher where there are areas with curvature. In the Figure 3.40 can be seen an example of how we expect this field of speeds.

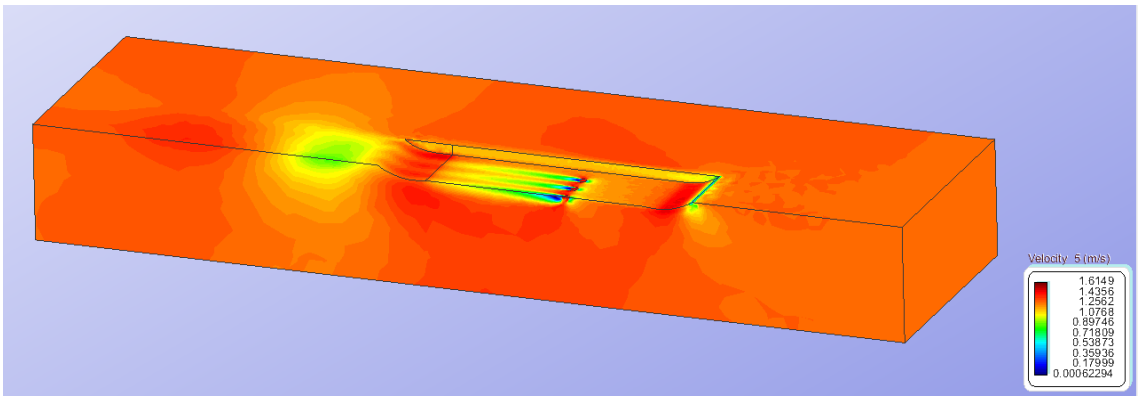

Figure 3.40: Example of velocity distribution on the short barge.

Section IV

Results Comparison

4.1 Comparison: Experimental and Numerical results

In this section takes place a comparison between the different values of the drag resistance obtained from the experimentation and the numerical simulations. In order to make a judgment of the air lubrication phenomenon, the drag resistance results are exposed in graphics because is a direct way of making relationships.

First of all, the results of the experimental tests for the short and long barge models are shown:

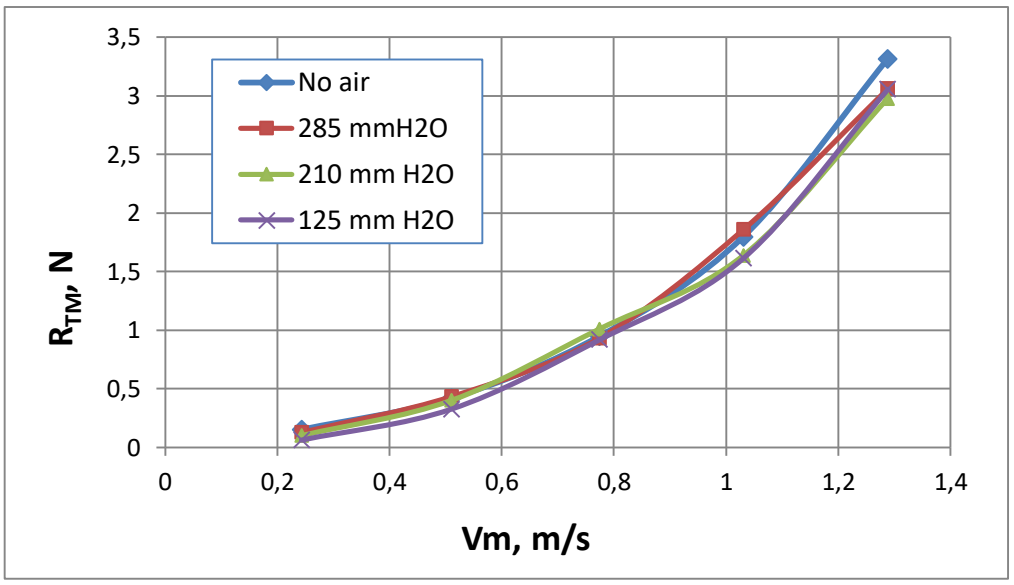

Figure 4.1: Resistance vs. speed, Short barge.

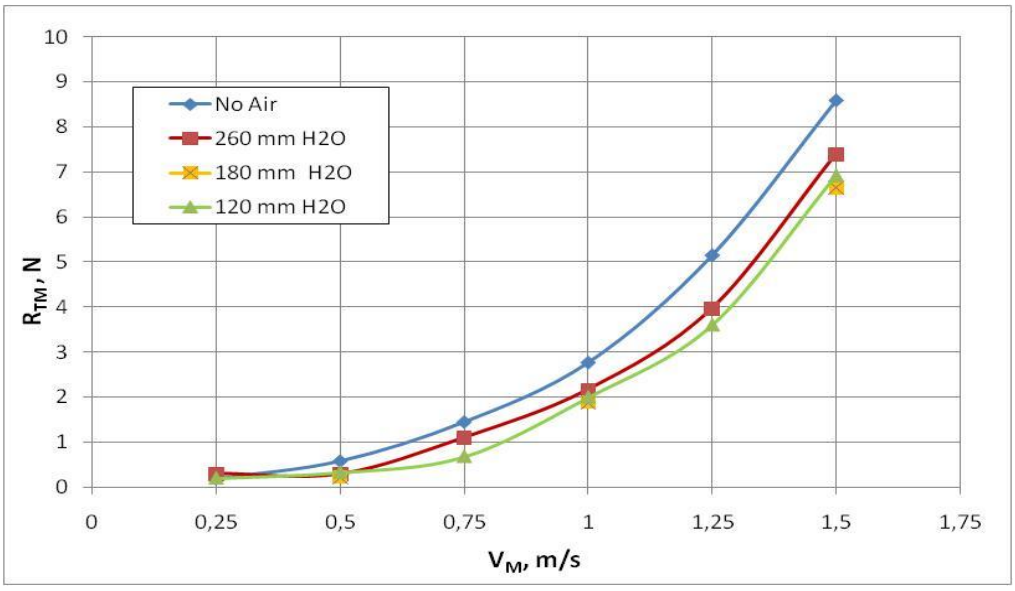

Figure 4.2: Resistance vs. speed, Long barge.

In both cases (short and long barge) there is a resistance reduction effect with the discharge of air which is more pronounced in the case of the long barge. Moreover, there is a noticeable optimum of air pressure in the range of 150 to 200 mm H_2O for all speeds tested.

After checking the experimental results, it is made a comparison with the results obtained for the short barge in the case without air with the same turbulence model (κ – ε) in the software Tdyn CFD and ANSYS Fluent. It may be noted that the final values obtained for total resistance are very close which leads to think that the simulations in both cases are similar. The differences between them are shown below in Table 4.1 and Figure 4.3.

Short barge

Vm, m/s	ANSYS	Tdyn CFD	Towing Tests
0,25	0,310	0,260	0,150
0,5	0,740	0,817	0,420
0,75	1,490	1,640	0,947
1	2,640	2,898	1,798
1,25	4,340	4,672	3,316

Table 4.1: Resistance vs. speed, Short barge.

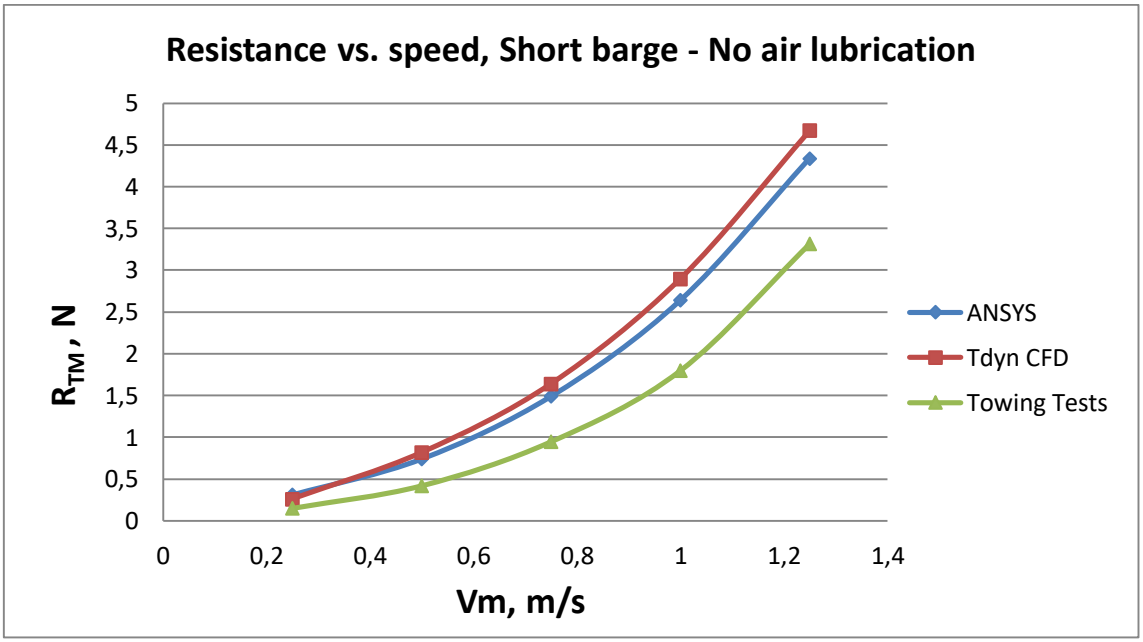

Figure 4.3: Resistance vs. speed, Short barge in the case without air lubrication.

Regarding with the towing tests the numerical simulations give higher resistance values, but within an acceptable range.

The Spalart Allmaras and k - ε turbulence models give the best results for the drag resistance estimation in the case of the simulation with Tdyn software. For the towing analysis of the models without air lubrication, the k - ε model was chosen and it is noticeable a reduction in the drag resistance with the use of air lubrication. Anyway all the simulations with different air flows have practically the same resistance values.

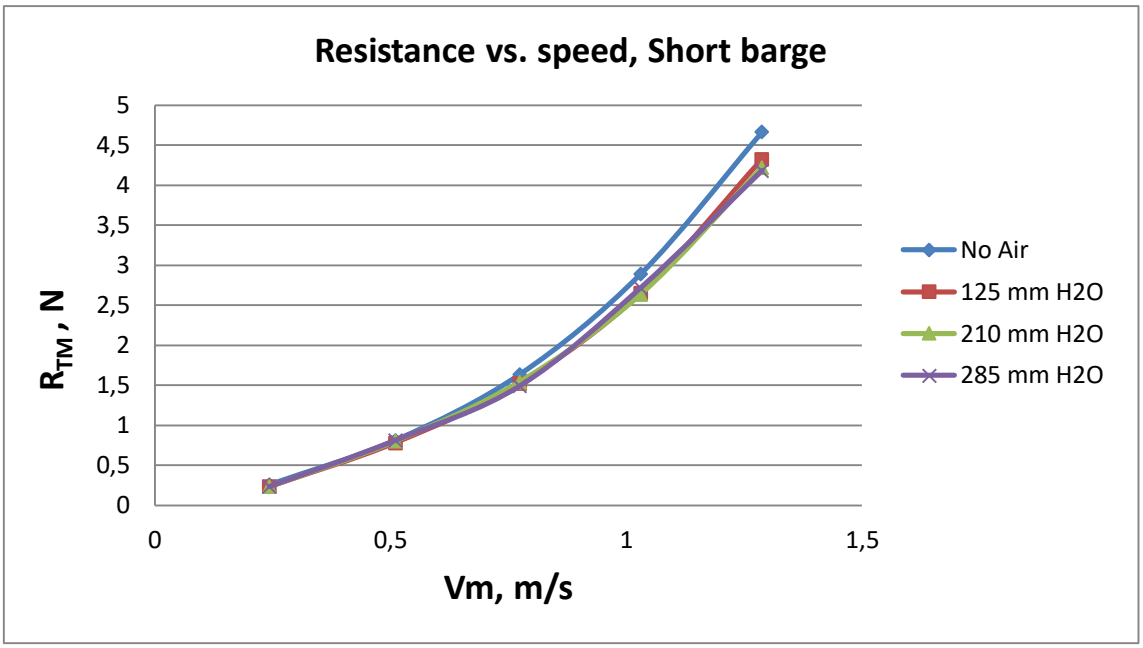

Figure 4.4: Numerical results (Tdyn) for resistance vs. speed, Short barge.

It is difficult to distinguish the lines corresponding to the cases with air lubrication because they have a very close values. There is hardly any difference in the use of different air flow rates.

The drag reduction in the case with air injection is the result of the lower density of the mixture and the turbulence model chosen (Spalart Allmaras). It seems that the effect is more noticeable in the case of the long barge (see Figure 4.5) but again, there is no reduction of the resistance as a function of the air flow injected. Simply it is due to the lower density of the fluid mixture in contact with the bottom of the barge.

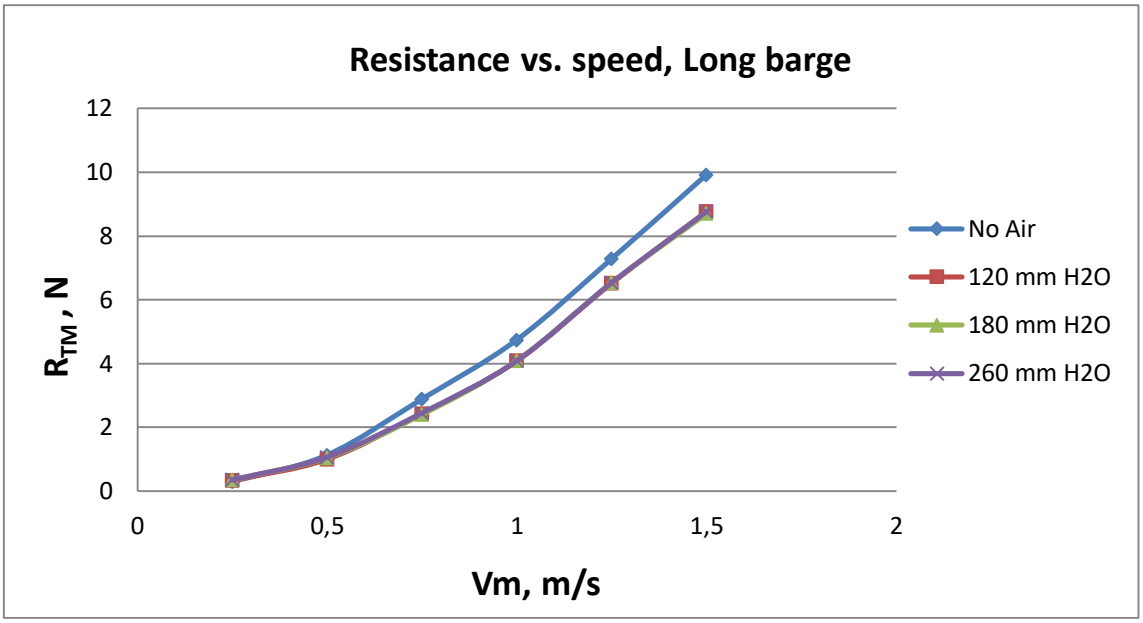

Figure 4.5: Numerical results (Tdyn) for resistance vs. speed, Long barge.

This lower density is not enough to make a conclusion about the effect of this system through the used software. Is necessary to work on a more complex model to get better results close to experimental.

Is a fact that the towing tests report a remarkable drag reduction and the simulations follow the same line at least in the case without air lubrication. Once the air lubrication is implemented for the analysis with the software, the results are not conclusive to validate those obtained in the tank.

The implementation of a more complex model as is the case of an air layer between the hull and water, perhaps may bring better results so it can be the starting point for a new study of the phenomenon.

The following figures show a comparison between the barge models simulated with Tdyn and those tested in the tank. In them it can be observed that the resistance obtained by software is greater than the experimental resistance. They are very similar with a reasonable values and the graphs present a similar form.

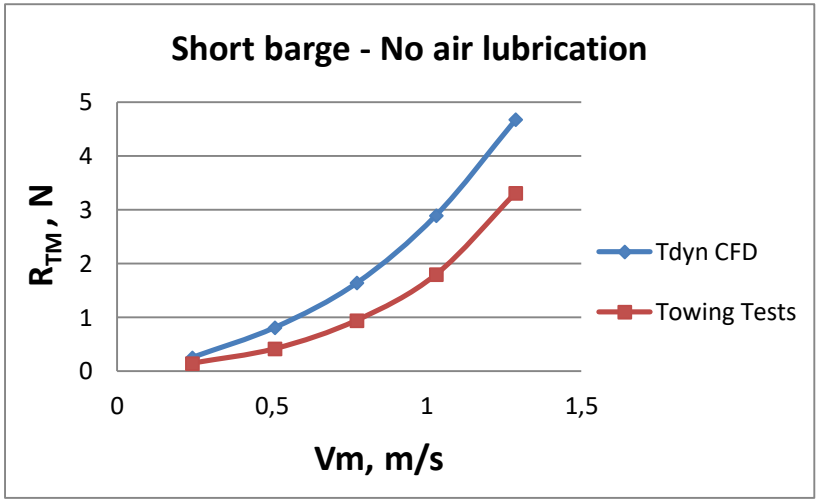

Figure 4.6: Resistance vs. speed, Short barge.

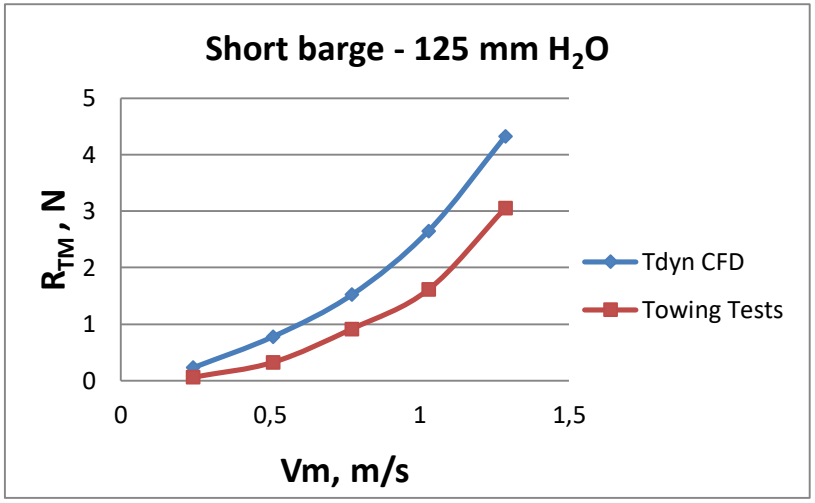

Figure 4.7: Resistance vs. speed, Short barge.

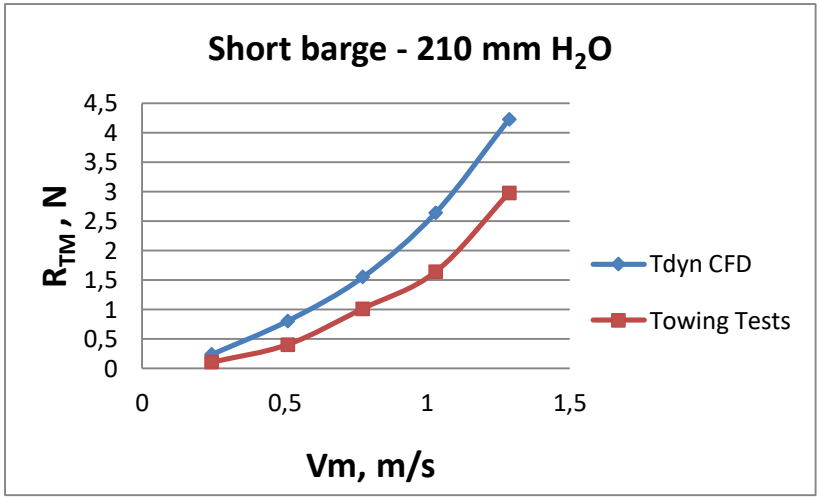

Figure 4.8: Resistance vs. speed, Short barge.

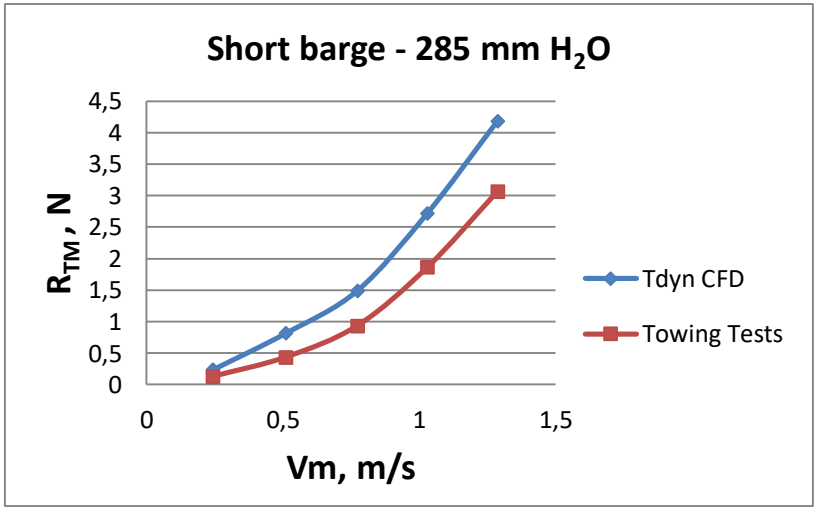

Figure 4.9: Resistance vs. speed, Short barge.

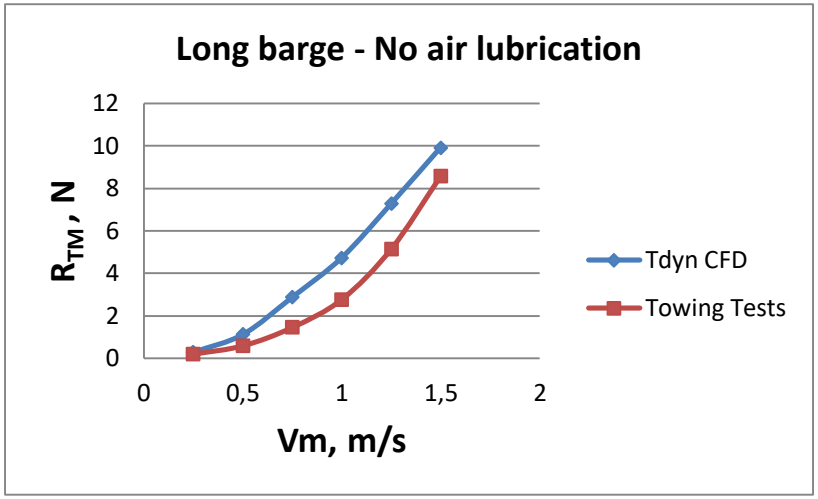

Figure 4.10: Resistance vs. speed, Long barge.

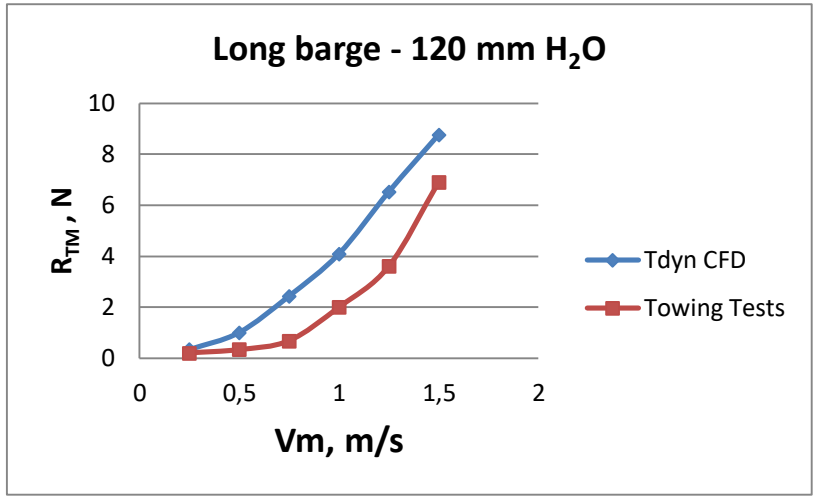

Figure 4.11: Resistance vs. speed, Long barge.

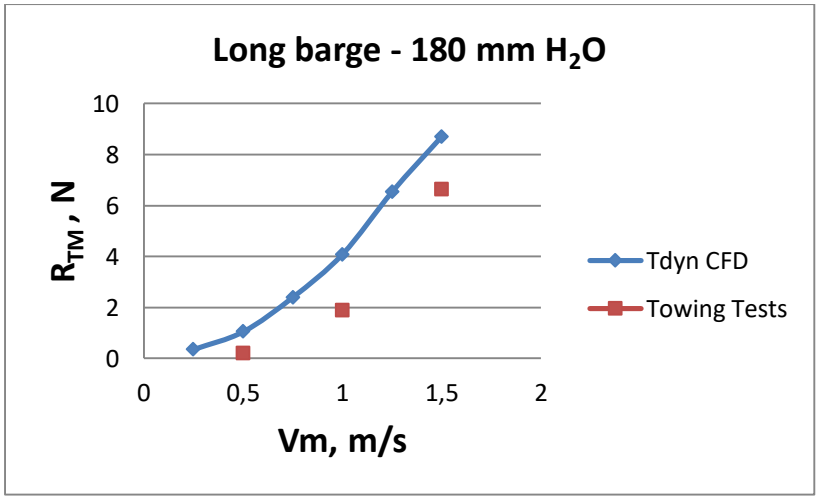

Figure 4.12: Resistance vs. speed, Long barge.

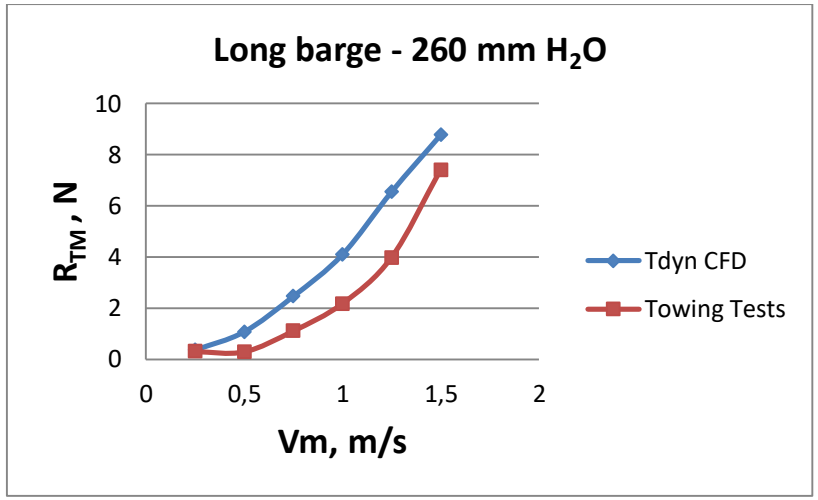

Figure 4.13: Resistance vs. speed, Long barge.

Section V
Conclusions

This investigation has gone in depth with this innovative approach for reducing ship drag. The fluid problem has been studied from two different ways, both complementary. On the one hand, experimental tests have shown the air-lubrication effect, it is a fact that friction resistance goes down when one of these air-lubrication techniques are correctly applied. The reduction is around 10 - 15% of the total resistance. On the other hand, numerical simulations have verified in part the theoretical reduction, but still need more investigation.

In order to extend the results obtained to full scale, more simulations and tests would be needed. At least, another with a larger scale model to compare the results at higher velocities and dimensions.

The most direct way to obtain information about this new phenomenon was to take measurement of the parameters that define the process. Anyway several difficulties were found as are the following:

- Location and air flow rate of the feed holes have a prime importance for the optimum performance of air lubrication technique. In the model, the system with five air feed holes was simpler but an optimization of its location can lead to better results.
- Experimental flow visualizations have indicated that exist a complex interaction between the ship boundary layer and the shapes of the spread air beneath the hull bottom. Since it does not form a uniform air layer, it would be useful to find out a way of registering and using the percentage of hull bottom covered by air. So it could set a relation between the percentages of covered area and drag reduction.
- In order to covering the maximum hull surface with air, an optimization of the hole position and air flow rate is required.
- Numerical simulation with ANSYS finally did not lead to expected results for the air injection cases due to the difficulty to carry out the simulations. Therefore, was not possible to contrast it with the results obtained in Tdyn.
- Assumptions made during Tdyn simulations may not exactly represent the real physical phenomenon, in consequence the issues found (similar results for the different air flow rates).

5.1 Potential economic impacts

According to the current framework of the air lubrication investigations reviewed in Section I, the economic and environmental impacts of successfully implemented air lubrication could be significant, as a ship's fuel consumption may be reduced by 5 to 20% with the corresponding reduction of harmful gases. However, the techniques have yet to be implemented on a large number of real vessels and hence the potential benefits are yet to be realized.

For the BDR and ALDR techniques, there have been two sea trials. The first one was carried out on the Pacific Seagull ship resulted in 5 to 10% net energy savings according to Hoang *et al.* (2009) [14], while the second sea trial by Mitsubishi Heavy Industries achieved 8 to 12% net energy savings (Mizokami *et al.* 2010) [3].

As for PCDR technique, a scale test by MARIN showed 15% net energy savings (Foeth, 2011) [16] and for a 1:12th scale test by STENA they reported resistance reduction of 20 to 25% [17].

5.2 Future research

The first thing that comes to mind is to change air injection holes upstream. In this way is possible to create a higher air film and hopefully better results. However, the model was already elongate to supplement this handicap.

Changing the air injection configuration could have a different influence in the air layer created. This is easier in CFD simulation because the barge model would need extra work.

Covering the hull bottom with full air layer may not be possible with just discrete holes. This suggests that other techniques should be tested with the goal of maximize the layer of air underneath the hull. An interesting experiment to carry out would be the use of another air lubrication technique as Bubble Drag Reduction (BDR). With the same barge, only a small remodeling would be necessary to investigate how this system works once the model is towed in the tank.

Air bubbles obtained from pumping of air through porous media have been utilized in several researches and full scale applications with clear results. So the opportunity to continue the investigation is there.

A horizontal strip of porous media can be placed in the section where the five discrete holes are placed. Even though the bubbles will form discretely, these bubbles may be combined to form an air film.

Also placing the porous strip near the bow would be the best way to maximize the hull surface in touch with air. But a simple way is to replace a rectangular piece of the barge bottom and make a rectangular parallelepiped with a porous bottom and a ceiling with the supply of the same 5 pipes of the actual model. Air flow rates between 1 to 3,5 m^3/h are possible according to the employed pump power. In this way another experiment tests could be carry out to observe the changes in drag reduction.

Concerning to numerical simulation it should be emphasized the job with ANSYS code, is a fact that this software was used to test the air bubbles technique. Simulations of large geometries and bubbly flows were carried out to design a system that covered 34 percent of the wetted surface area with air bubbles and estimated a 10 percent reduction in total resistance.

Finally, a better approximation to the physical phenomenon in Tdyn software would lead to other results. It has been shown that the biphasic mixture with lower density is not enough to achieve a reduction effect of the drag resistance as a function of the flow of air injected.

5.3 Resistance and propulsion open questions

Air-lubrication does indeed reduce drag resistance but there are still questions that will be important to study as are the following:

- **Air´s effect on propeller efficiency**. Although some studies say there is no interaction, more model tests and simulations are needed.
- **Additional drag from strakes and other appendices on the hull.** Again are needed more detailed calculations, model test and simulations.

- **Effect of sea state (perturbations) in air lubrication**. Some experiments performed as PELS, but more needed.
- **ALDR: Air layer persistence?** It has been seen in the experiment with the barge that the layer of air remains until arrival astern, but the point is, will happen the same during sea-trials?
- **PCDR: Is one multi-wave partial cavity enough?** Sea trials are required to answer this, maybe is necessary divide the length in several cavities which would increase the cost.

5.4 Life cycle cost open questions

The energy net balance positive is necessary but not sufficient condition. It must be taking into account the initial cost. This includes labor, materials, machinery, and lost opportunity cost during retrofit.

Also is possible to lose cargo capacity because air lubrication works with a system composed by compressor and pipes. Moreover, the air delivery system requires maintenance so these costs cannot be ignored. Maybe for new ship may be sufficient, because there may be offsets as a smaller engine and fuel tanks.

Not known what will be the price of fuel in the future, perhaps there may be “subsidies for being green”, which would compromise the effort to install an air lubrication system. For any air lubrication technique to be considered for implementation, the potential net energy savings must be sufficient to justify the added complexity of the air supply system and the capital, operational and maintenance costs.

To conclude, it can be said that air lubrication is a promising technique. However, the technique has not been fully developed. More research has to be done on the aspects of shape of the hull and positioning of the system and efficient distribution of air. Also, with the view of achieve the drag reduction goal, air lubrication should be considered as a good addition to the techniques that will help bring down fuel consumption and emissions.

Section VI

List of References

LIST OF REFERENCES

[1] Dr. ir. H. Prins, "*Sustainable Methods for Optimal design and Operation of ships with air lubricaTed Hulls (SMOOTH)"*, MARIN Report, July 2012 http://www.SMOOTH-ships.eu

[2] Thill, C.H., Toxopeus, S.L. and Walree, F. van, "*Project Energy-saving air-Lubricated Ships (PELS)*", 2nd International Symposium on Seawater Drag Reduction, Busan, Korea, May 2005

[3] Shuji Mizokami, Chiharu Kawakita, Youichiro Kodan, *"Experimental Study of ALM and Verification of Effects on Actual Hull by Means of Sea Trial"*, Mitsubishi Heavy Industries Technical Review Vol. 47 No. 3, Sept 2010

[4] M. Kawabuchi et al., *"CFD Predictions of Bubbly Flow around an Energy-saving Ship with Mitsubishi Air Lubrication System"*, Mitsubishi Heavy Industries Technical Review Vol. 48 No. 1 (March 2011)

[5] Steven L. Ceccio & Simo A. Mäkiharju, *"Air Lubrication Drag reduction on Great Lakes Ships"*, University of Michigan, February 2012

[6] Mäkiharju, S., Elbing, B.R., Wiggins, A., Dowling, D.R., Perlin, M. and Ceccio, S.L., *"Perturbed Partial Cavity Drag Reduction at High Reynolds Numbers"*, Proc. 28th Symposium on Naval Hydrodynamics, Pasadena, CA, 2010

[7] Lay, K.A., Yakushiji, R., Mäkiharju, S., Perlin, M. and Ceccio, S.L., *"Partial cavity drag reduction at high Reynolds numbers"*, Journal of Ship Research, v.54, n.2, pp. 109-119. 2010

[8] Shuji Mizokami, Manabu Kawakado, Mitsuhiro Kawano, Takeo Hasegawa, Ichiro Hirakawa, *"Implementation of Ship Energy-Saving Operations with Mitsubishi Air Lubrication System"*, Mitsubishi Heavy Industries Technical Review Vol. 50 No. 2, June 2013

[9] Insel M., Gokcay S., Helvacioglu I.H., "*Flow Analysis of an Air Injection Through Discrete Air Lubrication"*, INTERNATIONAL CONFERENCE ON SHIP DRAG REDUCTION (SMOOTH-Ships), 20-21 May 2010, Istanbul

[10] Dr. Stefan Kyulevcheliev, Dr. Petar Georgiev, *"Investigating the possibilities for ship resistance reduction by air lubrication"*, University of Varna, 2013

[11] M. Insel, I. H. Helvacioglu, S. Gokcay, *"Flow Analysis of an Air Injection through Discrete Air Lubrication"*, International conference on ship drag reduction, Istanbul Technical University, May 2010

[12] Dr. Blas Zamora Parra, *"Notas sobre simulación numérica de flujos de fluidos"*, Universidad Politécnica de Cartagena, 2008

[13] Manuel M. Sánchez Nieto, *"Mecánica de fluidos general"*, Universidad Politécnica de Cartagena, 2009

[14] Hoang, C. L., Toda, Y., and Sanada, Y. *"Full scale experiment for frictional resistance reduction using air lubrication method"* Proc. of the Nineteenth International Offshore and Polar Engineering Conference, 812-817, 2009

[15] Dr. José Enrique Gutiérrez Romero, *"Apuntes Hidrodinámica, Resistencia del buque"*, Universidad Politécnica de Cartagena, 2013

[16] Foeht, E.J., Eggers, R., *"The efficacy of air-bubble lubrication for decreasing frictional resistance"*, International conference on ship-drag reduction, Istanbul, May 2010

[17] B. M. Toemen Visser, P. van Kluijven, *"Air lubrication"*, Final report project, Rotterdam, March 2011

[18] Crespo, A., *"Mecánica de Fluidos"*; Thompson, 2006

[19] ANSYS Web site: http://www.ansys.com/

[20] Tdyn CFD Web site: http://www.compassis.com/

[21] CFD online Web site: https://www.cfd-online.com/